IMPORTANCE OF MOLECULAR PACKING AT INTERFACES AS WELL AS IN PRE-MICELLAR AND MICELLAR AGGREGATES FOR CONTROLLING VARIOUS TECHNOLOGICAL PROCESSES

By

JAMES RENE KANICKY

A DISSERTATION PRESENTED TO THE GRADUATE SCHOOL
OF THE UNIVERSITY OF FLORIDA IN PARTIAL FULFILLMENT
OF THE REQUIREMENTS FOR THE DEGREE OF
DOCTOR OF PHILOSOPHY

UNIVERSITY OF FLORIDA

2002

I dedicate this dissertation to my parents, who have waited
so long to see me get a real job!

ACKNOWLEDGMENTS

I would like to express my sincere gratitude and appreciation to my advisor, Professor Dinesh O. Shah, chairman of my supervisory committee, for his guidance, enthusiasm, and motivation throughout my career at the University of Florida. His philosophical lessons on life and happiness have been of great inspiration to me. I am also very thankful to my other graduate committee members, Professors Brij Moudgil, Gar Hoflund, and Anuj Chauhan for their valuable time and suggestions, and to the UF Department of Chemical Engineering for their kind support.

I wish to thank my colleagues from the Department of Chemical Engineering and the Center for Surface Science and Engineering for their help and cooperation: Dr. Alex Patist, Dr. Peter Kang, Dr. Steve Truesdail, Dr. Byron Palla, Dr. P. K. Patanjali, Dr. Brajesh Jha, Dr. Dibakar Dhara, Dr. Rahul Bagwe, Juan-Carlos Lopez-Montilla, Dr. Tapan Jain, Samir Pandey, Dr. Manoj Varshney, and Monica James. I would also like to thank all of my undergraduate student assistants, especially Adam Poniatowski, for their experimental contributions to this thesis.

I would also like to express my gratitude to Prof. Krister Holmberg for providing me with Gemini surfactant samples, and to the Engineering Research Center (ERC) for Particle Science and Technology at the University of Florida for sponsoring my research as well as for training me for my new career in industry. I also wish to thank ERC colleague Dr. Yakov Rabinovich for his help with the AFM measurements, as well as Dr. Joshua Adler, Dr. Pankaj Singh, Dr. Bahar Basim, Madhavan Esayanur, and Scott Brown

for their help with various aspects of my research and for very enlightening conversations.

Finally, but most importantly, my heartfelt gratitude goes to Elke Michalak, who has brought new meaning to my life, and to my parents, Anne-Marie and James Kanicky, to whom I owe everything.

TABLE OF CONTENTS

page

LIST OF TABLES

LIST OF FIGURES

Abstract of Dissertation Presented to the Graduate School
of the University of Florida in Partial Fulfillment of the
Requirements for the Degree of Doctor of Philosophy

IMPORTANCE OF MOLECULAR PACKING AT INTERFACES AS WELL AS IN PRE-MICELLAR AND MICELLAR AGGREGATES FOR CONTROLLING VARIOUS TECHNOLOGICAL PROCESSES

By

James Rene Kanicky

December 2002

Chair: Dinesh O. Shah
Major Department: Chemical Engineering

Molecular packing at interfaces and in micellar aggregates is investigated. Solutions of long-chain fatty acids and their soaps exhibit optimum behavior regarding foaming, contact angle, evaporation, surface viscosity, wetting, emulsification, solubilization, detergency, and dispersion stability when the pH of the solution is equal to the pKa of the fatty acid. The pKa of a fatty acid remains constant (at ~4.8) for chain lengths C_2–C_6, but increases with increasing chain length for C_8–C_{18}. The increase in pKa for C_8–C_{18} fatty acids can be attributed to increased molecular packing between soap molecules in the bulk solution and in the adsorbed film. Furthermore, upon mixing long-chain fatty acids of unequal chain lengths, pKa values decrease as compared with those of pure acids. This decrease is due to increased intermolecular distance caused by thermal motion of the unequal chains. pKa is also found to decrease upon increasing the degree of unsaturation in the chains as well as by dilution of fatty acid solutions below

the critical micelle concentration (cmc). Addition of small amounts of fatty acid to a micellar solution of dodecyltrimethylammonium bromide (C_{12}TAB) stabilizes the C_{12}TAB micelle both at low and high pH. Results indicate that even in nanomolar solutions of fatty acids, substantial molecular association exists in premicellar aggregates and in an adsorbed film.

The relaxation times of 12-s-12 quaternary ammonium bromide Gemini (or dimeric) surfactants have been shown to be much higher (seconds vs. milliseconds) than the stability of micelles of their monomeric surfactants (i.e. C_{12}TAB). The Gemini surfactants studied also have cmc values that are an order of magnitude lower than the cmc of C_{12}TAB. Finally, the Gemini surfactants studied have been shown to have very slow desorption rates as compared to single-chain surfactants.

The force-distance curves of 12-2-12 and 12-4-12 Gemini surfactants were correlated with AFM images in order to elucidate the mechanism by which these surfactants adsorb to the surface and the aggregation structures they form. Also, the strength of the adsorbed surfactant film on particles (i.e., the stability of the adsorbed layer) was correlated with the stability of dispersions.

CHAPTER 1
INTRODUCTION

1.1 Surfactants

Surfactants are surface-active agents that, when present at low concentration, have the property of adsorbing to the interface (gas/liquid, liquid/liquid or solid/liquid) of a two-phase system and decreasing the free energies of these interfaces. The ability of a surfactant molecule to adsorb at an interface arises from the physical structure of the molecule. A surfactant molecule is composed of a polar, hydrophilic "head" group attached to a hydrophobic "tail," usually an alkyl chain 8 to 20 carbons in length (Figure 1-1).

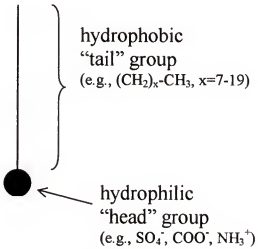

Figure 1-1. Schematic representation of a typical surfactant molecule.

The surface activity of a surfactant is derived from thermodynamic considerations of the minimum free energy locations for the molecules. When a surfactant molecule is placed in an aqueous solvent, the polar head of such a molecule interacts favorably with

the surrounding water molecules. The hydrophobic tail portion, however, exists in a high-energy condition caused by the tail's disruption of the surrounding hydrogen bonds connecting water molecules. The free energy of the entire system can be minimized when the surfactant molecule aligns itself at an interface with polar head facing towards the aqueous solution and hydrophobic tail facing away from the water. This leads to surfactant accumulation at the interface and a greater concentration of surfactant molecules at the interface than in either of the two bulk phases.

The adsorption of surfactant molecules at an interface is a dynamic process; that is, at a given moment in time, there are surfactant molecules adsorbing and desorbing from the interface, and a dynamic equilibrium exists between the surfactant molecules in the adsorbed film and those in the bulk. If the bulk surfactant concentration increases, then the surface concentration also increases. The rate of adsorption and desorption of a surfactant molecule depends on the driving force for adsorption and desorption as well as diffusion rate of the molecule.

Surfactants can be divided into two general types: ionic and nonionic. Ionic surfactants can be further categorized into cationic, anionic, and zwitterionic types, with the latter referring to a molecule that has both a positive and negative charge present on the head group. By far the most widely used surfactants are anionic surfactants . These surfactants have a negatively charged polar head counterbalanced by a cationic counterion. Anionic surfactants make up the majority of surfactants consumed in the world (Rosen, 1989). They have traditionally consisted of sodium salts of naturally occurring animal and plant fatty acids, and have been used for thousands of years for their stain-lifting and detergency characteristics. Other common anionic surfactants are

those synthesized from petrochemicals, and include alkyl sulfates and sulfonates (Miller and Neogi, 1985). Due to its solubility in water at low temperatures and low cost, sodium dodecyl sulfate (SDS) is the most common surfactant found in surfactant research literature.

Nonionic surfactants are the next most commonly used class of surfactant (Rosen, 1989). These surfactants include alcohols, polyoxyethylenated alkylphenols, and alcohol ethoxylates. An advantage of nonionic surfactants is that they are compatible with all other types of surfactants. They are also found as pure material without counterion electrolyte, and are soluble in both aqueous and hydrocarbon solvents. The major disadvantages of nonionics are that they cannot be made into a dry powder, they show an inverse solubility dependence on temperature (i.e., solubility decreases with increased temperature), and they become insoluble at a temperature called the 'cloud point', at which they come out of the aqueous phase and cause phase separation.

The third major class of surfactant is the cationic surfactant. These surfactants have a positively charged polar head group, allowing them to adsorb to most solid surfaces (which are usually negatively charged). As a result, they can change the characteristics of the substrate. This makes them efficient fabric softeners, dispersants, corrosion inhibitors, and antistatics and anticaking agents. Also, because they readily adsorb to and lyse cell membranes of microorganisms, they are often used as germicides and antiseptics. Cationic surfactants are generally more expensive and show less detergency than anionic surfactants. Typical cationic surfactants include long-chain amines, diamines, polyamines, and their salts, as well as quaternary ammonium salts and amine oxides (Rosen, 1978; Miller and Neogi, 1985).

Today, surfactants are among the most versatile performance products of the chemical industry, appearing in motor oils, detergents to clean laundry and homes, cosmetics, foods, oil recovery, pharmaceuticals, mineral flotation, and contact lenses (Rosen, 1989). Lately, basic research in the area of surfactants has turned to the so-called specialty surfactants. These include biodegradable, sugar-based surfactants (Holmberg 1998; von Rybinski and Stoll, 1997); fluorocarbon-based surfactants; zwitterionic surfactants; surface-active polyelectrolytes; and dimeric, or "Gemini" surfactants (Bernheim-Groswasser et al., 2000; In et al., 2000).

Specialized applications of surfactants are also being discovered. The past decade has seen the extension of surfactant applications to such high-technology areas as electronic printing, magnetic recording, enhanced filtration systems, medicine, biotechnology, and microelectronics (Holmberg, 1998).

1.2 Surfactant Adsorption

The adsorption of surfactant molecules at the air/water interface can be described by the Gibbs adsorption equation (Guggenheim and Adam, 1933; Adamson and Gast, 1997). As early as 1878, Gibbs (1931) derived a differential equation relating the surface tension, the number of moles and the chemical potentials of the components at the interface,

$$d\gamma = -\sum_i \Gamma_i d\mu_i \tag{1.1}$$

where $d\gamma$ is the change in interfacial tension of the solvent, Γ_i is the surface excess concentration of species i, which can be approximated by the number of moles per unit area, and $d\mu_i$ is the change in chemical potential of component i in the system. The Gibbs equation can be used to calculate the surfactant concentration of surfactant at the

interface and hence the area per molecule of the surfactant from the simple measurement of surface tension as a function of surfactant concentration (See Appendix 1 for a detailed description of how this is done). For dilute solutions of a nonionic surfactant or a 1:1 ionic surfactant in the presence of electrolyte, equation (1.1) can be written as (Adamson and Gast, 1997),

$$\Gamma = -\frac{1}{RT}\left(\frac{d\gamma}{d\ln C}\right)_T \tag{1.2}$$

where R is the gas constant, T the absolute temperature and C the concentration of surfactant. The surface excess concentration, Γ, can be obtained from the slope of a plot of the surface tension γ versus ln C at constant temperature, which then can be used for the calculation of the area per molecule a (in angstroms squared),

$$a = \frac{10^{20}}{N_{Avog}\Gamma} \tag{1.3}$$

where N_{avog} is Avogadro's number (~ 6.023 x 10^{23}) and Γ is the surface excess concentration of the surfactant. Further detail can be found in Appendix 1. A list of area per molecule values for a variety of surfactants and their counterions is given by Rosen (1989) and Oh and Shah (1993b).

The adsorption of surfactants at liquid-liquid and solid-liquid interfaces is very important in controlling large scale industrial processes such as dispersion stability in paints, detergency, water purification, oil recovery and ore flotation (Rosen, 1989; Adamson and Gast, 1997). Many studies have been undertaken over the last three decades to investigate the characteristics of aggregates formed by a surfactant on a solid surface or particle, using calorimetric studies, neutron-scattering, ellipsometry and the surface force apparatus developed by Israelachvili (1991). These techniques provide

quantitative information on the adsorption process little information on aggregate structure.

Much is known about structures of aggregates in bulk solution, leading to spherical or cylindrical micelles, bilayers and bicontinous phases in bulk solution. At interfaces however, the self-assembly process is influenced by additional surfactant-surface and solvent-surface interactions, including surface roughness, heterogeneity and charge behavior (Manne et al., 1994). Recently, the structure and shape of those adsorbed aggregates have been revealed by atomic force microscopy (AFM) (Manne and Gaub, 1995). The results suggest that the solid surface can alter the micellar structure of adsorbed aggregates. Other studies from UF and other groups indicate that dispersion stability can be modified by the strength of the adsorbed surfactant layer on the solid surface (Adler et al., 2000; Singh et al., 2001).

1.3 Micellization

Above a surfactant concentration known as the critical micelle concentration (cmc), surfactant monomers begin to aggregate into structures called micelles. When this occurs, the physical properties of surfactant solutions, such as surface tension, osmotic pressure, electrical conductivity and solubility (as a function of temperature), show an abrupt change in the neighborhood of the cmc. Therefore cmc can be determined from the discontinuity or inflection point in the plot of a physical property of the solution as a function of the surfactant concentration (Shinoda and Nakagawa, 1963; Mukerjee and Mysels, 1971). It is important to note that the free surfactant monomer concentration in the bulk solution remains constant above cmc because any newly added surfactant

immediately forms new micelles. Therefore the concentration profile in the system will follow the trend shown in Figure 1-2.

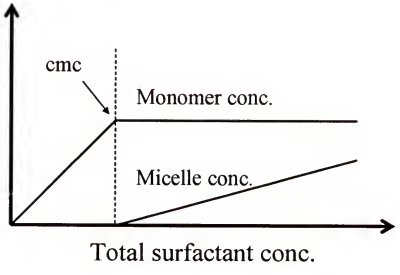

Figure 1-2. Effect of total surfactant concentration on the concentrations of species present in solution.

The unusual behavior of aggregation of fatty acid salts in dilute aqueous solution was first investigated by McBain (1913a,b; McBain and Salmon, 1920) in the 1910's and 20's, and later by Hartley (1936) in the 1930's. Other evidence for molecular aggregation was obtained from vapor pressure measurements and the solubility of organic material in the surfactant solutions. Colloidal-sized clusters of individual surfactant molecules in solution known as micelles are formed by the process known as micellization. Although first suggested by McBain (1913a), the earliest concrete model for spherical micelles is attributed to Hartley et al. (1936).

Figure 1-3 schematically shows the environments in which a surfactant can exist in aqueous solution. In a typical surfactant solution surfactant molecules disperse as monomers in the aqueous phase, form aggregates (micelles), and adsorb as a film at the air/liquid interface and at the solid/liquid interface of the container.

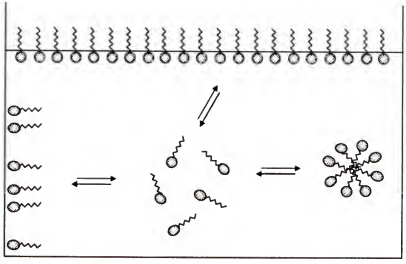

Figure 1-3. Schematic representation of the possible states in which a surfactant monomer can exist in water (free monomers, an adsorbed layer at the air/water or solid/water interface, and micelles).

The surfactant is in dynamic equilibrium between free monomers and each of the other states. Thus, at a given temperature, pressure and concentration, the number of monomers adsorbed at the air/water interface and the number of monomers and micelles present in solution are fixed under equilibrium conditions. The concentration of monomers and micelles changes with changes in equilibrium conditions such as pressure, temperature or surfactant and salt concentration.

Micellization above the cmc is a thermodynamically favored process that is primarily entropy driven (Hiemenz and Rajagopalan, 1997; Hunter, 1987). When surfactants are dissolved in water, the hydrophobic tails of the molecules are in a less favorable environment of hydrogen-bonded water. These tails therefore disrupt the matrix of hydrogen-bonded water molecules, resulting in an increase in the overall free energy of the system. At low concentrations, surfactant monomers adsorb individually at an interface, with the hydrophobic tails facing away from the water. However, when the surfactant concentration is increased to cmc, the diffusion length between individual

monomers in the bulk solution becomes short enough that aggregation begins to occur. Individual monomers associate with each other and begin to form aggregates which also serve to remove--or at least partially shield--the hydrophobic tails from the aqueous solution.

This scenario, however, is not favorable from the surfactant monomer's viewpoint. Several key forces arise that oppose the formation of micelles. A major one is the monomer's loss of possible conformations and range of motions. When the monomer is confined to the space of a tightly packed aggregate "cage," the energy of the system increases. Furthermore, because the molecules are so close together, they feel a great force from the normal phenomenon of diffusion that causes molecules to move from high concentration to a low concentration region. For ionic surfactants, another force is felt by the repulsion of head groups of similarly charged molecules within the micelle. These forces increase the free energy of the system and oppose micellization. Hence, micelle formation depends on the balance of forces between the factors favoring micellization (van der Waals and hydrophobic forces) and those opposing it (kinetic energy of the molecules and electrostatic repulsion). The explanation for the entropy-dominated association of surfactant molecules is called the "hydrophobic effect" or "hydrophobic bonding" (Tanford, 1980). The entropic increase due to greater freedom or conformation of water molecules is predominant over the energy decrease due to confinement of surfactant molecules in the micelle.

1.4 Structure of a Micelle

As mentioned above, a micelle is made up of a number of surfactant monomers that aggregate above the critical micelle concentration. The structure of a micelle has

been studied extensively. In the last few decades, the observation that surfactant association structures can mimic biological structures has sparked considerable interest in self-assembled surfactant aggregates such as cylindrical, lamellar and reverse micelles (Bergethon and Simons, 1990). The ability of micelles to catalyze reactions involving certain enzymes makes their investigation an interesting area of biomedical and detergent research (as enzymes are often added to laundry detergents to improve performance) (Gloxhuber and Kunstler, 1992; van Ee et al., 1997). Self-assembled structures such as micelles or reversed micelles (surfactant aggregates with hydrophilic head groups shielded from, and lipophilic tails sticking out to an organic solvent) also play an increasingly important role in catalysis and separation processes in engineering and environmental science and technology (Fendler, 1975; Myers, 1991; Gratzel and Kalyanasundaram, 1991).

The micellization process can be described by the reaction

$$nS \rightleftharpoons S_n \tag{1.4}$$

where S is a surfactant monomer and S_n is a micellar aggregate composed of n surfactant molecules. The so-called aggregation number n (which represents the number of surfactant molecules in a micelle) differs from one surfactant system to the next. It has, for example, been found to increase with increasing length of the hydrophobic group and decrease with increasing size of the hydrophilic group (Rosen, 1989). It is also affected to some degree by the number of counterions in solution and the surfactant concentration.

The factors that increase the aggregation number of a micelle also tend to decrease the cmc. For example, increasing the alkyl chain length of a surfactant decreases the cmc. The presence of electrolyte also decreases the cmc, due to charge shielding as

well as the so-called "salting out" effect (Rosen, 1989). The work required to accommodate a nonpolar solute in a given volume of water is increased in an electrolyte solution because of strong water-ion interactions. When surfactant monomers are "salted out" by the presence of electrolyte, micellization is favored and the cmc is decreased (Rosen, 1989).

Micelles tend to be regarded as spherical aggregates containing monomers with the polar head facing towards the aqueous medium and the hydrophobic tails pointed towards the center of the micelle. In reality, micelles most likely begin as loosely packed aggregates that have only a slight resemblance to a spherical object (Laughlin, 1994). As the surfactant concentration increases, the packing density of the micelles increases and a more spherical shape is approached. However, changes in temperature, surfactant concentration or additives in the solution may change the size, shape, aggregation number and stability of the micelles. The structure of a micelle could vary from spherical to rod-like to lamellar in shape (Figure 1-4). In concentrated solutions (much higher than the cmc), lamellar micelles form, such that water molecules occupy the region between parallel sheets of surfactants. Micelles may also form long cylinders packed together (known as lyotropic mesomorphs or liquid crystalline phases) at high surfactant concentrations (Miller and Neogi, 1985; Ekwall, 1967).

The shape of a micelle is also dependent upon the geometry of the individual monomers. In aqueous media, for example, surfactants with bulky or loosely packed hydrophilic groups and long, thin hydrophobic groups tend to form spherical micelles, while those with short, bulky hydrophobic groups and small, close packed hydrophilic

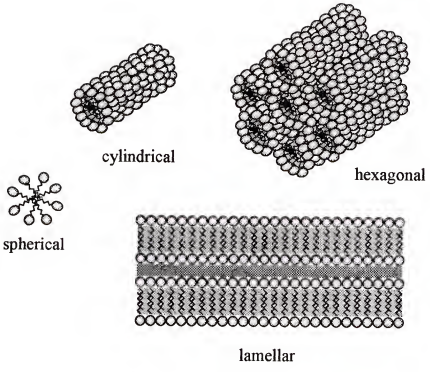

Figure 1-4. Several of the different types of micellar shapes encountered in a surfactant solution.

groups tend to form lamellar or cylindrical micelles. Molecular packing plays an important role in determining allowed micellar structures. The theory of micellar structure, based upon the geometry of various micellar shapes and the space occupied by the hydrophilic and hydrophobic groups of the surfactant molecules, has been developed by Israelachvili et al. (1976) and Mitchell and Ninham (1981). It was determined that a dimensionless group known as the packing parameter, P, can be used as an indicator of the shapes one can expect for the aggregate. The packing parameter is defined as

$$P = \frac{V}{a_h l_t} \tag{1.5}$$

where V is the hydrophobic chain volume, a_h the average surface area per surfactant head group, and l_t the critical chain length of the hydrocarbon tail.

The average surface area per surfactant head group, a_h, can be determined experimentally using surface tensiometry, or it can be estimated from interfacial free energy calculations (Hiemenz and Rajagopalan, 1997). The volume, V, and the critical chain length, l_t, of the hydrophobic chain are estimated from known geometric parameters such as volume of the micelle, aggregation number, as well as bond angles and lengths (e.g., the carbon-carbon bond in an alkyl chain has an angle of 109.5° and a length of 0.154 nm). Tanford (1980) has given the following expressions for l_t and V for saturated carbon chains of n carbon atoms:

$$l_t \leq l_{max} = (0.154 + 0.1265\, n) \text{ nm} \tag{1.6}$$

$$V = (27.4 + 26.9\, n) \times 10^{-3} \text{ nm}^3 \tag{1.7}$$

As shown in Figure 1-5, different packing parameters result in different micellar structures formed.

Packing parameter information can be used to predict the changes in structure of the aggregates as variables such as pH, charge, electrolyte concentration, and chain length of the tail are varied. For example, one can change the optimal head group area (a_h) by changing pH or electrolyte concentration in the case of ionic surfactants. One can also change the ratio (V/l_t) by increasing the number of alkyl chains, or introducing branches or unsaturation in the hydrocarbon chains (Hiemenz and Rajagopalan, 1997).

1.5 Dynamic Properties of Surfactant Solutions

The study of surfactant aggregation began in the 1910's, and the concept of micelles and a "critical micelle concentration" was put forth in the 1930's (McBain, 1913a; 1920; Hartley, 1936). However, at that time micelles were thought of as static and stable surfactant aggregates.

Packing Parameter, *P*	Surfactant Monomer Shape	Structure Formed
< 1/3		Spherical micelle
1/3 – 1/2		Cylindrical micelle
1/2 - 1		Vesicle
1		Bilayer (Lamellar phase)
> 1		Reverse (Inverse) micelle

Figure 1-5. Packing parameter and its relation to micelle structure.

It was not until more than 30 years later in the 1960's and 70's that researchers first discovered and observed the dynamic aspect of surfactant association and dissociation by various experimental methods such as pressure-jump (Mijnlieff and Ditmarsch, 1965), temperature-jump (Kresheck et al., 1966; Bennion et al., 1969; Bennion and Eyring, 1970; Lang and Eyring, 1972), concentration-jump (i.e., stopped-flow) (Lang et al., 1972; Yasunaga et al., 1973; Takeda et al., 1974), and ultrasonic relaxation studies (Yasunaga et al., 1967; Yasunaga et al., 1969; Zana and Lang, 1968a,b). Micelles are in dynamic equilibrium with individual surfactant molecules that are constantly being exchanged between the bulk and the micelles. Additionally, the micelles themselves are continuously disintegrating and reassembling. There are two relaxation processes involved in micellar solutions. The first one is a fast relaxation process referred to as τ_1 (generally on the order of microseconds), which is associated with the quick exchange of monomers between micelles and the surrounding bulk phase.

This process can be considered as the collision between surfactant monomers and micelles. The second relaxation time, τ_2 (of the order of milliseconds), is attributed to the micelle formation and dissolution process (i.e., the lifetime of the micelle). Figure 1-6 shows the two characteristic relaxation times, τ_1 and τ_2, associated with micellar solutions.

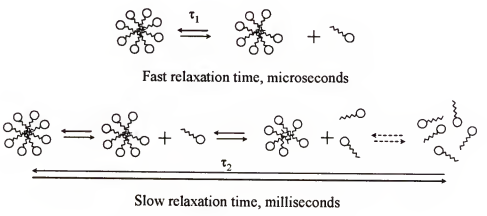

Figure 1-6. Mechanisms for the two relaxation times, τ_1 and τ_2, for a surfactant solution above cmc.

In 1965, Mijnlieff and Ditmarsch reported results on the rate of formation of sodium alkyl sulfate micelles in water studied by the pressure-jump technique. They did not at first distinguish between fast (τ_1) and slow (τ_2) relaxation times. This report was soon followed by temperature-jump (Kresheck et al., 1966; Bennion et al., 1969; Bennion and Eyring, 1970; Lang and Eyring, 1972), ultrasound (Yasunaga et al., 1967; Yasunaga et al., 1969; Zana and Lang, 1968a,b), and stopped-flow (Lang et al., 1972; Yasunaga et al., 1973; Takeda et al., 1974) studies on micelle association/dissociation kinetics. These studies showed that there are well-defined τ_1 and τ_2 values for each surfactant system, and that the time scale for τ_1 was on the order of microseconds while that of τ_2 was on the order of milliseconds.

1.5.1 Micelle Formation by Step-Wise Incorporation of Monomers

Experimental research on the kinetics of micellization reached its peak in the 1970's, from which point attention switched focus to analysis of the relaxation process in micellar solutions on the basis of stepwise formation and disintegration of micelles (Sams et al., 1972; Graber and Zana, 1970; Muller, 1972; Teubner et al., 1978). The primary breakthrough in this area was the discovery of the existence of two (fast and slow) relaxation processes (Lang et al., 1975; Yasunaga et al., 1967; Teubner et al., 1978) and the development of a model for the kinetic process of micelle formation and disintegration by Aniansson and coworkers (Aniansson and Wall, 1974; 1975; Aniansson et al., 1976).

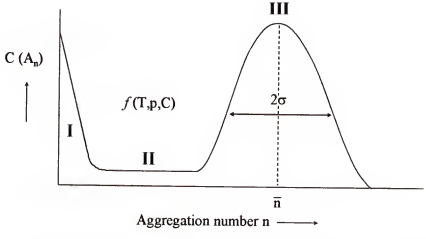

Figure 1-7. Typical size distribution curve of aggregates in a micellar solution according to the Aniannson-Wall model of step-wise micellar association. Region (I) corresponds to monomers and oligomers; Region (III) to abundant micelles with a Gaussian distribution around the mean aggregation number, $\bar{n}$; and Region (II) to the connecting "wire" (heat transfer analogy) or "tube" (mass transfer analogy) between Regions (I) and (III).

The first major assumption of this seminal work, which was derived for nonionic surfactants and later supplemented by Lessner et al. (1981) and Hall (1981) to include ionic surfactants, was that the free surfactant monomers are assumed to be completely

dissociated and the size distribution of the aggregates in a surfactant solution is assumed to have the shape schematically shown in Figure 1-7, where $C(A_n)$ denotes the total concentration of aggregates containing n monomers and is a function of temperature (T), pressure (p) and total surfactant concentration (C). Notice the existence of three distinct regions where one can find monomers and oligomers (Region I), proper micelles (Region III), and a narrow passage connecting monomers and micelles (Region II). In other words, only monomers and proper micelles are assumed to be present in the solution in significant quantities.

The second major assumption Aniansson and coworkers make is that the association and dissociation of micelles is a stepwise process involving the entry and departure of one monomer at a time from the micelle. Thus, there is a series of equilibria,

$$A_1 + A_{n-1} \underset{k_n^-}{\overset{k_n^+}{\rightleftharpoons}} A_n \qquad n = 2,3,4,... \tag{1.8}$$

where A_n denotes an aggregate containing n monomers, and k_n^+ and k_n^- are the forward and reverse rate constants for a given step, respectively. Therefore, when the equilibrium of a surfactant solution is perturbed (e.g., by temperature or pressure jump), the excess population has to move through regions of different aggregation numbers (Region II of Figure 1-7). According to Equation 1.8, this occurs in steps that are very small compared to the distance in aggregate space traveled. Therefore, the process will have the characteristics of a flowing system, which is important because it allows the abstract process of micelle aggregation kinetics to be studied in terms of the more familiar phenomena of heat or material flow.

The kinetic equation was put into a form first analogous with a heat conduction problem (Aniansson and Wall, 1974), and later (more appropriately) with a mass transfer

diffusion problem (Aniansson and Wall, 1975). Using this second analogy, the mechanism of micelle aggregation was likened to mass flow through a tube of variable width--two wide ends (Regions I and III in Figure 1-7) connected by an extremely narrow section (Region II in Figure 1-7). The diffusion of material through the narrow tube was considered to be the slow, rate-limiting step in the reaching of equilibrium between the two thick ends. Likewise, the extremely low concentration of transient intermediate submicellar aggregate states (Region II) that surfactant monomers must pass through (i.e., $A_2 \leftrightarrow A_3 \leftrightarrow A_4 \leftrightarrow \ldots \leftrightarrow A_{n-1}$ in Equation 1.8) when a micelle is formed from, or disintegrated into, free monomers is the rate-limiting step in the formation or disintegration of a micelle. Assuming the aggregation number n to be a continuous variable and applying the above analogy to mass transfer, Aniansson and coworkers derived the following expression for the fast relaxation process τ_1:

$$\frac{1}{\tau_1} = \frac{k^-}{\sigma^2}\left(1 + \frac{\sigma^2}{n}a\right), \qquad \text{with } a = \frac{C - CMC}{CMC} \tag{1.9}$$

where σ is the half-width of the distribution curve of micellar sizes (assumed to be Gaussian, Figure 1-7), k^- is the stepwise dissociation rate constant, which is assumed to be independent of n in the micellar region, C the total surfactant concentration and CMC the critical micelle concentration (cmc). Equation 1.9 predicts a linear relationship between $1/\tau_1$ and the total surfactant concentration, in agreement with pressure-jump and sound absorption experiments (Aniansson and Wall, 1975; Rassing et al., 1974). It is obvious that as the total surfactant concentration increases, so too does the number of micelles, resulting in a decrease in intermicellar distance. Hence, the time required for a monomer to collide with a micelle is shorter at higher surfactant concentration. The

magnitude of τ_1 depends on the length of the hydrocarbon tail of the surfactant--the shorter the chain length, the faster the relaxation time--since micelles composed of shorter chain surfactants are more loosely packed structures due to smaller van der Walls attractive forces and less hydrophobic effect.

Using the same analogy of diffusion through a tube as described above, an expression for slow relaxation time τ_2 was derived and simplified to

$$\frac{1}{\tau_2} = \frac{n^2}{CMC * R}\left(1 + \frac{\sigma^2}{n}a\right)^{-1} \tag{1.10}$$

where R is a term which may be visualized as the resistance to flow through the critical region (i.e., Region II in Figure 1-7) connecting the monomers to the micelles, and is given by

$$R = \sum_{n=n_1+1}^{n_2} \frac{1}{k_n^- A_n} \tag{1.11}$$

where n is the aggregation number of surfactant aggregate and A_n is the equilibrium concentration of aggregates, each aggregate having n molecules. The dependence of $1/\tau_2$ upon ionic strength, concentration and temperature has been interpreted in terms of their effect on R. Interestingly, the two relaxation times can be used to calculate two important parameters of a micellar solution: (1) the residence time of a surfactant molecule in a micelle, and (2) the average lifetime or stability of micelles (Attwood and Florence, 1983; Muller, 1979; Gormally et al., 1980; Lang and Zana, 1987). The residence time of a surfactant monomer in a micelle is equal to $\bar{n}/k^-$, where $\bar{n}$ is the mean aggregation number ($\bar{n}$ in Figure 1-7) and k^- the dissociation rate constant of a monomer from a micelle. The average micellar lifetime T_m is given by (Aniansson, 1985):

$$T_m = \tau_2 \frac{na}{1+\frac{\sigma^2}{n}a} \approx n\tau_2 \qquad (1.12)$$

When the concentration of surfactant is much greater than cmc, the micellar lifetime is approximately equal to $n\tau_2$. This implies that the larger the micelle or the greater the aggregation number (n), the longer the lifetime of the micelle, even if τ_2 is the same. However, it has been observed that for sodium dodecyl sulfate (SDS), the τ_2 increases by three to four orders of magnitude at 200 mM concentration, while the aggregation number changes insignificantly (Leung and Shah, 1986).

1.5.2 Micelle Association by Coagulation of Submicellar Aggregates Due to a Fusion-Fission Mechanism

Although first derived for nonionic surfactants, the results of Aniansson and Wall's theory on micellar aggregation kinetics were compared primarily with experiments on ionic systems, simply because it was much easier to detect the relaxation times in ionic systems than in nonionic systems. Even so, the agreement between theory and experiment was, in general, satisfactory in the regime of low surfactant concentrations (Aniansson et al., 1976). At higher concentrations, however, the theory did not match experimental results (Lessner et al., 1981). Equation 1.10 predicts that τ_2 should increase with concentration of a surfactant. However, it has been reported that for some ionic surfactant systems, τ_2 first increases, passes through a maximum, and then decreases again (Lang et al., 1975; Lessner et al., 1981; Innoue et al., 1980). This behavior in the slow relaxation process of ionic micelles is not predicted in the Aniannson-Wall model. Kahlweit and coworkers, using their own T-jump and p-jump results (Kahlweit and Teubner, 1980; Kahlweit, 1982; Herrmann and Kahlweit, 1980),

concluded that in ionic surfactant systems at high concentration, the reaction path for the formation of micelles must be different than that at low concentration. Therefore, the following model was proposed explaining the occurrence of a maximum in τ_2 (Figure 1-8):

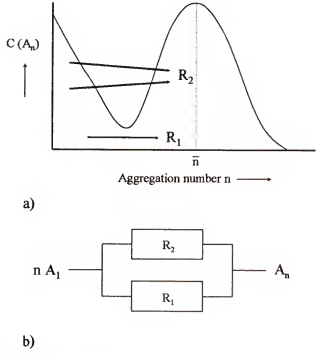

Figure 1-8. Schematic representation of the two possible reaction paths for the formation of micelles (a), and the corresponding resistances (b). (1) Formation by incorporation of monomers (Equation 1.8); (2) Formation by coagulation of submicellar aggregates (Equation 1.13).

Ionic micelles, including submicellar aggregates, can be considered charged particles. When ionic surfactant molecules such as SDS are added to water, the surfactant molecules dissociate into negatively charged dodecyl sulfate molecules and their positively charged counterions. These counterions are present in solution as a cloud surrounding the negatively charged micelle. At low surfactant counterion concentration, the micelles are stable with respect to coagulation due to repulsive electrostatic forces.

Consequently they can grow only by stepwise incorporation of monomers according to Equation 1.8 above.

As more and more surfactant is added into the system, the counterion concentration also increases, which compresses the electrical double layer and reduces charge repulsion, allowing the micelles to come closer to each other so that attractive dispersion forces (i.e., van der Waals forces) lead to a reversible fusion-fission coagulation according to

$$A_k + A_l \rightleftharpoons A_i \qquad k + l = i \tag{1.13}$$

where k and l are classes of submicellar aggregates.

Kahlweit (1982) then represented the micelle formation reaction path by two parallel resistors, R_1 and R_2 (Figure 1-8b) and compared the formation of micelles to the discharge of a capacitor through two parallel resistors (Halliday et al., 1993), so that the change in the monomer concentration with time was given by

$$\frac{-d \ln A_1}{d t} = \frac{1}{\tau_{21}} + \frac{1}{\tau_{22}} \tag{1.14}$$

where τ_{21} refers to the reaction path in Equation 1.8 and τ_{22} to the reaction path in Equation 1.13.

At low surfactant concentration, and hence at correspondingly low counterion concentration, R_2 (the resistance to coagulation of submicellar aggregates) is very high due to electrostatic repulsion between submicellar aggregates, so step-wise aggregation dominates and R_1 (the resistance to step-wise association, the same resistance term proposed by Aniansson and Wall in Equation 1.11) determines the rate of micelle formation. Equation 1.10 above can therefore be written as:

$$\frac{1}{\tau_{21}} = \frac{n^2}{CMC * R_1}\left(1+\frac{\sigma^2}{n}a\right)^{-1} \qquad (1.15)$$

which is identical to the Annianson and Wall model.

As the surfactant concentration is increased, the counterion concentration also increases. Thus, the resistance to coagulation of submicellar aggregates, R_2, decreases and ultimately becomes similar to the resistance to step-wise incorporation, R_1. The concentration where R_1 equals R_2 is the point where $1/\tau_2$ passes through a minimum and τ_2 is highest (for the SDS micelle, this occurs at 200 mM) (Lessner et al., 1981). If the counterion concentration is still further increased, R_2 becomes so low that coagulation of submicellar aggregates determines the rate of micelle formation according to the reaction mechanism in Equation 1.13:

$$\frac{1}{\tau_{22}} = \beta \;\; n \;\; a\left(1+\frac{\sigma^2}{n}a\right)^{-1}, \qquad \text{with } a = \frac{C-CMC}{CMC} \qquad (1.16)$$

where β is a measure for the mean dissociation rate constant in Equation 1.13 and is a function of counterion concentration. This result holds only at sufficiently high counterion concentration. A detailed explanation of β and its functionality with counterion concentration has been provided by Lessner et al. (1981). This theoretical development by Kahlweit and coworkers has helped to explain the existence of a maximum in τ_2 of ionic surfactants.

For ionic surfactant systems, the concept of one of two possible reaction pathways available depending on surfactant (and counterion) concentration does a good job of predicting and explaining the experimental maxima of slow relaxation times found in ionic surfactant micelles. The model also accurately predicts a shift of the maximum

τ_2 to lower surfactant concentrations by the addition of electrolyte and by the addition of nonionic amphiphiles such as alcohols (Lang et al., 1975; Lessner et al., 1981).

In the case of nonionic systems, electrostatic repulsion forces are absent, and both reaction paths compete right from the cmc on. Because of this, no pronounced maximum in τ_2 is ever encountered. Instead, the shape of the τ_2 versus concentration curve resembles that of an adsorption isotherm with an asymptotic increase to a maximum value and no decrease of τ_2 at higher concentrations (Lessner et al., 1981).

1.5.3 Computer Simulations of the Kinetics of Micelle Formation and Disintegration

Computer molecular simulations have recently been used to complement experimental studies and further our understanding of surfactant structure and aggregation behavior at a molecular level. The basic idea of computer simulation is that one may explicitly follow and statistically analyze the trajectory of a system involving many degrees of freedom in order to simulate the behavior of a real assembly of particles (Chandler, 1987). However, computer capacities, while growing, are finite. This implies that one may consider only a finite number of particles and a trajectory of finite length.

Two general classes of simulations exist: molecular dynamics and stochastic simulations. The most widely used molecular simulation technique presently in use is molecular dynamics (MD) simulation, in which forces derived from an assumed potential are used to generate phase space trajectories from which observable properties are calculated by using statistical thermodynamics principles (Frenkel and Smit, 1996).

Most MD simulations performed on micellar aggregation to date have focused on structure, shape, and size of micelles. More recently, however, there has been interest in

using MD to study the kinetics of micellar self-assembly (Tarek et al., 1998; Smit et al., 1991; Esselink et al., 1994; DeBolt and Kollman, 1995; Maillet et al., 1999; Wymore et al., 1999; Tieleman et al., 2000; Marrink et al., 2000). Smit and coworkers (1991) have used simplified models of surfactants and a Lennard-Jones solvent to examine micelle formation. Because micelle formation takes a long time (milliseconds) compared to atomic time scales, it requires great computational power to use fully atomistic MD models to reproduce such self-assembly. However, DeBold and Kollman (1995) were able to observe aggregation of alcohol molecules in an octanol-water system within a 2.0 nanosecond MD simulation. Nowadays, due to the increase in computer power and due to algorithmic advances, it has become possible to simulate the self-aggregation of surfactants using atomistic MD simulations. Maillet et al. (1999) simulated the self-aggregation of both short and long chain ionic surfactants, while others (Wymore et al., 1999; Tieleman et al., 2000; Marrink et al., 2000) have shown self-aggregation of dodecylphosphocholine (DPC) surfactant molecules in water into a single micelle, either spherical or worm-like, depending on surfactant concentration.

The main stochastic computer simulation technique is the Monte Carlo method. It is essentially a stochastic sampling experiment involving the generation of random numbers followed by a limited number of arithmetic and logical operations, which are often the same at each step. This method aims to generate a trajectory in phase space which samples from a chosen statistical ensemble. Several different variables, including chemical potential and number of molecules can be fixed while the positions and momenta of molecules can be followed over a series of steps to an equilibrium state (Allen and Tildesley, 1987).

Extensive studies of the equilibrium properties of surfactant systems using Monte Carlo simulations have been performed in the past (Care, 1987; Talsania et al., 1997; Nelson et al., 1997; Larson et al., 1985; Mackie et al., 1996). However, work on the dynamics of micellization is very limited (Haliloglu and Mattice, 1994; von Gottberg et al., 1998; Mavelli and Maestro, 1999; Mayer and Rasmussen, 2000; Wang et al., 1997). Recently there have been studies on the dynamic properties of micelles at equilibrium and of the micellization process (Haliloglu and Mattice, 1994; von Gottberg et al., 1998; Mavelli and Maestro, 1999; Mayer and Rasmussen, 2000). There have also been studies on the exchange kinetics between the bulk solution and a spherical absorbent (Wang et al., 1997). These studies have successfully demonstrated the process whereby a single monomer enters and exits an existing micelle, as well as the aggregation of many monomers to form a micelle, and the subsequent break-up of the micelle. However, because the time scales of micelle formation are so large compared to the picosecond time steps involved with molecular diffusion, there has been limited success in simulating micelle formation/breakup kinetics in real time.

1.6 Importance of Micellar Relaxation Time on Technological Processes

For many years, research in the area of micelle kinetics was purely academic. It was discovered early on that micelle break-up rate affects processes involving an increase in interfacial area (Mijnlieff and Ditmarsch, 1965). However, researchers were unable to correlate the micellar relaxation time, τ_2, with equilibrium properties of micellar solutions such as surface tension and surface viscosity. A surfactant's effectiveness at lowering surface tension, for example, in no way depends on the stability of micelles formed by the surfactant. However, for interfacial phenomena involving *the rapid formation* of

interfacial area, micelle stability *was* found to have an effect (Leung and Shah, 1986). A strong correlation of τ_2 with various dynamic processes such as foamability, textile wetting time, bubble volume, emulsion droplet size, and solubilization rate of benzene in micellar solutions was found by Shah and coworkers (Shah, 1998; Patist et al., 2000; Patist et al., 2002).

The mechanism by which micelle stability influences various dynamic interfacial phenomena is outlined below. Processes such as foaming, emulsification, and wetting depend on the stabilization of a newly created interface by surfactant monomers. So for example, when air is injected into a surfactant solution and a bubble begins to form, the newly created air/water interface must be stabilized by adsorption of surfactant molecules to keep the bubble from bursting. Free surfactant molecules from the bulk solution diffuse to and accumulate at the interface, thereby decreasing the free energy and hence the surface tension, and stabilizing the surface. If there is not sufficient concentration of monomers to stabilize the bubble, then it will burst.

If a large number of bubbles are created in a surfactant solution below the cmc, the free monomer concentration decreases over time as the existing monomers diffuse to the bubble interfaces to stabilize the foam. After the free monomers are used up, no more stable foam will be created and the foam height will level off. For a surfactant solution above cmc, any spent free monomers will in time be replaced by new monomers when the micelles break up. The key phrase in the previous sentence is "in time". If the micelles are weak and break up quickly, then the free monomer concentration in the bulk will continually be replenished by new monomers. This would lead to increased foaming and a larger foam volume. However, if the micelles are very stable and take a long time

to break up, then a scenario can exist where the free monomers in solution are depleted and there are no new monomers supplied to replace them. This would lead to a decreased foam volume. Thus, micelle stability can become the key rate-controlling parameter in processes where there is a rapid increase in interfacial area such as foaming or emulsification. Figure 1-9 shows schematically the importance of micelle break-up in foaming processes.

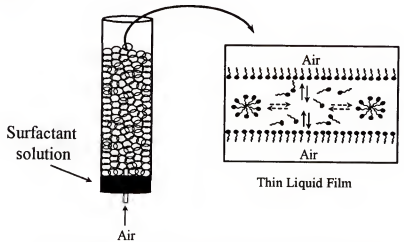

Figure 1-9. Schematic representation of adsorption of surfactant onto the newly created air/water interface due to disintegration of micelles during foam generation.

The micelle break-up process is also important in fabric wetting (Figure 1-10). When a piece of fabric (e.g. 1" x 1") is placed to float on top of a surfactant solution, the solution begins to penetrate the inter-fiber spaces of the fabric. The monomers deposit onto the hydrophobic sites of the surface and at the same time decrease the interfacial tension between the water and fabric as well as water and air. More stable micelles will cause less monomer flux to the fabric surface, which will slow down the wetting process and result in a longer wetting time.

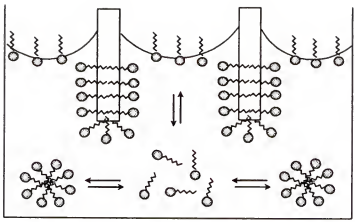

More stable micelles → Less monomer flux →
Slower wetting process (longer wetting time)

Figure 1-10. Schematic representation of adsorption of surfactant onto fabric due to disintegration of micelles during wetting.

A similar picture can be drawn for micelle break-up during emulsification processes (Figure 1-11). When mechanical energy is applied to increase the interfacial area between oil and water to produce oil droplets, the newly created interface must be stabilized by the adsorption of monomers from the aqueous phase. More stable micelles cause less monomer flux, which leads to a higher interfacial tension at the oil/water interface. The relationship between surface tension or interfacial tension and the amount of interfacial area created in foams or emulsions can be given by (Walstra, 1983):

$$W = \gamma \cdot \Delta A \tag{1.17}$$

where W is the work done, γ the surface or interfacial tension at the air/water or oil/water interface and ΔA the increase in interfacial area. If the work on a system is kept constant, a lower surface tension results in more interfacial area (either by decreasing the bubble size or by increasing foam volume). Thus, one would expect a larger emulsion droplet size when micelles are very stable.

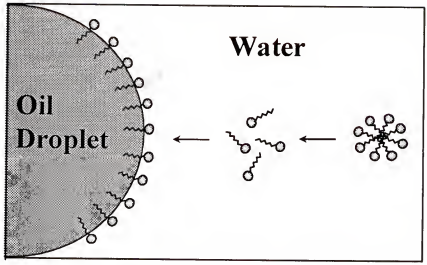

More stable micelles ⟶ Less monomer flux ⟶
Higher interfacial tension ⟶ Larger droplet size

Figure 1-11. Schematic diagram for the adsorption of surfactant monomers from the bulk to the oil/water interface during emulsification.

The micellar stability of sodium dodecyl sulfate (SDS) solutions was determined by Oh and Shah (1993) using pressure-jump with electrical conductivity detection. Figure 1-12 shows the micellar relaxation time τ_2 as function of SDS concentration. A maximum micellar stability was found at 200 mM (τ_2 = 5 sec), in agreement with previous observations (Lessner et al., 1981).

The maximum micellar stability at 200 mM SDS can be explained by the following proposed Intermicellar Coulombic Repulsion Model (ICRM) (Patist et al., 2002). Knowing the aggregation number of the SDS micelles and the total SDS concentration, one can calculate the number of micelles at a specific SDS concentration in the solution. By dividing the solution into identical cubes equal to the number of micelles, one can equate the distance between the centers of the adjacent cubes to the average intermicellar distance. By this approach, the intermicellar distance was found to

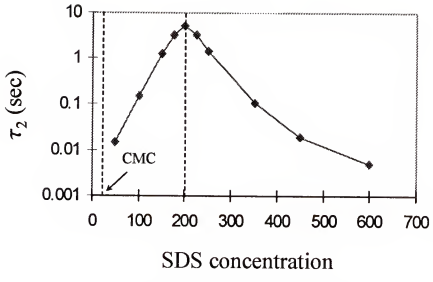

Figure 1-12. The slow relaxation time, τ_2, of SDS micelles at various surfactant concentrations.

be 130 Å, 100 Å, and 78.6 Å respectively at 50 mM, 100 mM and 200 mM SDS concentration. This suggests that the adjacent micelles are one diameter apart at 200 mM concentration. The small gap of about 40 Å between the surfaces of adjacent micelles causes Coulombic repulsion and hence induces a rapid uptake of counterions to minimize the charge repulsion between adjacent micelles. This provides considerable stability to the micellar structure, resulting in a long relaxation time. Above 250 mM SDS concentration, a structural transition from spherical to cylindrical SDS micelles occurs. However, this structural transition is gradual and hence in this concentration range (250 to 400 mM) the solution consists of a mixture of spherical and cylindrical micelles (Ekwall, 1967; Reiss-Husson, 1964). Since the number of spherical micelles is less as compared to that at 200 mM concentration, as some of them have become cylindrical micelles, the distance between spherical micelles increases, which leads to shorter relaxation times. In a binary mixture, it is the most labile structure (i.e., spherical micelles) which responds quickly as compared to cylindrical micelles to the change in

pressure in the pressure-jump studies (Huibers et al., 1996). The intermicellar distances obtained from the procedure at various SDS concentrations are shown in Figure 1-13. This model also explains the shift of the maximum micellar stability to lower concentrations of SDS by the addition of salt or cosurfactants (Lessner et al., 1981b).

In summary, SDS solutions exhibit maxima and minima for various properties at 200 mM concentration due to maximum stability of SDS micelles at this concentration. Most ionic surfactants may exhibit such a characteristic concentration at which the micellar stability will be maximum due to an increase in Coulombic repulsion and reduction in intermicellar distance.

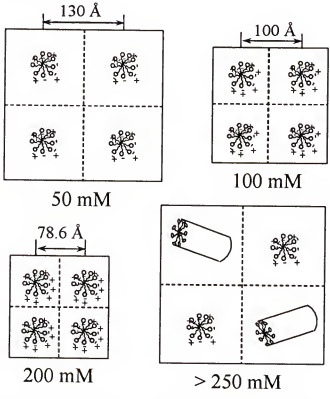

Figure 1-13. Schematic diagrams showing micellar packing at 50, 100, 200 and 250 mM SDS concentration.

Figure 1-14 presents the various phenomena exhibiting minima and maxima at the liquid/gas interface as a function of SDS concentration. At 200 mM SDS, minimum

foamability, maximum single film stability, maximum single bubble volume and a minimum frequency of bubble generation were found. These phenomena were explained based upon the monomer flux to newly created interfaces. If the micelles in solution are very stable, they cannot provide monomers quickly enough to the interface and thus the interfacial tension remains higher. Therefore, lower foamability, larger single bubble foam volumes and a minimum frequency of bubble generation were found (Oh and Shah, 1991; Oh et al., 1992). Very unstable micelles, however, provide monomers quickly enough to the surface to reduce the interfacial tension. Maximum single film stability was found at 200 mM, when the micelles are most stable (Patel et al., 1996). An important factor influencing single film stability is the arrangement of micelles inside the thin liquid film, which has been investigated by Wasan and coworkers (Nikolov and Wasan, 1989; Nikolov et al., 1989). The stratification of thin liquid films can be explained as a layer by layer thinning of ordered structures of micelles inside the film. This structured phenomenon is affected by micellar effective volume fraction, their stability, interaction and polydispersity. Therefore, the results from this study indicate that very stable micelles contribute to the stability of thin liquid films, by stabilizing layers of micelles.

Interfacial phenomena occurring at the liquid/liquid and solid/liquid interface in SDS solutions are shown in Figure 1-15. The wetting time and droplet size in emulsions exhibit maxima at 200 mM. The wetting time is the time during which the fabric floats on a surfactant solution before it actually sinks into the solution. During this time, water penetrates into the fabric structure to replace the air until the gravitational force exceeds the buoyancy of the entrapped air.

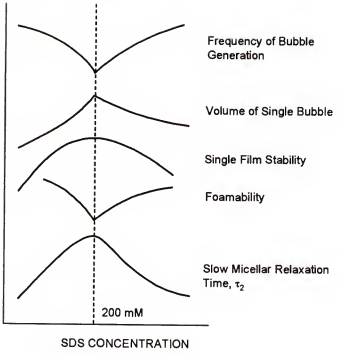

Figure 1-14. Liquid/gas interfacial phenomena exhibiting minima and maxima at 200 mM SDS concentration.

When micelles are very stable, the flux of monomers decreases and hence the wetting process slows down. Different types of fabrics, such as polyesters, Dacron, Nylon, cotton and silk were investigated. The maximum wetting time of the investigated fabrics occurs at 200 mM SDS concentration. Although the absolute magnitude of the wetting time depends on the fabric, the maximum which always occurred at 200 mM, is a property of the SDS solution and not of the fabric.

The liquid/liquid and solid/liquid phenomena can also be explained based upon the monomer flux necessary to stabilize a newly created interface. Very stable micelles result in high dynamic surface tensions and hence larger droplet sizes and longer wetting times are obtained (Oh et al., 1993; Oh and Shah, 1992). The solubilization rate of benzene in SDS solutions as well as the detergency or removal of orange OT dye from the surface of a fabric show maxima at 200 mM concentration. The time required to

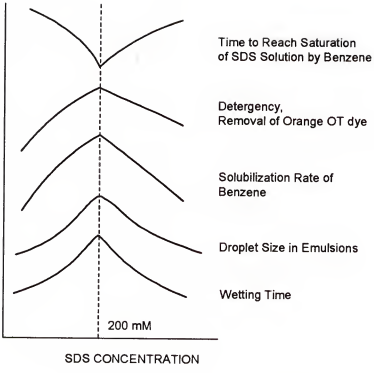

Figure 1-15. Liquid/liquid and solid/liquid interfacial phenomena exhibiting minima and maxima at 200 mM SDS concentration.

reach saturation of the SDS solution upon the addition of benzene is minimum at 200 mM SDS concentration. This suggests that very stable micelles (i.e., tightly packed micelles) are more effective in the solubilization of oil (Oh and Shah, 1993). This can be explained by examining the interior of the micelles. The interior of rigid (i.e., tightly packed) micelles is more hydrophobic as compared to that of loosely packed micelles, and hence the stronger hydrophobic core causes more rapid partitioning or solubilization of benzene and Orange OT dye into the micelles at 200 mM SDS concentration.

1.7 Long-Chain Fatty Acids and Soaps

Vegetable oils and animal fats have been used to make soaps--salts of long chain fatty acids--since ancient times. The saponification process, which once involved the boiling of oils and fats with caustic wood ashes, has since evolved into a very important

global industry. The majority of surfactants used in the world today are still derived from natural ingredients and a chemical reaction over two millennia old (Rosen, 1989). However, most higher fatty acids were not known until the beginning of the nineteenth century, when it was found that both odd and even numbered alkanoic acids of molecular formula $C_nH_{2n}O_2$ occur naturally. Since this time, hundreds of long-chain fatty acids have been isolated from natural sources and characterized (Pryde, 1979).

1.7.1 Physical and Chemical Properties of Fatty Acids

Fatty acids, which are so called because they have traditionally been produced from plant and animal fats, are composed of a carboxylic acid head group attached to an alkyl chain. As mentioned above, the general formula for a fatty acid is $C_nH_{2n}O_2$. The alkyl chain length can vary significantly. However, we will limit our interest to the series of acids with chain lengths of $C_2 - C_{18}$. Table 1-1 shows the basic properties of these selected fatty acids.

As can be seen in Table 1-1, melting and boiling points for carboxylic acids vary widely depending on the molecular weight, structure, and the presence of unsaturation in the alkyl chain. Acetic, propionic, and butyric acids are miscible with water at room temperature. Solubility in water decreases rapidly for the higher alkanoic acids as the chain length increases (Pryde, 1979). The melting points of these saturated fatty acids increase from C_8 to C_{18}. The hydrophilic nature of the carboxylic acid group balanced against the hydrophobic nature of the alkyl chain makes fatty acids of chain length above C_6 surface active. Above approximately C_{18}, the solubility of the fatty acid in water is so small that virtually none of the acid is found in bulk aqueous solution. Therefore, only fatty acids in the range $C_8 - C_{18}$ are useful as surfactants.

Table 1-1. Physical properties of selected fatty acids.

Systematic name (common name)	# of Carbon Atoms and Degree of Saturation	Molecular Weight	Melting Point Temp. (°C)	Boiling Point Temp[a] (°C)
Ethanoic (acetic)	2:0	60.05	16.6	118.1
Propanoic (propionic)	3:0	74.08	-22	141.1
Butanoic (butyric)	4:0	88.11	-7.9	163.5
Pentanoic (valeric)	5:0	102.13	-34.5	187.0
Hexanoic (caproic)	6:0	116.16	-3.4	205.8
Octanoic (caprylic)	8:0	144.21	16.7	239.7
Decanoic (capric)	10:0	172.27	31.6	270.0
Dodecanoic (lauric)	12:0	200.32	44.2	298.9
Tetradecanoic (myristic)	14:0	228.38	53.9	326.2
Hexadedanoic (palmitic)	16:0	256.43	63.1	351.5
Octadecanoic (stearic)	18:0	284.48	69.6	376.1
trans-9-Octadecenoic (elaidic)	18:1;*(trans)*9	282.47	43.7	234[b]
cis-9-Octadecenoic (oleic)	18:1;*(cis)*9	282.47	13.6	234[b]
cis,cis-9,12-Octadecadienoic (linoleic)	18:2;*(cis)*9,12	280.45	-5	202[c]
cis,cis,cis-9,12,15-Octadecatrienoic (α-linolenic)	18:3;*(cis)*9,12,15	278.44	-11 - -10	157[d]

[a] At 101.3 kPa = 1 atm unless otherwise noted.
[b] At 15 kPa = 113 mm Hg.
[c] At 1.4 mm Hg.
[d] At 0.001 mm Hg.

The hydrocarbon chain and carboxylic acid group of fatty acids undergo the usual reactions. Reactions in the carboxyl group include salt and acid chloride formation, esterification, pyrolysis, reduction, and amide, nitrile, and amine formation (Fox and Whitesell, 1994).

Salt formation occurs when the carboxylic acid reacts with an alkaline substance (Levy, 1968), in the reaction

$$RCOOH + MOH \rightarrow RCOO^{-}M^{+} + H_2O \quad (1.18)$$

where M = Li, Na, K, NH_4, R_3HN, etc. The alkaline substance can also be an oxide, hydroxide, or carbonate of a metal of higher valence such as Ca, Mg, Zn, or Al. Water-soluble soaps are generally produced by the above hyrolysis (i.e., saponification) process.

1.7.2 Associative Interactions in Soap Solutions

A fundamental characteristic of all surfactant species is their amphiphilic nature, which allows them to adsorb to and accumulate at an interface. The same surface activity of these molecules that gives rise to their adsorption properties also causes them to interact with each other in the bulk solution to minimize the interaction between water and the hydrophobic tails. As described above, micellization is known to take place above a critical surfactant concentration. This phenomenon has been a topic of research for many decades. However, micelles are not the only types of aggregates that are formed in solution. There has also been interest in the formation of lower molecular weight aggregates and, in particular, dimers. McBain (1913b; McBain and Stewart, 1927), Ekwall (1940; Ekwall and Lindblad, 1941), Ananthapadmanabhan (1980), and others have studied the existence of premicellar aggregates. Supporting evidence for the existence of premicellar aggregates has come from a number of studies such as that of specific conductivity (Mukerjee, 1958a; Mukerjee and Mysels, 1958), transport number (Mukerjee, 1958b), molar volume (Franks et al., 1968), osmotic coefficient (Bangs, 1964), pH-hydrolysis behavior (Ekwall, 1940; Ekwall and Lindblad, 1941; Cook, 1951; Eagland and Franks, 1965; Lucassen, 1966) and partitioning of surfactant between and organic and aqueous phase (Mukerjee, 1965).

Fatty acids are weakly ionizable surfactants that demonstrate a very complex range of premicellar associative interactions. In fact, a large number of different species in chemical equilibria exist in a fatty acid solution. The typical equilibrium chemical reactions between these species are listed below:

$$RH \rightleftharpoons R^- + H^+ \qquad K_a \qquad (1.19)$$

$$RH + R^- \rightleftharpoons R_2H^- \qquad K_{as} \qquad (1.20)$$

$$R_2H^- \rightleftharpoons H^+ + R_2^{2-} \qquad K_d \qquad (1.21)$$

$$2RH + R_2^{2-} \rightleftharpoons (R_2H^-)_2 \qquad K_{as2} \qquad (1.22)$$

where RH is the fatty acid, R^- is the carboxylate anion, R_2H^- is the "acid soap," R_2^{2-} is the dimer, and $(R_2H^-)_2$ is a larger oligomer. K_a is the equilibrium constant of acid dissociation. K_{as} is the equilibrium constant of acid soap formation. K_d is the equilibrium constant for dimer formation, and K_{as2} is the equilibrium constant for formation of a larger oligomer. From the above equilibrium reactions, we see that a fatty acid molecule dissolved in water can ionize (Equation 1.19) or undergo any number of changes. Equation 1.20 indicates that the fatty acid can immediately interact with an ionized fatty acid molecule to form the so-called "acid soap" with an equilibrium constant of K_{as}. Also, fatty acids and acid soaps can undergo a reaction to become dimers. The prevailing species in solution depends on the driving force for ionization, which is a function of the solution pH. Figure 1-16 below shows the probable state of fatty acid versus pH in the sub-micellar solution.

At acidic pH values the predominant molecule is the undissociated fatty acid (RH). At alkaline pH, mainly carboxylate anions (R^-) and to a lesser extent ionic dimers (R_2^{2-}) are present, although the acid soap salt, R_2HNa, is also found in extremely alkaline

solutions or if sufficient Na^+ ions are added (Mysels, 1959). At pH 4 to 8, acids, anions, as well as so-called acid-soaps, $(RCOO)_2H^-$, all coexist in the aqueous bulk solution (Small, 1986).

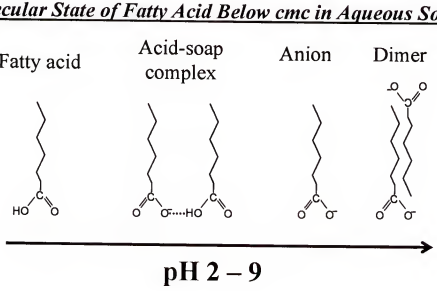

Figure 1-16. Molecular state of fatty acid below cmc in aqueous solution.

Extensive studies by McBain (McBain and McHan, 1948), Ekwall (1940; Ekwall and Lindblad, 1941), Jung (1976), and Ananthapadmanabhan (1980) have provided evidence for the existence of acid-soaps in a number of systems including myristate, palmitate, and oleate. Furthermore, these investigators have developed equilibrium species distribution diagrams of several fatty acids after careful research on their chemical equilibria.

1.7.3 Chemical Equilibria in Soap Solutions

As mentioned above, the number of different types of chemical species in a soap solution is quite large. Furthermore, the concentration of each species in solution is strongly dependent on the pH of the solution. For this reason, species distribution diagrams must be computed for each system of interest in order to keep track of the

species present at a particular pH. These species diagrams are computed using thermodynamic data such as estimates for energy of interaction between molecules, as well as solubility and acidity constants (K_a, K_{as}, K_d, K_{as2} in Equations 1.19 – 1.22). Unfortunately, values for these thermodynamic constants tend to vary from system to system and from one investigator to the next. For example, the energy of hydrogen bonding has been reported to vary from 0.5 to 6 Kcal/mole (Ananthapadmanabhan, 1980), making it difficult to choose any specific value for this constant.

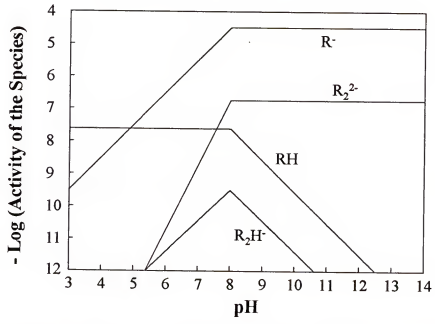

Figure 1-17. Species distribution of potassium oleate (3×10^{-5} M) as a function of pH (Ananthapadmanabhan, 1980).

The above problems notwithstanding, it is possible to create a species distribution diagram for a system in order to study in general terms the effect of pH on the fatty acid. Figure 1-17 is such a diagram for potassium oleate drawn by Ananthapadmanabhan (1980) with thermodynamic constants computed by Bangs (1964). As can be seen here, at any given pH, at least two or more species exist in a significant concentration. At low pH, for example, the protonated fatty acid, RH, and to a lesser extent the ion, R^-, are

active. At very high pH, the R^- and R_2^{2-} species, as well as the R_2HNa species (not shown in Figure 1-17, but described above) are active. At pH around 8, the activity of the acid-soap, R_2H^-, is at a maximum. While in Bangs' estimate this activity is lower than that of the other species present, other research has indicated that the acid-soap may actually play a large role with respect to surface activity within this system. Species distribution diagrams based upon different thermodynamic data show the activity of R_2H^- to be much higher than in Figure 1-17 (Mukerjee, 1965; Jung, 1976; Ananthapadmanabhan, 1980). Figure 1-18, for example, shows the species distribution based upon Ananthapadmanabhan's estimate of the thermodynamic constants.

While estimates of the activity of acid-soap in a fatty acid solution vary from one investigator to the next, it has nonetheless been shown that this molecule plays a very important role in the mineral floatation industry (Jung, 1976; Ananthapadmanabhan, 1980). Past research conducted in the area of fatty acid surface activity and aggregation behavior has been applied extensively to floatation (Somasundaran and Moudgil, 1988). Fatty acid salts, especially oleate, are used as selectively adsorbing surfactants (i.e., collectors) in mineral floatation. Collection efficiency of oxide minerals such as hematite with weakly anionic collectors such as oleic acid has been shown to have a distinct maximum at pH around 8.0.

From the application of the above equilibrium species distribution diagrams and the knowledge that not all of the possible species are present in significant quantities at any given pH, a hypothesis was developed to explain the reason for maximum floatation of hematite by oleate at pH 8.0. Oleate anion and dimer activities do not change appreciably when decreasing pH from the alkaline to the neutral region. However, the

activities of undissociated acid and acid-soap complexes do increase significantly, leading to increased oleate surface activity and, hence, greater floatation of hematite and lower surface tension at the air/water interface.

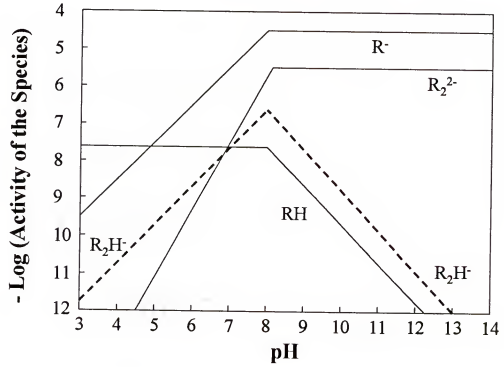

Figure 1-18. Species distribution of potassium oleate (3×10^{-5} M) as a function of pH using different estimates of thermodynamic constants than in Figure 1-17 (Ananthapadmanabhan, 1980). The R_2H^- curve is a dashed line.

If pH is further decreased to the acidic region, the activities of the ionic monomers, dimers, and acid-soap complexes decrease while that of the undissociated acid remains the same. This results in a decrease in hematite floatation and an increase in surface tension. Therefore, the maximum in hematite floatation and minimum in surface tension are encountered in the neutral pH range where the greatest number of surface active species exists (DeCastro, 1995).

1.8 Rationale of the Proposed Research

From the previous section, it is clear that fatty acids are an important class of surfactant with very complex behavior in aqueous solutions. Like other surfactants, fatty acids form spherical, cylindrical, and lamellar micelles at different concentrations, as well as adsorb at the air/liquid, liquid/liquid, and solid/liquid interfaces. Fatty acids, unlike other surfactants, are also very much affected by solution pH. As was shown in Section 1.7, the fatty acid molecular species distribution is the key factor in determining surface activity, which has led to applications of fatty acids in the mineral floatation industry, a direct application of the solid/liquid adsorption properties of soaps.

The purpose of this dissertation is twofold. The first is to study the molecular interactions between fatty acids and soap molecules in order to apply the principles outlined in Section 1.7 to phenomena involving air/liquid, liquid/liquid, as well as other solid/liquid interfacial phenomena, and to extend the technological applications of fatty acids in these areas--in essence, to extend the application of fatty acids as surfactants beyond the solid/liquid adsorption realm of mineral floatation.

The second purpose of this project is to elucidate the connection between molecular mechanisms of adsorption and molecular packing at interfaces and in micelles of fatty acid soaps and other surfactants, and to study the consequent effect on macroscopic interfacial phenomena such as foaming, contact angle, evaporation, surface viscosity, wetting, emulsification, solubilization, detergency, and dispersion stability. This is in fact a continuation of Professor Shah's ongoing project to study the mechanisms by which micelles form and break, and to determine the factors influencing micellar stability--the ultimate goal of this project being the ability to tailor the lifetime of

a micelle for application to various interfacial phenomena. Figure 1-19 illustrates how the principles of micelle kinetics can be combined with fatty acid adsorption studies in order to tailor the kinetics of a micelle.

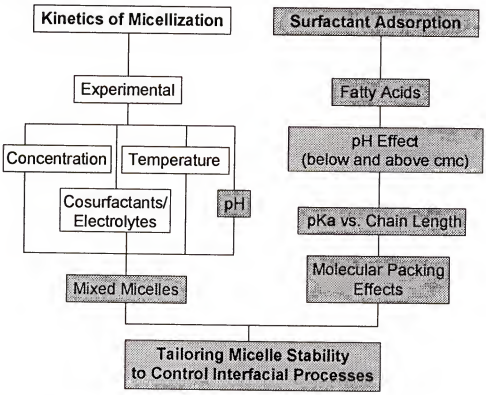

Figure 1-19. Flowchart illustrating how principles of micelle kinetics can be combined with fatty acid adsorption studies in order to tailor the kinetics of a micelle. Gray-filled boxes indicate the scope of this dissertation.

Long-chain fatty acids have the unique property among simple surfactant systems of being very sensitive to solution pH. Chapter 2 shows how bulk solution pH affects the adsorption of fatty acids to an air/liquid or liquid/liquid interface. This chapter further illustrates how fatty acid solution pH can be tailored to optimize performance of various interfacial phenomena.

In Chapter 3, the effect of chain length on the observed pKa of a fatty acid molecule is shown. Furthermore, the performance of mixed chain length fatty acids is

compared to that of pure solutions. Finally, the effect of unsaturation in the fatty acid alkyl chain on pKa is investigated.

In Chapter 4, the effect of surfactant concentration on fatty acid pKa is explored. This leads to a discussion of the probability of premicellar aggregation occurring at very low fatty acid concentrations. Finally, the self-interaction behavior of long-chain fatty acids is compared to that of their short-chain cousins.

Chapter 5 extends the study of micellar kinetics to the realm of mixed surfactant micelles. Specifically, the influence of solution pH on micelle stability will be investigated. Also, the possibility of creating mixed micelles containing fatty acids will be explored. This should give valuable insight to the forces controlling micelle formation, as well as provide an added means of designing or tailoring a surfactant solution with a micelle stability specific to the requirements of a given process. Chapter 5 also describes research on a new type of surfactant called Gemini (or dimeric) surfactants, which show interesting adsorption, desorption, and aggregation properties. This research leads to Chapter 6, which is a study of the ability of Gemini surfactants to adsorb to the surface of particles and stabilize a dispersion of such particles in water by creating a repulsive barrier when the two particles approach each other.

Chapter 7 then summarizes the conclusions of this dissertation and the scope of the future extension of these studies.

CHAPTER 2
DETERMINATION OF FATTY ACID pH FOR OPTIMAL PERFORMANCE IN VARIOUS INTERFACIAL PHENOMENA

2.1 Introduction

The manner in which surfactant molecules align at an interface is an important factor in systems involving interfacial films. Among the important properties of a surfactant that dictate the strength, elasticity, and stability of a surface film are chain length compatibility (Shiao et al., 1998), the distance between molecules in the monolayer (Shiao et al., 1997), and surface activity. The presence of a net charge on a surfactant polar group affects its surface activity. Fatty acids, for instance, can become ionized by an increase in the pH of the solution. If all the fatty acid molecules become ionized, repulsion between similarly charged molecules in the monolayer can result in an expansion of the monolayer at high pH (Adam, 1921; Adam and Miller, 1933), which in turn can lead to a weak and unstable film. However, this expansion upon ionization depends upon the chain length. The greater the chain length, the less the expansion in area/molecule due to ionization of carboxyl groups. The change in monolayer characteristics of fatty acids as a function of pH of the bulk solution was first reported by Schulman and Hughes (1932), who found that the surface potential (ΔV)-pH relation resembled an acid-base titration curve. For weakly ionized monolayers such as those created by fatty acids, it was proposed that the difference in pKa between the surface and the bulk is small (Davies and Rideal, 1961). This suggests that one may calculate surface properties, including surface pH, using the normal bulk value of pKa. However, the

present paper reports that pKa of soap depends on the chain length of the soap molecule, and can be as high as about 9.0 as the chain length increases to C_{16}.

Most short-chain carboxylic acids have a pKa value of *ca.* 4.8. For example, when acetic acid (CH_3COOH) and propionic acid (CH_3CH_2COOH) are dissolved in water, their pKa values are found to be 4.74 and 4.87, respectively (Budavari, 1996). The pKa value represents the ionic environment of the solution where 50% of hydrogen atoms are removed from the carboxyl group by the existing OH^- ions in the solution. The pKa can be decreased by attaching an electron-accepting substituent to stabilize the carboxylate anion (Sutherland, 1979). Note in Table 2-1 the drop in pKa when a chlorine atom substitutes for a hydrogen, or when the chain becomes unsaturated.

The converse effect--that of electron-releasing substituents lowering the acidity and raising the pKa--is true, though less dramatic. The pKa can be raised by increasing the carbon chain length of the carboxylic acid. However, because electronic effects are not felt beyond 2-3 carbons, when the chain length is increased beyond about four carbons, the pKa tends to level off. Increasing the chain length from pentanoic to hexanoic acid, for example, increases the pKa from 4.82 to 4.83. Therefore, we know that *intra*molecular interactions (i.e., the effects on the carboxylate anion by the rest of the carbon chain) become negligible beyond four carbons in the alkyl chain.

The present chapter attempts to explain various pKa-related phenomena and elucidate their technological applications (e.g., foamability, foam stability, retardation of water evaporation, contact angle on PMMA, surface viscosity, and single-bubble stability) as a function of the pH of the soap solution.

Table 2-1. pKa values of selected carboxylic acids*

Name	Formula	pK_a^{25oC}
Formic (methanoic)	HCOOH	3.75
Acetic (ethanoic)	CH_3COOH	4.75
Chloroacetic (chloroethanoic)	$ClCH_2COOH$	2.85
Dichloroacetic (dichloroethanoic)	$Cl_2CHCOOH$	1.48
Trichloroacetic (trichloroethanoic)	Cl_3CCOOH	0.7
Propionic (propanoic)	CH_3CH_2COOH	4.87
3-Chloropropanoic	$ClCH_2CH_2COOH$	3.98
Acrylic (propenoic)	CH_2=CHCOOH	4.25
Propiolic (propynoic)	CH≡CCOOH	1.84
Butyric (butanoic)	$CH_3CH_2CH_2COOH$	4.81
Crotonic ((E)-but-2-enoic)	CH_3CH=CHCOOH	4.69
But-2-ynoic	CH_3C≡CCOOH	2.59

*Sutherland, 1979.

2.2 Materials and Methods

Materials. Sodium caprylate (C_8), sodium decanoate (C_{10}), sodium laurate (C_{12}), sodium myristate (C_{14}), and sodium palmitate (C_{16}) were supplied by Sigma Chemical Company (St. Louis, MO) and were of 99% purity. Sodium phosphate (monobasic and dibasic), concentrated sodium hydroxide, light mineral oil, and anhydrous calcium chloride were supplied by Fisher Scientific (Fair Lawn, NJ). All solutions were prepared using water that was both deionized and distilled. All experiments were carried out at 23 ± 1 °C unless otherwise stated.

Solution preparation. Monobasic and dibasic sodium phosphate were used to prepare 0.02 M phosphate buffer solutions (Dawson, 1959). 0.05 wt% phosphate-buffered fatty acid solutions were prepared by dissolving 0.5 g of fatty acid in water and adding phosphate buffer to adjust the solution to 100 mL of a desired starting pH. pH was monitored with an Orion (model 720A) pH meter and adjusted with sodium hydroxide.

Equilibrium Surface tension and area/molecule. Surface tension measurements were obtained from freshly prepared solutions by the Wilhelmy plate method, whereby a 2.54 cm x 1 cm platinum blade is dipped into the solution and the force exerted on the blade by the solution is measured and translated to surface tension. Before each measurement, the platinum plate was cleaned by heating it to a red/orange color with a Bunsen burner. Area/molecule was calculated using the Gibbs adsorption equation (see Appendix A):

$$\Gamma = \frac{-1}{2.3RT}\left(\frac{d\gamma}{d\log C}\right) \qquad (2.1)$$

where Γ is the surface concentration of surfactant (mol/cm^2), γ is the surface tension (mN/m), and C is the bulk concentration of surfactant in the solution (mol/L). The area/molecule at the air/water interface is given by 1/Γ. The slope can be obtained from surface tension measurements plotted against $\log_{10}$C.

Dynamic surface tension. The maximum bubble pressure apparatus was constructed using a differential pressure transducer purchased from Omega Engineering, Inc. (Stanford, CT), with a sensitivity of 0 to 10 in. (25 cm) H_2O (0 to 2500 Pa). A #23 steel needle was used as a capillary, with a nominal 0.025 in. (0.64 mm) external

diameter, 0.013 in. (0.33 mm) internal diameter, and a flush cut tip. The capillary diameter was chosen so that the viscous resistance of water to bubble growth could be ignored. Such internal and viscous effects are a potential source of error in these measurements that need to be taken into consideration (Garrett and Ward, 1989). All measurements were conducted with the capillary tip 1 cm beneath the liquid surface. Compressed air was used as the bubbling gas and an oscilloscope connected to the pressure transducer was used to determine the bubble frequency and the dynamic surface tension. A schematic diagram of the setup is shown in Figure 2-1. Note that the tip of the capillary tube can be pointed either upward or downward.

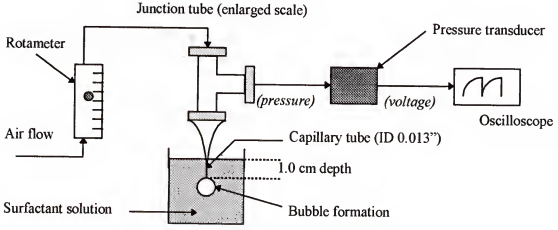

Figure 2-1. Setup for the measurement of dynamic surface tension by the maximum bubble pressure method.

Surface viscosity. A deep-channel surface viscometer (Wasan et al., 1971; Chattopadhyay et al., 1992) was used to measure the surface viscosity of 0.05 wt% sodium laurate as a function of pH. Two concentric cylinders form the deep channel of a viscometer. The walls of this channel are stationary, while the floor moves at a constant angular velocity. To measure the centerline velocity of the air/water interface, a small

Teflon particle was placed on the surface, and the time for that particle to make one revolution was recorded from visual observation. Using this value, the surface viscosity can be determined by

$$\epsilon = \frac{\eta y_0}{\pi}\left[\frac{8V_b}{\pi V e^{\pi D}} - 1\right] \qquad (2.2)$$

where ϵ is the surface viscosity, η the bulk viscosity of the solution, y_0 the channel width, V_b the plate rotational speed, V the centerline velocity of the air/water interface, and D the ratio of depth to width of the liquid channel.

Foamability by shaking. Foamability measurements on sodium decanoate, sodium laurate, and sodium myristate were carried out at 40 °C. Measurements for sodium palmitate were performed at 50 °C because the soap precipitated out of solution very quickly at temperatures lower than this. Sodium caprylate exhibited little or no foaming at low concentration. Experiments were carried out by vigorously shaking 20 ml of the sample solution for 30 seconds in a 100-ml graduated cylinder and recording the foamability as the volume of foam produced immediately after shaking. Each solution was tested at least five times as a function of pH.

Foamability by air bubbling. A quartz column, 3.5 cm in diameter, was used to measure the foamability of 0.05 wt% sodium laurate by air bubbling (Figure 2-2). At the base of the cylinder a single capillary, 1 mm in diameter, was used to generate the bubbles. Fifty milliliters of the sample solution was poured into the column using a long funnel that reached to the bottom to ensure that the walls of the cylinder remained dry and could not act as an additional supply of surfactant molecules, which would increase the foam stability. The air was then turned on at a constant flow rate of 158.2 cc/min.

The foam volume produced after 2 min was recorded. The measurement was repeated at least five times for each pH value tested.

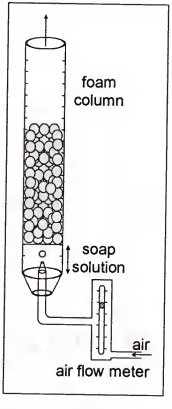

Figure 2-2. Schematic diagram of foam column used for foamability and foam stability studies.

Foam stability. Foam stability measurements were performed in the same quartz column used in the foamability by air bubbling experiments. Air was blown through 50 ml of 0.05 wt% sodium laurate solution at a rate of 158.2 cc/min and turned off when the foam reached a desired height (20 cm). The foam half-life (i.e., the time required for the foam to collapse to half of its original height) was measured as a function of pH. The measurement was repeated at least five times for each pH value tested.

Single bubble stability. A No. 23 steel needle (nominal 0.64 mm external diameter, nominal 0.33 mm internal diameter) with a flush-cut tip was positioned 2 cm

below the surface of a covered 0.05 wt% sodium laurate solution. Air was injected by micrometer rotation through the needle and a single air bubble was formed and allowed to rise to the surface. The time until collapse of the bubble was recorded. Over twenty measurements at each pH were made and averaged to give a mean bubble lifetime for each pH value tested.

Contact angle on PMMA. The contact angle between a 0.05 wt% fatty acid salt and air on a clean PMMA surface was observed using the low-power microscope of a Ramé-Hart contact angle goniometer, model A100. Over five measurements were made and averaged to give a mean contact angle for each pH value.

Evaporation studies. A known amount of anhydrous calcium chloride was measured and placed in a petri dish (Figure 2-3). The petri dish was then covered with vinyl cloth, inverted, and placed 3 mm above the surface of a 0.05 wt% 40-ml fatty acid solution. The rate of evaporation was measured by the increase in weight of the desiccant, anhydrous $CaCl_2$. The percent change in desiccant weight was measured every 15 minutes over a period of two hours as a function of solution pH.

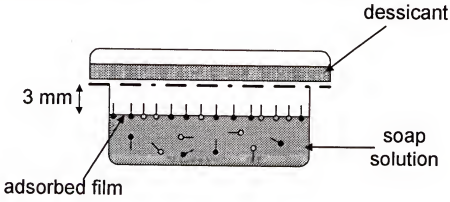

Figure 2-3. Schematic diagram of the experimental setup for evaporation measurements. The dessicant used was $CaCl_2$.

Determination of pKa. The pKa values of sodium caprylate, sodium decanoate, sodium laurate, sodium myristate, and sodium palmitate were determined by titration at 25 °C with 0.1 M sodium hydroxide using a METROHM 726 Titroprocessor. The neutralization endpoint was first determined. This is the point of inflection on the S-shaped titration curve. Then, the pKa was calculated as the pH of the solution at half the neutralization volume (i.e., half the volume needed to reach the neutralization endpoint). Five titrations were performed on each solution and mean pKa values for each soap were calculated.

Emulsions. 0.05 wt% sodium laurate solution was combined with light mineral oil to create emulsions containing 5 vol% oil at various values of pH. These solutions were first stirred and later sonicated for 30 minutes to create O/W emulsions. A drop of emulsion was placed on a microscopic glass slide and a cover slip was placed on top. The photographs of emulsions were taken with an optical microscope fitted with a camera.

2.3 Effect of pH on Performance of Fatty Acid in Various Interfacial Phenomena

The concentration of sodium laurate used in this study was 0.05 wt% (2.25 mM), which is approximately one-tenth of cmc for sodium laurate as reported by Mukerjee and Mysels (1971). Therefore, the concentration of monomers in solution is high enough that, while micelles are not created, the formation of small aggregates such as dimers, trimers and tetramers cannot be ruled out.

It is obvious that when dissolving sodium laurate in water in the pH range 6-9, the solution will be made up of different fractions of ionized carboxylate ($RCOO^-$), unionized fatty acid (RCOOH), and at very high pH values, unionized fatty acid salt (RCOONa). It

is known that unionized lauric acid is nearly insoluble in water (Seidell, 1941; Lide and Milne, 1995). This makes it the most surface active of the three species in an air/water system. It is also well accepted that long-chain fatty acids undergo an ionization process between pH 4.0 and 10.0 (Rosano et al., 1966; Higashiyama and Takenaka, 1974). At pH around 8.0 there is an ion molecular complex (RCOOH--RCOO-) present in 1:1 proportion (Somasundaran and Moudgil, 1988), which is more commonly regarded as the acid-soap. We see in Figure 2-4 that surface tension of sodium laurate increases with pH. In view of this fact, we propose that the salt form is more water soluble than the ($RCOO^-$) and (RCOOH) species found in solution. Therefore, our interpretations of results are mainly in terms of the interactions between ($RCOO^-$) and (RCOOH) in the range 6.5 to 8.5 at the air/water interface.

In the majority of studies on surface activity of a chemical compound, one very frequently begins by examining the change in surface tension with respect to change in a solution property (e.g., concentration, pH, temperature). Using surface tension data exclusively to deduce surface activity, however, one may overlook some interesting effects due to subtle molecular interactions in the adsorbed film. Figure 2-4 shows a plot of surface tension vs. pH of sodium laurate. This figure indicates that surface tension increases monotonically with increasing pH. There seem to be no unusual changes occurring anywhere within the pH range studied (pH 7.0 – 8.0). The only conclusion that one can draw from this figure, therefore, is that higher pH leads to lower surface activity (i.e., higher surface tension of the solution).

The results shown in Figure 2-4 for equilibrium surface tension were verified by dynamic surface tension studies. Dynamic surface tension measurements of sodium

laurate at a 2 second bubble lifetime also show a monotonic increase in surface tension with pH (Figure 2-5).

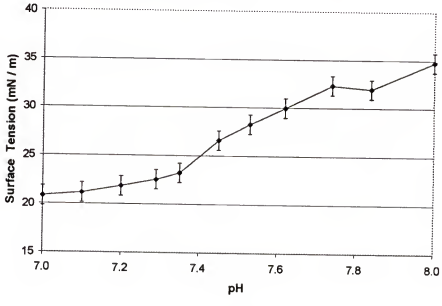

Figure 2-4. Surface tension (γ) vs. pH of 0.05 wt% sodium laurate solution.

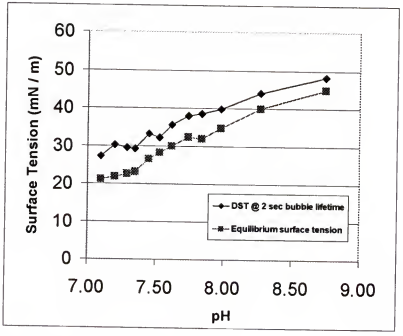

Figure 2-5. Dynamic surface tension (DST, 2 sec lifetime) and equilibrium surface tension measurements for 0.05 wt% sodium laurate solution vs. pH.

However, by depending on the results of a single parameter, one can easily miss very interesting phenomena occurring in such systems. Contrary to the results shown in Figures 2-4 and 2-5, the remainder of this chapter reports very interesting phenomena that occur at or near the pKa of a fatty acid salt solution.

Figure 2-6 shows results of the foamability (i.e., foam height) by single-capillary air injection test for sodium laurate. It is evident that the foam height is maximum in the pH range of 7.4 – 7.6. The foam height at pH 7.5 is three to five times greater than the foam heights near 7.0 and 8.0.

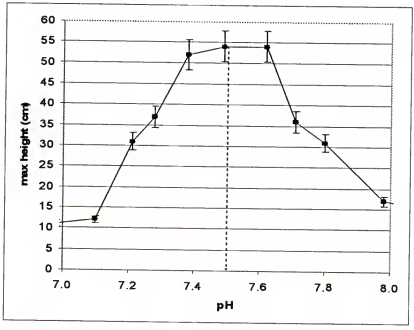

Figure 2-6. Foam height of 0.05 wt% sodium laurate solution vs. pH in foam column prepared by single-capillary injection of air.

The effect of pH on foam stability is shown in Figure 2-7. It is interesting that such a dramatic difference in the foam stability--a 30-second half-life near pH 7.1, to a half-life of nearly 350 seconds at pH 7.5, back to a 40-second half-life at pH near 8.0--can occur within 1 pH unit.

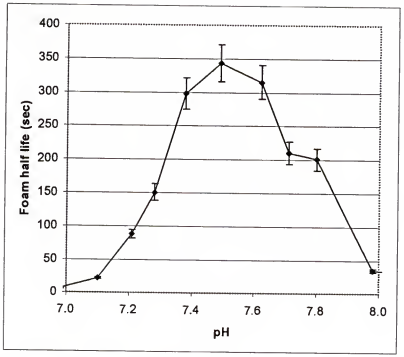

Figure 2-7. Maximum foam stability of 0.05 wt% sodium laurate solution vs. pH in foam column prepared by single-capillary injection of air.

The bulk pKa value of the 0.05 wt% sodium laurate solution at 25 °C was determined by titration to be 7.48. This suggests that the improved foamability and foam stability observed occur at or very near to the bulk pKa of sodium laurate.

Foamability and foam stability are not the only interfacial phenomena that show dramatic change near the pKa value of sodium laurate. The surface viscosity (Figure 2-8), as well as the single bubble stability (Figure 2-9) of the solution were found to increase dramatically. These two phenomena help to explain the dramatic increase in foamability and foam stability, since high bubble stability and surface viscosity are required to produce a stable foam.

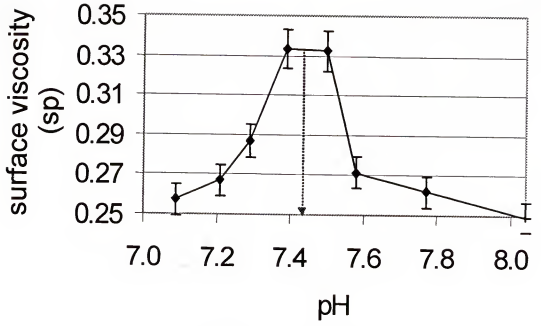

Figure 2-8. Surface viscosity vs. pH of a 0.05 wt% sodium laurate solution.

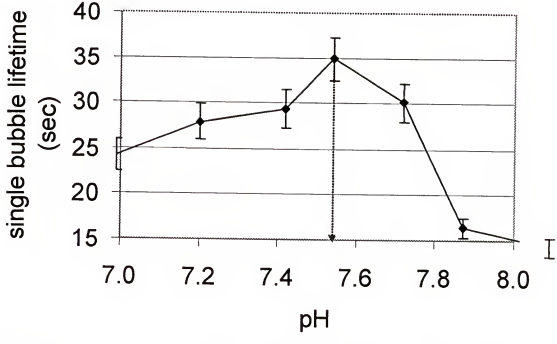

Figure 2-9. Single bubble stability vs. pH of a 0.05 wt% sodium laurate solution.

Evaporation studies, whereby the amount of water molecules evaporating through an adsorbed monolayer of fatty acid, were conducted. Results of these experiments show that evaporation of water is minimum at a sodium laurate solution at pH of 7.5 (Figure 2-10).

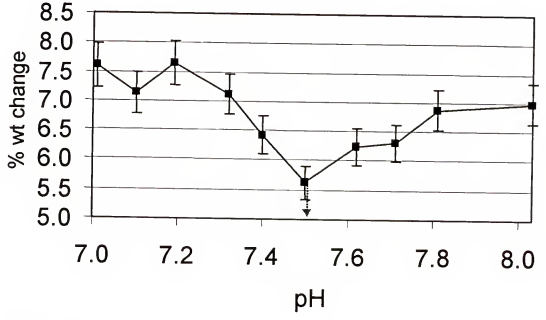

Figure 2-10. Water evaporation through a monolayer of sodium laurate vs. pH of the solution. The y-axis is a measure of the % weight change of the desiccant.

The air/water interface was not the only system affected by a change in fatty acid solution pH. Contact angle of sodium laurate on polymethylmethacrylate (PMMA), a hydrophobic surface, was also found to show optimum behavior (in this case, minimum contact angle) at pH 7.5 (Figure 2-11).

Figure 2-12 is a compilation of the data presented thus far. As one can see, all of the interfacial phenomena studied show optimum performance at a pH of 7.5 for sodium laurate. As was mentioned above, acid-base titration of the sodium laurate/lauric acid system shows the apparent pKa of this fatty acid to be 7.48, or approximately 7.5. Because of the 1:1 ratio of ionized to unionized fatty acid molecules at this pH, increased

intermolecular interaction and association is occurring, both in the bulk solution and at the surfaces and interfaces. This leads to the results shown in Figure 2-12: increased foamability, foam stability, single bubble stability, and surface viscosity, as well as a smaller contact angle and decreased evaporation at the pKa of the solution.

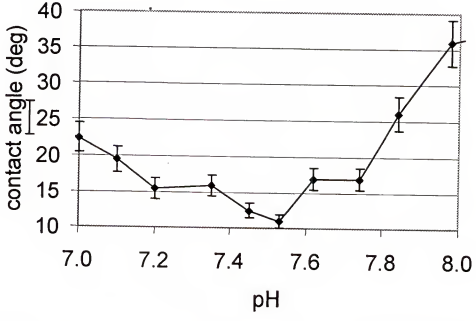

Figure 2-11. Contact angle on PMMA (a hydrophobic surface) vs. pH of a 0.05 wt% sodium laurate solution.

Other results corroborate these findings. In an emulsification experiment, it was found that an O/W emulsion at pH near pKa results in a higher concentration of emulsion droplets compared to other values of pH. This can be seen in Figure 2-13. Figure 2-13 also shows that at high pH values, the concentration of emulsion droplets is very small, as the ionized soap becomes more water soluble and less surface-active.

We propose that at pKa, since 50% of the molecules are in ionized form and 50% in unionized form, a strong ion-dipole interaction occurs between these two types of molecules that leads to a dimer formation at this pH. The interaction is much stronger than ordinary hydrogen bonding where no formal charge is present on any atoms.

Therefore, this association may be responsible for the effects that are seen in soaps near the pKa value. At pH values lower than pKa, the film becomes largely unionized and prefers to partition to a lipophilic medium (or to the fatty acid droplets in the surface in the case of an air/water system).

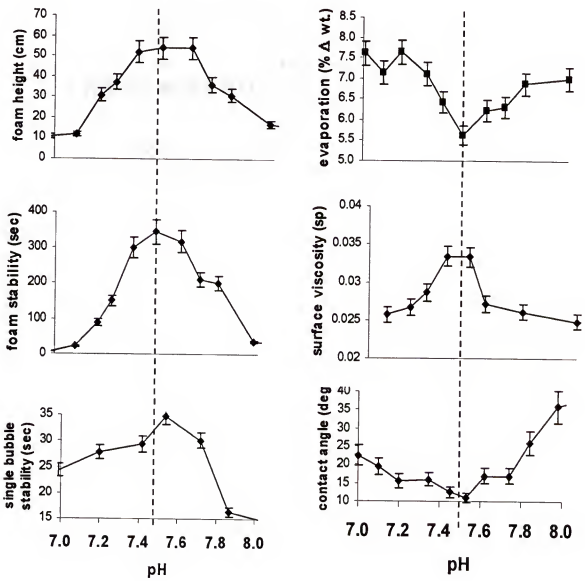

Figure 2-12. Diagram depicting maxima or minima in various interfacial properties with respect to pH of sodium laurate ($C_{11}H_{23}COO^-Na^+$) solution.

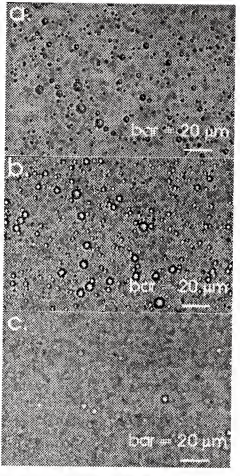

Figure 2-13. Comparison between O/W emulsions at different values of pH of sodium laurate solution. (a) pH 7.0, (b) pH 7.5, and (c) pH 8.0

At pH values higher than pKa, the film is almost completely ionized, leading to ionic repulsion between the polar groups and greater solubility in water. Figure 2-14 schematically shows the ion-dipole interaction between ionized and unionized molecules of fatty acid at pH values near the pKa.

The predicted minimum in area per molecule at pH near pKa is confirmed by area per molecule experiments for sodium laurate. Table 2-2 lists parameters of the Gibbs adsorption equation used to determine area per molecule of 0.05 wt% sodium laurate as a function of pH (see Appendix A). As can be seen in Table 2-2 and Figure 2-15, a

minimum in area per molecule and intermolecular distance is observed at pH ~7.5, which corresponds to the pKa of sodium laurate.

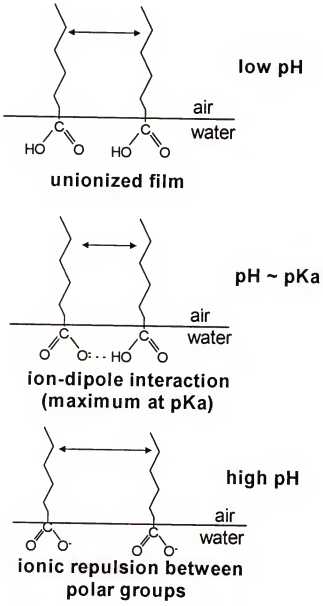

Figure 2-14. A strong ion-dipole interaction among the carboxyl groups near the pKa value decreases the intermolecular distance at the air/water interface.

Table 2-2. Calculated parameters of Gibbs adsorption equation used in determination of area/molecule of 0.05 wt% sodium laurate solution vs. pH.

Determination of area / molecule using Gibbs Adsorption Equation

Temperature =	298	Kelvin
sodium laurate FW =	222.3	g / mol
R =	8.31473E+15	dynes angstrom mol^{-1} K^{-1}

pH	$d\gamma$ / d logC	Γ (molecules / $Å^2$)	$1/\Gamma$ ($Å^2$/ molecule)	intermolecular distance (Å)
7.00	-14.07	0.015	67.2	8.20
7.25	-15.523	0.016	61.0	7.81
7.50	-16.699	0.018	56.7	7.53
7.75	-16.556	0.017	57.2	7.56
8.00	-16.182	0.017	58.5	7.65
8.25	-14.481	0.015	65.3	8.08
8.50	-12.311	0.013	76.9	8.77

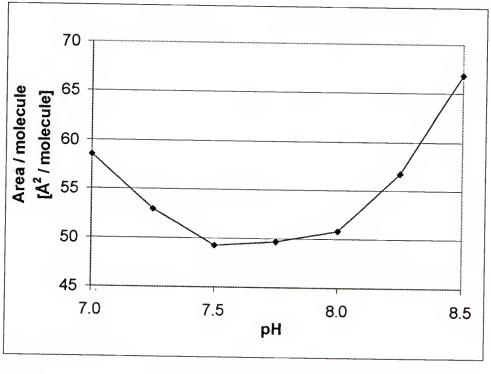

Figure 2-15. Area/molecule of 0.05 wt% sodium laurate vs. pH of solution.

2.4 Effect of Chain Length on Fatty Acid pKa

As the chain length of a fatty acid salt increases, the pKa value also increases. This is a very interesting phenomenon, since pKa is governed by ionization in the carboxylic acid moiety of the molecule and not by the electronic distribution in the carbon chain. If one goes from a C_{10} fatty acid chain length to C_{12}, the electronic distribution in the polar group region cannot be significantly altered. It is known (Hughes and Rideal, 1933; Shah and Schulman, 1965) that electronic effects do not go beyond 3-4 carbon atoms. Thus, the effect of the carbon chain length on pKa must be explained by intermolecular interactions.

We propose that as one increases the chain length of a soap molecule, the surface concentration (i.e., moles/cm^2) increases due to greater van der Waal interactions between alkyl chains and greater surface activity, and hence area per molecule decreases. This will decrease the intermolecular distance between the molecules of soap. Thus, the shift in pKa as one increases chain length must be due to closer packing of soap molecules at the interface.

Figure 2-16 shows the foam heights obtained by shaking method. It was observed that the foam height is maximum at pH values of 6.5, 7.5, 8.8, and 9.15 for C_{10}, C_{12}, C_{14}, and C_{16} soap molecules, respectively. The pH value for maximum foam height of C_{16} soap falls in between the two pKa values of C_{16} fatty acid found in the literature. Heikkila et al. (1970) reported an apparent pKa for hexadecanoic acid (i.e., palmitic acid) of 9.7, and Peters (1931) reported a pKa of 8.5 for the same fatty acid. We found the pKa of sodium palmitate to be 8.6-8.8 by titration (see Table 2-2). Christodoulou and Rosano estimated pKa values of 9.0 for octadecanoic (C_{18}) acid. Our values of pKa increased with increasing chain length. Table 2-3 shows a comparison between experimentally

determined pKa values and observed phenomena near pKa for fatty acid salts of (C_8-C_{16}) chain lengths. As can be seen in this table, pH values corresponding to minima in contact angle on PMMA and evaporation rate are similar to experimentally determined pKa values. Again, the shift in pKa due to increase in chain length seems directly related to increased van der Waals interaction between soap molecules. Thus, the above results indicate that *cooperativity* among molecules at interfaces induced by the van der Waals interactions between chains and the concomitant polar group interactions cause reduced intermolecular distance leading to optimum behavior of various properties exhibited by the soap solution near its pKa value.

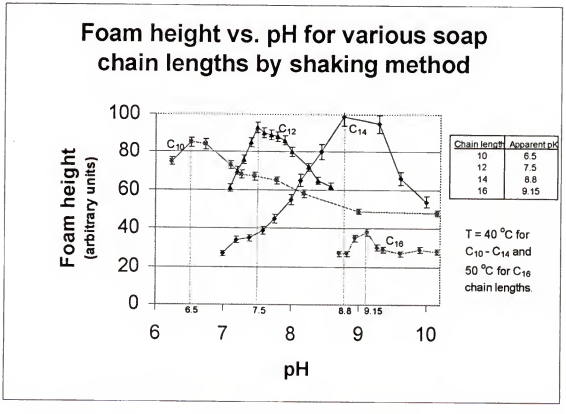

Figure 2-16. An increase in soap chain length leads to a shift in apparent pKa, as reflected by foamability (shaking method).

Table 2-3. Comparison between experimentally determined pKa values and observed phenomena for fatty acid salts of (C_8 – C_{16}) chain lengths.

Soap chain length	measured pKa	pH of maximum foam height	pH of minimum evap rate	pH of minimum contact angle
8	6.3 - 6.5	*	6.9	7.0
10	7.1 - 7.3	6.5	7.1	7.2
12	~ 7.5	7.5	7.5	7.5
14	8.1 - 8.2	8.8	8.1 - 8.3	7.6
16	8.6 - 8.8	9.15	8.9 - 9.0	**

* negligible foam generated
** insoluble at room temperature

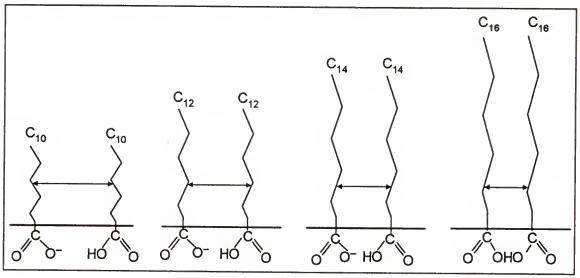

Figure 2-17. Schematic illustration of the proposed mechanism for the effect of chain length on the intermolecular distance between molecules in the adsorbed film at their respective pKa values.

Figure 2-17 schematically illustrates the proposed mechanism for the effect of increasing chain length on intermolecular distance of fatty acids at their respective pKa values. It was shown previously by Shiao et al. (1997) that changes in intermolecular distance as small as 0.04 Å induced by mixing surfactants of different chain lengths can significantly influence performance of various technological processes such as foaming, emulsification, lubrication, wetting, and retardation of evaporation by films. We have shown further in Table 2-2 that similar sub-angstrom changes (0.03 Å) in intermolecular

distance can be produced by ionization of the polar head groups near their respective pKa's, and this in turn will cause striking changes in the performance of various technological processes.

2.5 Conclusions

It has been shown that soap exhibits optimum properties at a pH near its pKa in various technological processes. Specifically, foam height, foam stability and bubble lifetime show maximum values, and contact angle on PMMA and water evaporation rate show minimum values at the bulk pKa of sodium laurate. Further studies indicate that an increase in the chain length of the soap molecule results in a shift in pKa towards a greater value due to molecular cooperativity induced by van der Waals interactions between hydrophobic chains and greater interactions among ionized and unionized polar groups.

CHAPTER 3
EFFECT OF CHAIN LENGTH COMPATIBILITY AND DEGREE OF UNSATURATION ON THE pKa OF LONG-CHAIN FATTY ACID SOAPS

3.1 Introduction

In 1917, Irving Langmuir showed that monolayers of fatty acids of various chain lengths compress to almost the same limiting area, indicating that the different acids must all form films in which the molecules are orientated vertically with respect to the surface (Langmuir, 1917). It was further shown that fatty acids with a *cis* double bond in the chain showed increased limiting areas as compared to those with a saturated chain. Addition of double bond to an alkyl chain 1) limits flexibility of the chain in this region, and 2) decreases adhesion between molecules (Heikkila et al., 1970; Seelig and Seelig, 1977). It was found, for example, that a saturated fatty acid chain (e.g., stearic acid) has a limiting area of 21 $Å^2$, while an unsaturated chain (e.g., oleic acid) has a limiting area of 32 $Å^2$ (Davies and Rideal, 1963; Schneider et al., 1949) per molecule.

Further evidence as to the effect of unsaturation on the packing of molecules at surfaces was shown by Shah and Schulman in the lecithin-cholesterol system (Shah and Schulman, 1965; 1967a). They showed that the limiting areas of synthetic (dipalmitoyl), egg, and yeast lecithin monolayers depend on the degree of unsaturation of the fatty acid residues, and that the addition of cholesterol to these systems serves to decrease the area per molecule as it occupies the molecular cavities in the monolayer created by the thermal motion of the chains or by the unsaturation of the alkyl chains. It is well known (Small, 1986) that the double bond in the chain produces a kink in the alkyl chain.

The compression data and limiting areas of the lecithin system obtained by surface pressure measurements were independently verified by an enzyme-catalyzed hydrolysis experiment (Shah and Schulman, 1967b). Shah and Schulman measured the action of snake venom phospholipase A on lecithin monolayers. It was shown that a lecithin monolayer does not hydrolyze when it is compressed above a critical pressure. The critical surface pressure required to block the penetration of the enzyme into the monolayer increased with molecular area (i.e., dioleoyl lecithin > soybean lecithin > egg lecithin > dipalmitoyl lecithin), which corresponded to their area per molecule as well as the increase in degree of unsaturation of the molecule. This and other experiments (Singh and Shah, 1993) corroborated previous limiting area results indicating that increasing degree of unsaturation yields increased area per molecule in a spread monolayer. Furthermore, Rao and Shah (1990) have shown that addition of a minimum of 20 mol% cholesterol to an arachidyl alcohol monolayer fluidizes the film and strikingly increases the evaporation of water through the film. Fang and Shah (1998) showed again using infrared imaging techniques that the molecular packing at the interface significantly affects heat transfer at the interface. These studies illustrate how monolayer packing and fluidity can influence important macroscopic phenomena.

The presence of a net charge on a surfactant polar group also affects its performance in an adsorbed monolayer. Fatty acids, for instance, can become ionized by an increase in the pH of the solution. If all the fatty acid molecules become ionized, repulsion between similarly charged molecules in the monolayer can result in an expansion of the monolayer at high pH (Adam, 1921; Adam and Miller, 1933), which in turn can lead to a weak and unstable film. The change in monolayer characteristics of

fatty acids as a function of pH of the bulk solution was first reported by Schulman and Hughes (17), who found that the surface potential (ΔV)-pH relation resembled an acid-base titration curve. As previously mentioned, for weakly ionized monolayers such as those created by fatty acids, it was proposed that the difference in pKa between the surface and the bulk is small (Davies and Rideal, 1961).

In Chapter 2, it was shown that the pKa values of long-chain fatty acids depend on the chain length of the fatty acid molecule, and can increase to values much higher than those for the shorter-chained analogs. These pKa's can reach values higher than 9 as the chain length increases to C_{16} and beyond. Heikkila et al. (1970) reported a pKa for hexadecanoic acid (i.e., palmitic acid) of 9.7, and Peters (1931) reported a pKa of 8.5 for the same fatty acid. In Chapter 2 we find the pKa of palmitic acid to be 8.6-8.8 by acid-base titration. Christodoulou and Rosano (1968) estimated pKa values of 9.0 for octadecanoic (i.e., stearic, C18) acid.

Figure 2-17 shows how the chain length of the fatty acid might affect its pKa. It is known (Tanford, 1980; Israelachvili and Pashley, 1982) that as the chain length increases, van der Waals interactions between the chains of adjacent molecules increases, bringing these molecules closer to each other. When this happens, the carboxylic acid groups of the fatty acids are also packed closer, shielding the hydrogen atom between the two oxygen atoms and hence increasing its interaction with adjacent oxygen atoms. The closer the molecules, the more strongly bonded is the hydrogen atom and consequently the higher the pKa.

This chapter presents our studies on the observed pKa values of C_{18} fatty acid solutions or aqueous dispersions, and attempts to describe how the pKa's of these fatty

acids can be influenced by the degree of unsaturation and subsequent molecular packing of the alkyl chains.

3.2 Materials and Methods

Materials. Stearic acid (97+% purity) and oleic acid (97+% purity) were supplied by Fisher Scientific (Fair Lawn, NJ). Elaidic acid (99% purity) and linoleic acid (95% purity) were supplied by Sigma Chemical Company (St. Louis, MO). Linolenic acid (acid value: 203, saponification value: 200, iodine value: 192) was supplied by Pfaltz and Bauer (Waterbury, CT). Sodium caproate (C_6), sodium caprylate (C_8), sodium caprate (i.e., sodium decanoate, C_{10}), and sodium laurate (C_{12}) were supplied by Sigma Chemical Company (St. Louis, MO) and were ≥98% purity. Sodium phosphate (monobasic and dibasic), concentrated sodium hydroxide, light mineral oil, and anhydrous calcium chloride were supplied by Fisher Scientific (Fair Lawn, NJ). Potassium hydroxide pellets and hydrochloric acid were supplied by Fisher Scientific (Fair Lawn, NJ). All solutions were prepared using water that was both deionized and distilled. All experiments were carried out at 20 ± 1 °C unless otherwise stated.

Solution preparation. Each of the C_{18} fatty acids listed above were placed in a clean beaker containing 10 mol% excess solid potassium hydroxide pellets. Water was very slowly titrated to the mixture until all of the fatty acid and potassium hydroxide had dissolved, producing a clear solution for each fatty acid. Because C_{18} fatty acids are insoluble in water, it was assumed that this solution was composed of water-soluble potassium salts of these fatty acids. The concentrations of these fatty acid salt solutions varied (stearic acid: 0.30 M, elaidic acid: 0.293 M, oleic acid: 0.35 M, linoleic acid: 0.66

M, linolenic acid: 0.61 M). The solutions were filtered with a 0.22 μm Cameo syringe filter and diluted with water to 100 mmols for determination of pKa by titration.

Determination of pKa. See "Determination of pKa" in Chapter 2, Section 2.2.

Evaporation studies. See "Evaporation studies" in Chapter 2, Section 2.2.

3.3 Effect of Degree of Unsaturation on pKa

It was shown in the previous chapter that the molecules of a fatty acid monolayer are packed closest together when the pH of the solution is close to the pKa of the fatty acid (Figure 2-14). When the pH is very high, ionic repulsion between the carboxylate ions keeps the molecules apart. When the pH is close to pKa, approximately 50% of the acid groups in the adsorbed film are protonated. The added ion-dipole interaction between the ionized and unionized acid groups is absent when all of the acid groups are protonated (i.e., pH is very low).

Figure 3-1 shows the structures of the C_{18} fatty acids with increasing degree of unsaturation studied. Stearic acid is completely saturated and consequently has a straight chain that can be packed tightly in a monolayer. Elaidic acid has a double bond at the number 9 carbon, but because the double bond is *trans*, the molecule remains straight and can still pack well in a monolayer. Oleic, linoleic, and linolenic acids have increasing numbers of *cis* double bonds, resulting in chains that kink and bend at the position of the *cis* double bond (Davies and Rideal, 1963). These molecules, therefore, become more and more difficult to pack easily in a monolayer.

Stearic acid has a limiting area of approximately 20 $Å^2$ (Hifeda and Rayfield, 1985; Tomoaia-Cotisel et al., 1987) and packs into a solid state. Elaidic acid, even though it packs nicely, does not become fully condensed like stearic acid because of its

double bond. Elaidic acid has a limiting area of approximately 31-33 $Å^2$ (Hifeda and Rayfield, 1985). Oleic, linoleic, and linolenic acids do not pack as tightly and as a result form a liquid expanded state for which the limiting areas are approximately 41 $Å^2$ for oleic acid (Davies and Rideal, 1961; Tomoaia-Cotisel et al., 1987) and 48 $Å^2$ for linoleic acid (Tomoaia-Cotisel et al., 1987; Peltonen and Rosenholm, 1989). The limiting area for linolenic acid is a difficult value to obtain because of the inherent characteristics of the linolenic acid molecule. This molecule contains three unsaturated bonds and a carboxyl group. Together these polar groups seem to be sufficient to allow the molecule to leave the spread film and dissolve into water when compressed to a sufficient pressure. Therefore, calculations of area per molecule may incorrectly assume a higher number of molecules in the monolayer, and result in a low value of area per molecule (Figure 2 of Reltonen and Rosenholm, 1989).

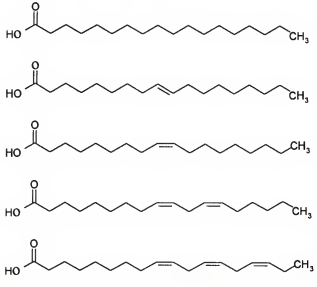

Figure 3-1. Molecular structure of stearic, elaidic, oleic, linoleic, and linolenic acids.

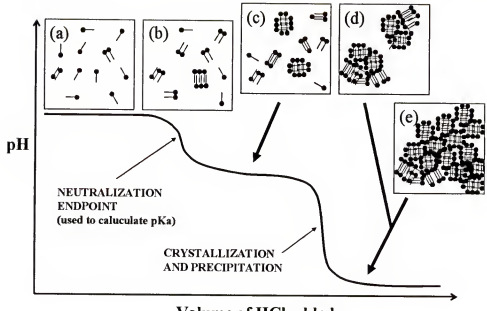

Figure 3-2. Schematic diagram of a typical C_{18} fatty acid pH titration curve and the degree of aggregation vs. pH expected in the aqueous solution. At pH > pKa (a) the solution is clear and contains soluble potassium salts. At pH ~ pKa (b) crystals begin to appear in solution. The crystals keep forming at lower pH values (c) until total conversion to insoluble fatty acid (d) or (e).

Figure 3-2 is a schematic diagram of a typical pH titration curve obtained for fatty acids (Rosano et al., 1966). When the pH of the solution is high, the solution is clear and contains only soluble potassium salts (Figure 3-2a). As hydrochloric acid is added, the pH decreases until it is close to the pKa of the fatty acid. At this point (Figure 3-2b), crystals begin to appear in the solution. The pH then levels off and crystals continue forming (Figure 3-2c) until total protonation of the fatty acids and precipitation of fatty acid crystals occurs (Figure 3-2d,e). The pKa is calculated from the neutralization endpoint shown in Figure 3-2.

Figure 3-3 shows the results of the titrations of the various C_{18} fatty acids with hydrochloric acid. As can be seen in this figure, stearic acid has the highest pKa value

(pKa = 10.15), followed closely by elaidic acid (pKa = 9.95), and then oleic acid (pKa = 9.85), linoleic acid (pKa = 9.24), and finally linolenic acid (pKa = 8.28).

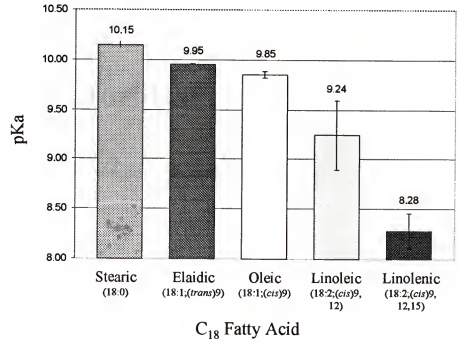

Figure 3-3. pKa values vs. degree and nature of unsaturation of C_{18} fatty acids, obtained by acid-base titration at 30 °C.

The results are not surprising if they are interpreted in the manner described above. These C_{18} fatty acids have a tendency to be expelled from water in order to minimize the total energy of the system (i.e., to maximize entropy of the water molecules). Even when slightly soluble in the form of potassium salts, these long-chain fatty acids arrange themselves into oligomers or clusters in order to minimize the free energy of the system. Stearic acid, with its straight alkyl chain, packs much tighter both in an adsorbed monolayer and in the small aggregates formed in solution as compared to unsaturated acids. Therefore it is more difficult for hydroxide ions in solution to strip away the acid's proton. On the other end of the series, linolenic acid contains many kinks in its chain caused by three *cis* double bonds. These kinks prevent the molecules from

packing closely, as is shown in Figure 3-4. Elaidic acid, with its *trans* double bond, packs much closer than its *cis* double bond counterpart oleic acid. As can be seen in Figure 3-3, this results in a higher pKa value as well.

Singh and Shah (1993) found similar results when studying the oxidation by potassium permanganate of monoglyceride, diglyceride, and triglyceride monolayers as a function of surface pressure. They found that oxidation rate is greatest for the molecule with the highest degree of unsaturation because of the increased intermolecular distance of this molecule in the monolayer.

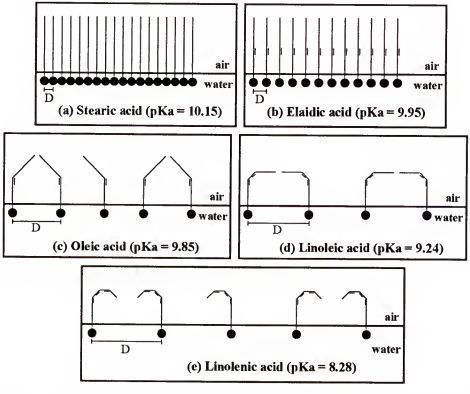

Figure 3-4. Schematic representation of C_{18} fatty acid monolayers at the air/water interface. Note the effect of degree of unsaturation on the area per molecule and the intermolecular distance, D, in the spread monolayers.

One must keep in mind that these molecules are always in a state of thermal kinetic motion. Even in a spread monolayer, fatty acid tails are spinning, rotating, and

colliding with the adjacent molecules. These collisions result in increased intermolecular distance, D, as illustrated in Figure 3-4.

Table 3-1 contains data on melting point temperatures (T_m), intermolecular distances between molecules in a spread monolayer, and the observed pKa values of the fatty acids studied. It is interesting to note that the decrease in pKa values corresponds to a decrease in melting point temperatures. This makes sense since the melting point temperature is an indication of the energy required to disrupt the molecular packing of crystals in the solid phase. For molecules that can pack very closely (e.g., stearic acid), T_m is relatively high. As degree of unsaturation increases, T_m decreases, and so too does pKa. However, melting point temperature and pKa do not have such a strong correlation. For example, there is an approximate 30 °C difference in T_m between elaidic and oleic acid, while only a 0.1 difference exists between their pKa's.

Table 3-1. Selected physical properties of C_{18} fatty acids.

C_{18} Fatty Acid	Structure and Degree of Saturation	Melting Point Temp. (°C) [a]	Limiting Area of Monolayer (Å^2)	Intermolecular Distance (Å) in Monolayer [f]	Observed pKa
Stearic acid	18:0	69 – 71	20[b]	4.47	10.15
Elaidic acid	18:1;*(trans)*9	44 – 45	31-33[c]	5.57-5.74	9.95
Oleic acid	18:1;*(cis)*9	13 – 14	41[d]	6.40	9.85
Linoleic acid	18:2;*(cis)*9,12	-5 – -1	48[e]	6.93	9.24
α-Linolenic acid	18:3;*(cis)*9,12,15	-11 – -10	---	---	8.28

[a] Sigma-Aldrich catalog
[b] Refs. Hifeda and Rayfield, 1985; Tomoaia-Cotisel, et al., 1987.
[c] Ref. Hifeda and Rayfield, 1985.
[d] Refs. Davies and Rideal, 1961; Tomoaia-Cotisel, et al., 1987.
[e] Refs. Tomoaia-Cotisel, et al., 1987; Peltonen and Rosenholm, 1989.
[f] Calculated from "Limiting Area of Monolayer" data using procedure in Appendix A

Area/molecule and intermolecular distance calculations of fatty acid monolayers made from π-area curves leave uncertainties as to whether or not the fatty acids present at the surface are actually present in uniform spread molecules, or if they have formed aggregates or islands at the surface. Fatty acid monolayer phase transitions can also be studied using methods such as x-ray diffraction (Ueno et al., 2000; Pen et al., 1997; Peng et al., 2000; Dutta, 2000; Tandon et al., 2000; Fainerman et al., 2000), FT-Raman spectroscopy (Tandon et al., 2000), and Brewster Angle Microscopy (BAM) (Fainerman et al., 2000; Johann et al., 2001). A correlation between fatty acid monolayer phase transition and solution pH has been shown using the BAM technique (Johann et al., 2001). Specifically, spread monolayers of fatty acids show maximum resistance to phase transition under compression when the pH of the solution equals pKa, indicating that the L_2 phase, which is characteristic of fatty acid monolayers, is stabilized by the ion-dipole interactions between carboxylic acid and carboxylate headgroups (Figure 10 of Ref. Johann et al., 2001).

3.4 Effect of Chain Length Compatibility on pKa of Mixed Fatty Acid Solutions

In many systems such as biological membranes, a mixture of fatty acids of different chain lengths often exists in the lipid layer. The way that these molecules interact at an interface must be influenced by the difference in chain lengths. Our group has shown by a series of studies (Patist et al., 1999; Shiao et al., 1997; Shiao et al, 1998; Sharma et al., 1986; Sharma and Shah, 1984; Shah, 1985) that compatibility between these molecules of unequal chain length is an important parameter that can affect surface concentration, area per molecule, surface viscosity, and intermolecular distance of a monolayer. These studies have shown that the mismatch between two adsorbed chains of

unequal length results in a poor molecular packing due to the extra vibrational energy created by the thermal motion of the extra segments of the longer chain.

The resulting increase in intermolecular distance can lead to a greater rate of evaporation from the adsorbed monolayers of mixtures as compared to pure components, as shown in Figure 3-5 for pH 6.5. As Figure 3-5 shows, addition of small amounts of the second component (e.g., 10% caprylate to a laurate solution or 10% laurate to a caprylate solution) can strikingly disrupt an adsorbed film to increase the rate of evaporation of water.

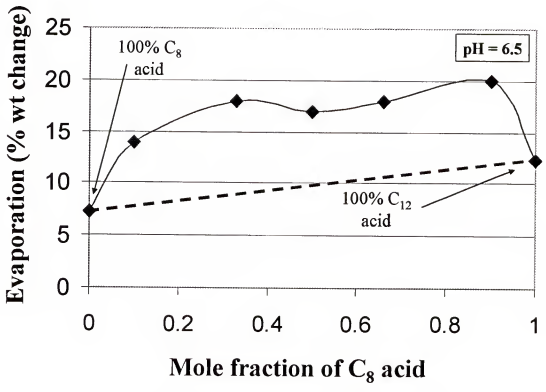

Figure 3-5. Evaporation of water through an adsorbed film of C_8/C_{12} mixed fatty acid salt solution at pH 6.5. Increased evaporation indicates decreased cohesiveness of the adsorbed film. The dashed line represents expected results using the additivity rule. Note: A similar trend exists for the entire pH range 6.5 – 9.

Similar results are encountered when measuring the pKa of mixed fatty acid solutions by pH titration. If a small amount of fatty acid of a different chain length is added to a pure fatty acid solution, the apparent pKa is found to decrease dramatically to values similar to those of short-chain fatty acids. For example, when adding small amounts of sodium caprylate (pKa = 6.5) to an aqueous solution containing only sodium decanoate (pKa = 7.2), the observed pKa drops down to approximately 5.5, which is one pH unit lower than that of caprylic acid (Figure 3-6). If the same amount of caprylate is added to a solution of sodium laurate, the pKa drops lower to a pKa of 5.0, much lower than pKa of 6.5 or 7.5 for the pure components. The unequal chain length leads to a disruption in molecular packing and a subsequent decrease in measured solution pKa (Figure 3-7).

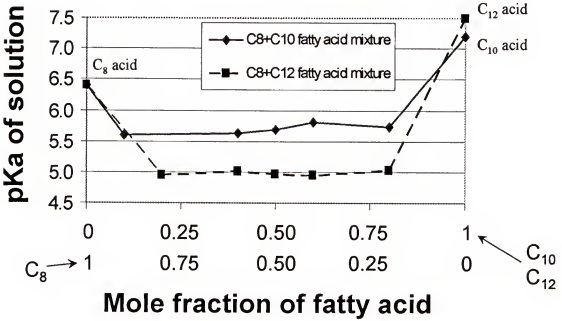

Figure 3-6. Measured pKa values of C_8, C_{10}, and C_{12} mixed fatty acid solutions obtained by acid-base titration at 23 °C.

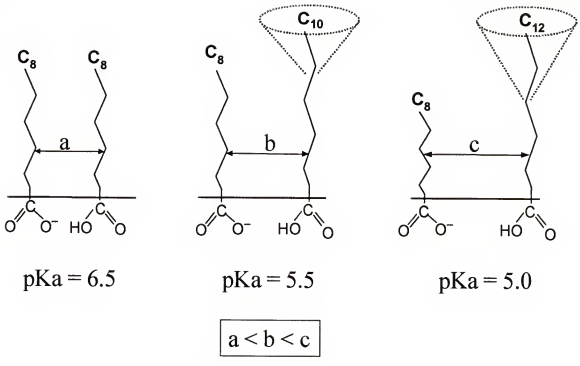

Figure 3-7. Chain length incompatibility increases intermolecular distance, which may lead to a decrease in apparent pKa of the solution.

A similar phenomenon must exist for the premicellar aggregates existing in the bulk solution. A lack of molecular cooperativity between the chains in these aggregates would most likely result in loosely packed molecular aggregates, which according to the above argument would explain the decrease in pKa with the addition of small amounts of surfactant of different chain length.

3.5 Conclusions

In summary, the results presented in this chapter report for the first time the effect of degree of unsaturation on the pKa value of oleic, linoleic, and linolenic acids, and further correlate the pKa value of a long-chain fatty acid with the intermolecular distance between the fatty acid molecules. The greater the intermolecular distance, the lower is the pKa value of the acid. Furthermore, upon mixing long-chain fatty acids of unequal

chain lengths, pKa values decrease as compared with those of pure acids. This decrease is due to increased area per molecule caused by thermal motion of the mismatched chains. Retardation of water evaporation from the films of pure vs. mixed fatty acids were carried out to show that the greater evaporation occurs in mixed films, indicating poorer molecular packing and hence increased intermolecular distance, and greater rate of evaporation.

CHAPTER 4
EFFECT OF PREMICELLAR AGGREGATION ON THE pKa OF FATTY ACID SOAP SOLUTIONS

4.1 Introduction

As shown in Chapter 2, the surface activity of a surfactant depends on the chain length as well as the state of ionization of the polar group of surfactant molecules. Strongly ionizable anionic surfactants such as dodecylsulfate exist predominantly as anions in the aqueous solution, with the undissociated "acid" form present only at very low pH values. Weakly ionizable surfactants such as long-chain fatty acid salts, however, are extremely sensitive to changes in solution pH and exist as different molecular species at various pH values in the aqueous solution (Small, 1986; McBain and Stewart, 1927; McBain and McHan, 1948; Ekwall, 1940; Ekwall and Lindblad, 1941; Mukerjee, 1965; Cook, 1951; Eagland and Franks, 1965; Pugh, 1986) as well as in monolayers (Goddard and Ackilli, 1963; Goddard et al., 1968; Johann and Vollhardt, 1999; Patil et al., 1972; Fainerman et al., 2000; Peng et al., 2001).

This chapter will illustrate how fatty acid concentration plays an important role in influencing the measured pKa in the premicellar concentration range. The objective here is to determine the molecular mechanisms leading to the unexpectedly high pKa values of long-chain fatty acids measured by acid-base titration, and to consider whether premicellar surfactant aggregation can explain this behavior.

4.2 Materials and Methods

Materials. Sodium caproate (C_6), sodium caprylate (C_8), sodium caprate (i.e., sodium decanoate, C_{10}), and sodium laurate (C_{12}) were supplied by Sigma Chemical Company (St. Louis, MO) and were ≥98% purity. Sodium phosphate (monobasic and dibasic), concentrated sodium hydroxide, light mineral oil, and anhydrous calcium chloride were supplied by Fisher Scientific (Fair Lawn, NJ). All solutions were prepared using water that was both deionized and distilled.

Determination of pKa. See "Determination of pKa" in Chapter 2, Section 2.2.

Evaporation studies. See "Evaporation studies" in Chapter 2, Section 2.2.

4.3 Effect of Chain Length on pKa

As mentioned in Chapter 2, electronic effects in a fatty acid are not felt beyond 2-3 carbons in the chain. Therefore, when the chain length is increased beyond about four carbons, the pKa tends to level off. Increasing the chain length from pentanoic to hexanoic acid, for example, increases the pKa only slightly from 4.82 to 4.83. Therefore, it is known that *intra*molecular interactions (i.e., the electronic effects on the carboxylic acid moiety by the rest of the molecule) become negligible beyond four carbons in the alkyl chain. However, Chapter 2 has shown that the observed pKa of long-chain fatty acids increases with increase in chain length of the molecule, and can be as high as about 9.0 as the chain length increases to C_{16} or greater.

Figure 2-14 shows the structure of a fatty acid polar group at different pH values. At low pH (pH ~ 1-2), unionized carboxyl groups are oriented at the interface to face the water. At the pKa value (where 50% of the molecules are ionized), there exists a strong ion-dipole interaction between the adjacent carboxyl groups, which causes the molecules

to pack more closely. This ion-dipole-stabilized complex is generally referred to as an acid-soap (Jung, 1976). This interaction and subsequent closer molecular packing is consistent with the minimum in evaporation rate of water through a fatty acid monolayer at the pKa (Chapter 2; Kanicky et al., 2000). However, at high pH (pH ~ 9-10), where complete ionization of the carboxyl groups causes ionic repulsion between adjacent polar groups and increases the solubility of fatty acid in water, the intermolecular distance is higher as compared to that at lower pH values.

As mentioned above, most short-chain carboxylic acids have a pKa value of about 4.8. This value reflects the ionization behavior of the fatty acid carboxylic acid group to dissociate in the aqueous solution. Because pKa depends only upon the electronic effects felt by the acid group, it is not expected to increase by addition of methylene groups to the fatty acid chain. If fatty acid pKa is measured using acid-base titration, we see that pKa in fact remains constant for chain length up to C_6 (caproic acid). However, when the fatty acid chain length is increased beyond C_6, a noticeable increase in pKa is observed when determined by acid-base titration (Figure 4-1).

We proposed in Chapter 2 that as the surfactant chain length is increased, the molecular packing between surfactant molecules at the interface and in the submicellar aggregates in the bulk solution becomes tighter due to van der Waals interactions between the chains. The surface concentration (i.e., moles/cm^2) increases and hence the area per molecule at the surface decreases (i.e., intermolecular distance between the surfactant molecules decreases).

As the fatty acid molecules get closer together, the proximity of other charged groups next to any given carboxyl group serves to stabilize the acid proton, making it

more difficult to remove it by the free hydroxide ions in the bulk solution. As a result, the measured pKa of the fatty acid increases. Thus, the above results indicate that *cooperativity* among molecules at interfaces and in the submicellar or micellar aggregates in the bulk solution induced by van der Waals interactions between chains and the concomitant polar group interactions results in reduced intermolecular distance and an increase in pKa as measured by acid-base titration.

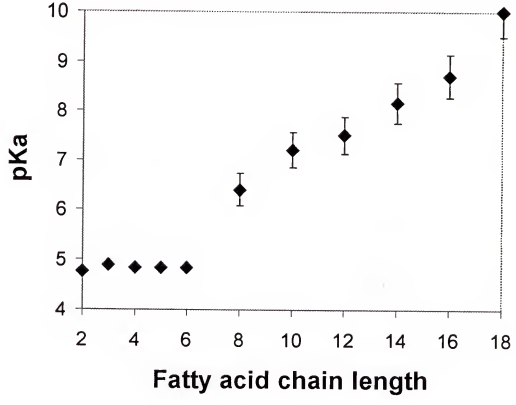

Figure 4-1. Effect of chain length on the pKa of fatty acid solutions. (Note: pKa values are for concentrations below cmc except for C16 and C18, which are slightly above cmc.)

If one focuses on the adsorbed film alone, it is easy to visualize that as chain length increases, the interaction between chains also increases, and hence intermolecular distance decreases. However, if we focus not only on the adsorbed film, but also on the

pre-cmc aggregates in the bulk fatty acid solution in the pre-cmc concentration region, it can be reasoned that as the concentration decreases below cmc, the premicellar aggregates do persist in the solution and reflect the effect of molecular cooperativity in the ionization behavior of the carboxyl groups. A number of investigators have shown that there exist premicellar aggregates (e.g., dimers, trimers, oligomers, etc.) in solution (Wangnerud and Jonsson, 1994; Kunjappu and Somasundaran, 1995). These aggregates are stabilized by interactions in hydrocarbon chains, and can be viewed as nothing more than small fragments of micelles existing in the bulk solution. As such, their behaviors are governed by the same interactions discussed previously for the adsorbed film. As long as premicellar aggregates exist in the bulk solution, they will behave similar to the adsorbed film at the surface (i.e., they will have a high pKa value). Therefore, if the solution is diluted and the pKa does not decrease to 4.8 (i.e., the pKa value for short-chain fatty acids ~4.8), we can presume that aggregates still exist in the bulk solution at that diluted concentration.

4.4 Effect of Surfactant Concentration on pKa

All of our previous studies on foamability, foam stability, contact angle, evaporation, and surface viscosity were performed on fatty acid solutions at concentrations below cmc. However, each of the interfacial phenomena studied here depends on the behavior of the adsorbed film. The similar associations found between adjacent molecules in the adsorbed film and molecules within a micelle are expected to lead to the same result--namely, an upward shift in pKa value. Thus if the fatty acid solution is continuously diluted to concentrations well below cmc, intermolecular associations in the bulk are expected to decrease and, ultimately, a concentration will be

reached where this association will not occur and all of the surfactant molecules will exist as individual monomers. In this case, one would expect the solution pKa to be 4.8, which is the pKa of non-associating short-chain fatty acids. Any deviation from 4.8 would indicate *premicellar association* between fatty acid molecules in that system.

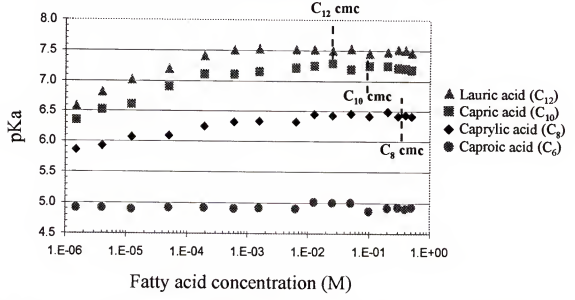

Figure 4-2. Effect of concentration on apparent pKa values of fatty acid solutions above and below cmc. Dashed lines indicate cmc.

As can be seen in Figure 4-2, measured pKa values of aqueous fatty acid solutions of chain lengths $C_8 - C_{12}$ are indeed found to decrease when these solutions are diluted to concentrations well below cmc. Solutions of caproic acid, however, maintain a constant measured pKa of approximately 4.8-5.0. If pKa values are extrapolated to increasingly dilute fatty acid concentrations (Figure 4-3), one can see that the estimated pKa values of each of the fatty acid solutions would intersect at a value of approximately 5.0 at a concentration of 5×10^{-11} M. It is possible that as the solutions are diluted to this concentration, the population of premicellar aggregates decreases to the point where only monomers are present in solution. Large intermolecular distances at this concentration

(10^{-11} moles/liter) would not facilitate molecular association in the form of premicellar aggregates. These monomers would have the same pKa value as short-chain fatty acids, namely 4.8 to 5.0. This suggests that upon increasing the chain length above C_8, the alkyl chain length association in the premicellar aggregate is very persistent even at a very dilute concentration (e.g. 10^{-10} moles/liter).

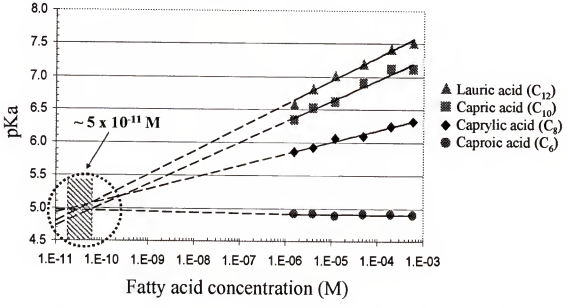

Figure 4-3. Extrapolated pKa values of very dilute fatty acid solutions. Values seem to intersect at a pKa of approximately 5.0 (5 x 10^{-11} moles/liter).

4.5 Conclusions

It has been shown that an increase in the chain length of a fatty acid from C_8 to C_{18} increases the apparent pKa of the solution. However, fatty acids of chain length C_6 and below have a constant pKa of about 4.8. pKa values are found to decrease upon dilution of C_8-C_{12} fatty acid solutions below cmc. However, they have to be reduced from 10^{-6} to 10^{-11} M to reach the pKa of short chain fatty acids, by extrapolation. These results indicate that even in nanomolar solutions of fatty acids of C_8-C_{12}, substantial molecular association exists in *premicellar aggregates* and in an *adsorbed film*. The

association between the ionized and unionized polar groups in such premicellar aggregates will shift the measured pKa to a higher value, depending upon its intermolecular distance.

CHAPTER 5
KINETICS OF GEMINI AND MIXED SURFACTANT MICELLES

5.1 Introduction

As was discussed in Chapter 1, micelle stability plays an important role in technological processes involving interfacial phenomena where a rapid creation of interfacial area occurs. One of these processes is the foaming process. As was shown in Figure 1-14, an increase in micelle stability results in a decrease in foamability (initial foam height) and an increase in foam stability (Shah, 1998). Micelle stability is a function of surfactant concentration (Figure 1-12) as well as salt concentration (Lessner et al., 1981a;1981b). And, of course, micelle stability is dependent upon the structure of the surfactant molecules. Another way of altering micelle stability is by the addition of other types of surfactants to the micelle. For example, Patist (1999) added small amounts of long-chain alcohol and oppositely charged surfactants to the SDS system, with stunning results. As Figure 5-1 shows, the micelle stability of 25 mM SDS jumped from 1 ms to over 200 ms with the addition of 1.25 mM $C_{12}OH$ (1-dodecanol), and to 2000 ms (2 seconds!) with the addition of 10 mM $C_{12}TAB$.

The concept of tailoring the stability of a micelle is an ongoing project in Prof. Shah's research group. Earlier investigations by Leung and Shah (1986) showed that short chain alcohols (C_1 to C_5) decrease the stability of SDS micelles. Research by Huibers (1996) showed that similar results are found with the addition of glycerol to SDS.

25 mM SDS, τ_2 = 1 ms.

25 mM SDS + 1.25 mM $C_{12}OH$, τ_2 = 230 ms.

25 mM SDS + 10 mM $C_{12}TAB$, τ_2 = 2000 ms.

Figure 5-1. Tailoring SDS micellar stability by the addition of 1-dodecanol ($C_{12}OH$) or alkyltrimethylammonium bromide ($C_{12}TAB$).

It is clear from Figure 5-1 that the addition of neutral or oppositely charged surfactant can dramatically increase micelle stability by charge shielding (as in the case of added neutral surfactant) or charge neutralization (for oppositely charged surfactant). Previous results obtained by Patist (1999) show that the addition of small amounts of long-chain alcohol to an SDS micellar solution increases the micelle stability. However, as shown in Figure 5-2, the increase in SDS micelle stability depends on the chain length compatibility between the surfactant and alcohol. Maximum increase in micelle stability occurs when the surfactant and alcohol chain lengths are equal.

Another factor influencing the effectiveness of added alcohol in increasing micelle stability is the surfactant concentration. As can be seen in Figure 5-2, the maximum increase in micelle stability occurs at 25 mM SDS. At this concentration, pure SDS micelles are very unstable, and the addition of alcohol results in a dramatic increase in stability. At 200 mM, however, pure SDS micelles are at maximum stability (see Figure 1-12) addition of $C_{12}OH$ does little to increase micelle stability. In fact, the alcohols with different chain lengths actually decrease the micelle stability due to chain length incompatibility.

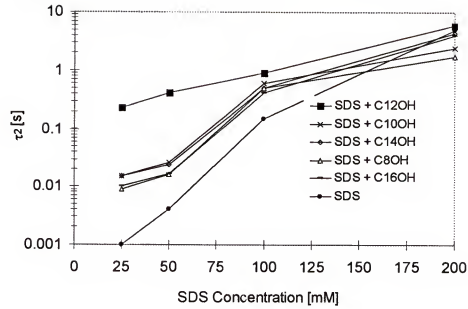

Figure 5-2. The effect of 5 mol% CnOH on the micellar relaxation time (τ_2) of 25-200 mM SDS solutions at 25°C.

A natural extension of the above research is to study the effect of added long-chain fatty acids to a micellar system. It stands to reason from discussions in previous chapters that solution pH will be an important factor in determining the ionization state of the added fatty acids. Therefore, it may be possible to further tailor micelle stability by varying the pH of the micelle solution.

Research on micelle stability will further be extended to other mixed and novel surfactant systems. One such novel system is the Gemini (or dimeric) surfactant, whose special properties are described in detail below.

5.2 Methods to Measure Micelle Stability

There are several ways to study the kinetics of micelle formation and disintegration. These methods are based on techniques which are used to perturb the equilibrium state of the micelle solution and monitor the system as it attains a new

equilibrium. Two such techniques described below are the pressure-jump and stopped-flow methods. The pressure-jump method perturbs the equilibrium state by very quickly changing the pressure of the system. The stopped-flow method works similarly by very quickly diluting the surfactant concentration. Not explained below is another popular technique to measure micelle kinetics: the temperature-jump method, which is similar to the other two methods except that the temperature is changed abruptly. All of these perturbations in the pressure, concentration, or temperature must be done in a time scale of a few microseconds.

5.2.1 Pressure-Jump with Electrical Conductivity Detection

One of the easiest methods used to measure micelle kinetics is the pressure-jump method with conductivity detection. A schematic diagram of the pressure-jump apparatus is shown in Figure 5-3.

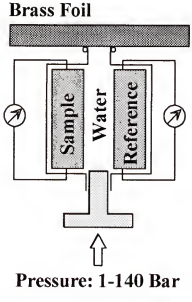

Figure 5-3. Schematic diagram of the pressure-jump apparatus.

The sample surfactant solution is placed in the "sample" cell, and a reference solution (e.g. KCl) with the same electrical conductivity as the sample is placed in the "reference" cell. The cells are separated from deionized water in the main pressure chamber by a deformable plastic diaphragm, usually made from polyethylene. The entire chamber is then pressurized to 140 bar, and the difference in conductivity between the sample and reference cell is monitored and allowed to equilibrate at high pressure. The pressure is then suddenly reduced to 1 bar by bursting the brass foil, and the time required for the conductivity difference to come to a new equilibrium is measured.

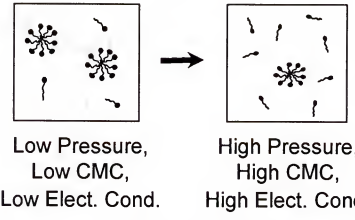

Figure 5-4. Aggregation state of a micellar solution at low and high pressure.

As is shown in Figure 5-4, at low pressure, the cmc is lower and more micelles are present in a micellar solution. The same solution at high pressure will have less micelles because the cmc is shifted to a higher value. So during the pressure-jump experiment, micelles are being created as the pressure drops from 140 to 1 bar. The conductivity of the reference cell remains the same throughout the experiment. However, since electrical conductivity depends upon the monomer concentration, we see a decrease in conductivity in the sample cell when the pressure is suddenly dropped from 140 to 1

bar. The result is an exponentially decaying conductivity signal like that shown in Figure 5-5 that can be used to determine the micellar relaxation time, τ_2, by the equation

$$\tau_2 = t\left[C = \frac{\Delta C}{e}\right] \tag{5.1}$$

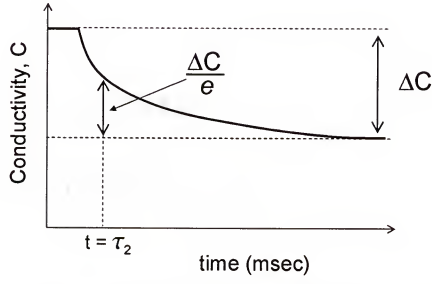

Figure 5-5. Exponentially decaying conductivity signal obtained in pressure-jump experiment and used to calculate micelle relaxation time, τ_2.

The major disadvantage of the pressure-jump technique with electrical conductivity detection is that only ionic surfactants have sufficiently high conductivity to be measured. Nonionic surfactants do not have sufficient conductivity to be detected by this method. Also, only low concentrations of ionic surfactant can be used, because if the concentration is too high, the conductivity change with pressure is too small to be detected.

5.2.2 Stopped-Flow Method

The stopped-flow method is generally used for nonionic surfactants, where the pressure-jump method does not work because conductivity is not a sensitive parameter. For this reason, it is necessary to use a dye to obtain information about the micellar

kinetics. A number of dyes or fluorescent compounds show an appreciable change of extinction coefficient depending on the medium in which the dye resides. Eosin, Merocyanine, and Rhodamine (Figure 5-6) have different light absorbance characteristics depending on whether they are present in an aqueous phase or in an oily phase. Because the interior of a micelle is oily in nature, these dyes absorb or emit differently inside and outside the micelles. This allows us to follow the relaxation kinetics upon a quick temperature, pressure, or (in this case) concentration-jump by employing spectrophotometric detection methods (Patist, 1999).

Eosin Y, for example, has a maximum light absorbance at 518 nm in water. This maximum shifts to 538 nm in the presence of micelles [Shinoda and Nakagawa, 1963; Hunter, 1987] as the dye partitions between the aqueous and micellar phases. As is shown in Figure 5-7, the maximum shift in absorbance occurs at 542 nm. The absorbance of 542 nm wavelength light increases with increase in surfactant concentration (Patist, 1999). Therefore, if the 542 nm absorbance peak is monitored before and after quick dilution, the kinetics of micelle breakup over time can be followed.

Figure 5-8 is a schematic diagram of a stopped-flow apparatus. This diagram shows how the surfactant + dye solution is diluted by a dye solution of the same concentration but without surfactant. The kinetics of the dilution process and subsequent disintegration of micelles is followed by monitoring the selected absorbance peak of the dye.

One of the drawbacks of the stopped-flow method is that there exists a "dead" time following the dilution of the sample and reference solutions, during which no measurement can be made. This dead time depends on the volume of solution injected

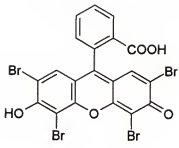

Eosin Y

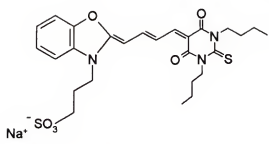

Merocyanine 540

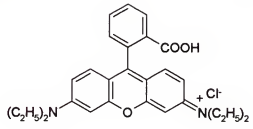

Rhodamine B

Figure 5-6. Molecular structure of Eosin Y, Merocyanine 540, and Rhodamine B.

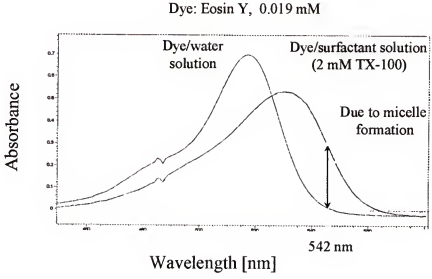

Figure 5-7. Absorbance spectra of Eosin Y in water and 2 mM Triton X-100 solution (Eosin Y concentration: 0.019 mM) (Patist, 1999).

and the design of the instrument. Long dead times have in the past prevented the use of the stopped-flow technique for measuring micelle kinetics of very unstable ionic micelles. These dead times have been of the same order as anionic micelle lifetime. Newer instruments that inject smaller liquid volumes have a much smaller dead time, however. The SX.18MV-R stopped-flow spectrometer used to collect data for this chapter, for example, has a dead time of only 2 ms.

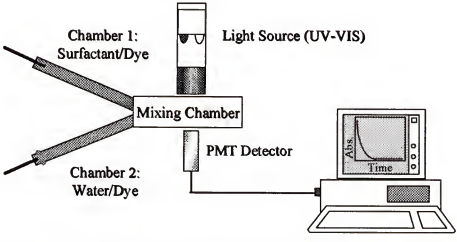

Figure 5-8. Schematic diagram of a stopped-flow apparatus with optical detection.

Another limitation of the stopped-flow method has to do with the intensity of projected light and/or sensitivity of the light absorbance detector. The SX.18MV-R stopped-flow spectrometer mentioned above has a relatively low light intensity. For this reason, changes in absorbance are sometimes difficult to observe for very dilute solutions.

5.3 Materials and Methods

Materials. Sodium caprylate (C_8), sodium decanoate (C_{10}), sodium laurate (C_{12}), dodecyltrimethylammonium bromide (C_{12}TAB), and sodium dodecyl sulfate were supplied by Sigma Chemical Company (St. Louis, MO) and were of 99% purity. Triton

X-100 was supplied by Aldrich Chemical Company (Milwaukee, WI). High purity grade dyes Eosin Y ($C_{20}H_6Br_4Na_2O_5$, anionic) and Merocyanine 540 ($C_{26}H_{32}N_3NaO_6S_2$, anionic) were supplied by Acros Organics (Fair Lawn, NJ). Bis(dodecyldimethylammonium bromide) (i.e., 12-n-12) Gemini cationic surfactants with ethylene (12-2-12), propylene (12-3-12), and butylene (12-4-12) spacer groups were generously supplied by Prof. Krister Holmberg of Chalmers University in Göteborg, Sweden. Sodium phosphate (monobasic and dibasic), and concentrated sodium hydroxide were supplied by Fisher Scientific (Fair Lawn, NJ). All solutions were prepared using water that was both deionized and distilled. All experiments were carried out at 23 ± 1 °C unless otherwise stated.

Equilibrium Surface tension. Surface tension measurements were obtained from freshly prepared solutions by the Wilhelmy plate method, whereby a 2.54 cm x 1 cm platinum blade is dipped into the solution and the force exerted on the blade by the solution is measured and translated to surface tension. Before each measurement, the platinum plate was cleaned by heating it to a red/orange color with a Bunsen burner.

Contact angle on PMMA. The contact angle between a surfactant solution and air on a clean PMMA surface was observed using the low-power microscope of a contact angle goniometer. Over five measurements were made and averaged to give a mean contact angle.

Pressure-Jump Method. The pressure-jump technique with conductivity detection from Dia-Log GmbH (Duesseldorf, Germany) was used to measure the slow relaxation time τ_2 of several ionic surfactants. The temperature was 23 ± 1 °C unless otherwise stated.

Stopped-Flow Method. The slow relaxation time τ_2 of several different types of surfactants was measured by the stopped-flow dilution method with an SX.18MV-R stopped-flow spectrometer (Applied Photophysics, Surrey, Great Britain). The dye concentration used was 0.019 mM. The mixing time of the instrument was approximately 2 ms. Absorbance measurements in the light range of 400-1000 nm (depending on the dye used) were taken as a function of time. The temperature was 23 ± 1 °C unless otherwise stated. The mean value from a series of 10 separate trials was used for calculations.

Gemini Surfactant Desorption Studies. A surfactant solution was made by adding surfactant to a 1:1:3 methanol:chloroform:n-hexane solution at a ratio of 1 mg/ml. 100 μL of the surfactant solution was deposited onto the clean surface of a 0.05 mol/liter NaCl solution in a container with a large ratio of reservoir volume to available air/water surface area. The surface tension was monitored as a function of time to determine the rate of desorption of surfactant from the air/water interface. Further experimental details are explained in the following sections.

5.4 Kinetics of Micelles with Added Fatty Acid

As was discussed in Section 5.1, micelle stability of a surfactant system can be modified by the addition of small amounts of additives. When Patist (1999) added small amounts of long-chain alcohol and C_nTAB to the SDS system, he saw that micelle stability increases dramatically. Addition of long-chain fatty acids to the same system should give similar results. Furthermore, from discussions in Chapter 2, one would expect the pH of the solution to make a noticeable difference on the stability of micelles containing long-chain fatty acids.

For example, as shown in Figure 5-9, an SDS micelle with added lauric acid should behave differently at low pH than at high pH. At low pH, the acid groups will be protonated, making the fatty acid molecule neutral in charge and able to shield the SDS molecules from each other. At high pH, the acid groups will be ionized, making the molecule anionic, which would cause them to act similarly to the SDS molecules. The micelle stability should be a function of the solution pH.

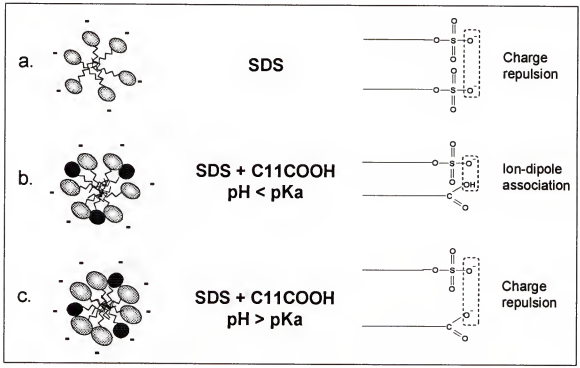

Figure 5-9. Tailoring micelle stability by addition of long-chain fatty acid.

Figure 5-10 shows the slow micellar relaxation rate, τ_2, of 100 mM SDS as a function of added sodium laurate for different pH values using the stopped-flow method. As can be seen, at every pH value the micelle stability increases with increasing sodium laurate concentration. The increase is very insignificant for pH 9.0, but becomes more significant for pH 7.5 and still more noticeable for pH 7.0 and 6.0.

These results agree with the prediction that at low pH, the fatty acid molecules present within the micelle would act to shield the charges between SDS molecules and effectively reduce their repulsive forces and hence increase the value of τ_2, while at high pH, the fatty acid molecules would themselves be anionic surfactants and act similarly to the SDS molecules and probably does not partition as much in micelles as at lower pH values. This explanation is further illustrated in Figure 5-11, which shows the micelle stability of 100 mM, 150 mM, and 200 mM SDS solutions with 5 mM sodium laurate added as a function of pH using the stopped-flow method. The figure shows the micelle stability for each concentration to be high at pH 7.0 and to gradually decrease to near pure SDS values (0.13, 1.1, and 5.0 seconds for 100 mM, 150 mM, and 200 mM SDS, respectively, as shown in Figure 1-12) at pH 10.0.

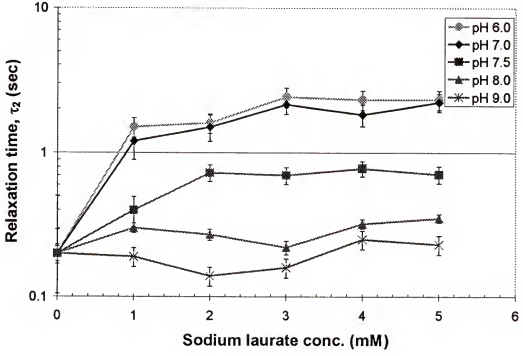

Figure 5-10. Micelle stability of 100 mM sodium dodecyl sulfate (SDS) as a function of added sodium laurate concentration for various pH values using stopped-flow method.

It is interesting to note that τ_2 values in Figures 5-10 and 5-11 approach those of pure SDS at higher pH. This makes sense since at high pH, the fatty acids in the micelle are in an anionic form with characteristics presumably similar to SDS molecules (Figure 5-9). Also noteworthy in Figure 5-11 is the very slight change in micelle stability vs. pH at 200 mM SDS. This can be attributed to the fact that SDS micelles are most stable at 200 mM as explained by the Intermicellar Coulombic Repulsion Model (ICRM) described in Chapter 1.

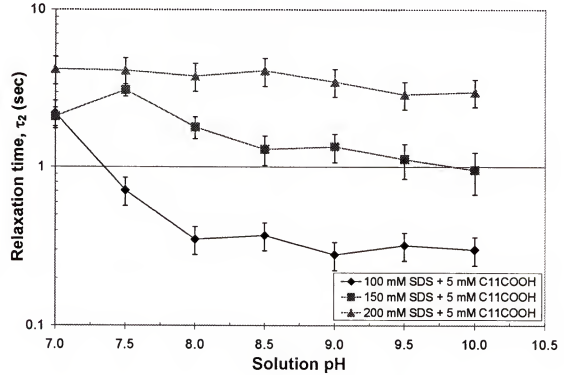

Figure 5-11. Micelle stability of 100 mM, 150 mM, and 200 mM sodium dodecyl sulfate (SDS) with 5 mM added sodium laurate as a function of solution pH using stopped-flow method.

Addition of fatty acid to a solution of cationic surfactants is expected to give different results. At low pH, the fatty acid molecules are protonated and neutral in charge. Any fatty acids within a cationic micelle would shield the cationic monomers

from each other, leading to a slight increase in micelle stability. At high pH, the fatty acids are ionized, and charge neutralization should occur between the fatty acid anions and the surfactant cations. This is expected to result in increased micelle stability.

Figure 5-12 shows the slow micellar relaxation rate, τ_2, of 20 mM $C_{12}TAB$ as a function of sodium laurate concentration for different pH values using the stopped-flow method. The figure shows the micelle stability to increase with addition of fatty acid despite the pH. However, the increase in micelle stability is significantly higher at higher pH values.

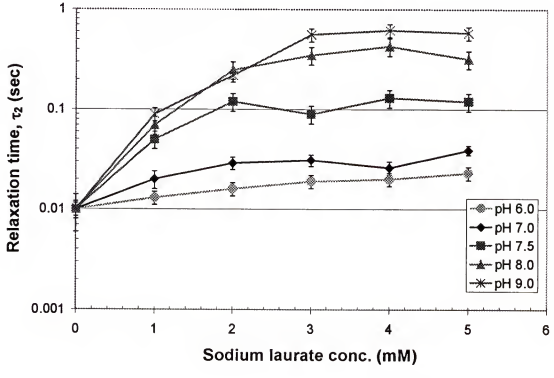

Figure 5-12. Micelle stability of 20 mM dodecyltrimethylammonium bromide ($C_{12}TAB$) with 5 mM sodium laurate added as a function of solution pH using stopped-flow method.

5.5 Kinetics of Mixed Surfactant Micelles

Research in the area of mixed micelles was extended to the ionic/nonionic surfactant system. Previous unpublished research by Patist and Huibers using the pressure-jump method showed that the addition of Tween 80 nonionic surfactant to an SDS solution increases the micelle stability. Further research performed on the SDS/Triton X-100 system showed similar results (Figure 5-13). Addition of approximately 10% Triton X-100 to the SDS system increased the micelle stability four-fold. However, micelle stability did not increase further with addition of more nonionic surfactant.

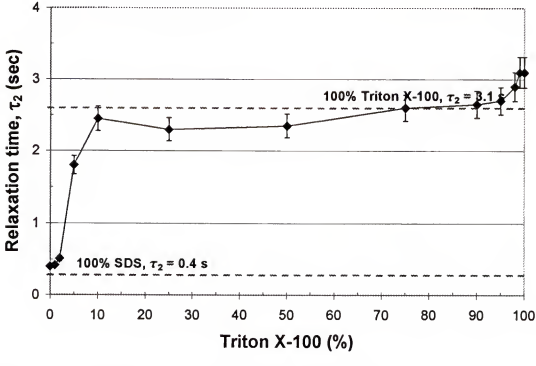

Figure 5-13. Relaxation time of sodium dodecyl sulfate/Triton X-100 mixed surfactant systems (100 mM total concentration).

5.6 Kinetics of Gemini Surfactant Micelles

A Gemini (or dimeric) surfactant is a molecule composed of two identical hydrophilic head groups and hydrophobic tail groups. It is very similar to two single chain surfactants linked covalently by a spacer group. The spacer group can vary in length and chemical structure, be flexible or rigid, and be hydrophilic or hydrophobic (Figure 5-14) (Zana, 1997).

Figure 5-14. Schematic diagram of a Gemini surfactant.

Gemini surfactants have three unusual solution and interfacial properties. First, Gemini surfactants have cmc values one to two orders of magnitude lower than that of corresponding single-chain surfactants (Rosen, 1993). Second, they are much more efficient than their corresponding monomeric surfactants at decreasing the surface tension of water (Devinsky et al., 1986; Zhu et al., 1993). For example, the C_{20} (i.e., surfactant concentration required for lowering the surface tension of water by 20 mN/m) for 12-2-12 Gemini is 0.0083 wt% while that for C_{12}TAB is 0.25 wt% (Zana, 2002). Finally, Gemini surfactants with short spacers form large, threadlike aggregates while the monomeric equivalent forms only small spherical micelles. For example, 12-2-12 Gemini has been shown to form long wormlike micelles at a concentration as low as 1.5 wt% (about 25 mM) (Zana and Talmon, 1993). As a result, aqueous solutions of these Gemini surfactants can have a very high viscosity at relatively low surfactant

concentration and can show shear-induced viscoelastic behavior at concentrations as low as 0.7 wt% (Schmitt et al., 1995).

Along with the properties mentioned above, Gemini surfactants have been shown to have better solubilizing, wetting, and foaming, properties than conventional surfactants (Rosen, 1993). Also, the Krafft temperatures of Gemini surfactants with hydrophilic spacers is very low (Rosen, 1993), allowing these surfactants to be used in cold water. Finally, Gemini surfactants have been shown to have interesting biological effects. For example, the alkyltrimethylammonium bromide-based Gemini surfactants induced various biological effects such as an inhibition of bacterial activity (Mlynarcik et al., 1976; Imam et al., 1983; Devinsky et al., 1985) and of photosynthesis (Kralova and Sersen, 1994).

The unusual characteristics listed above make Gemini surfactants a very interesting topic of study. The following sections of this chapter focus on results obtained from the study of bis(dodecyldimethylammonium bromide) (i.e., 12-n-12) Gemini cationic surfactants with ethylene (12-2-12), propylene (12-3-12), and butylene (12-4-12) spacer groups.

5.6.1 Gemini Surfactant Critical Micelle Concentration (cmc)

Figure 5-15 shows the surface tension vs. concentration curves used to calculate the cmc of 12-2-12, 12-3-12, and 12-4-12 Gemini surfactants. From Figure 5-15, cmc values are calculated and compared to literature values in Table 5-1.

As can be seen in Table 5-1, the cmc values of 12-2-12, 12-3-12, and 12-4-12 Gemini surfactant are very similar. They are also approximately one-tenth the value of the corresponding monomer, C_{12}TAB. C_{12}TAB has a cmc of 16 mM at 25 °C (Rosen,

1989). This characteristic of Gemini surfactants has great practical importance, because such a low cmc value means that only one-tenth the amount of Gemini surfactant (on a mole basis) is required to form micelles in solution as compared to $C_{12}TAB$. This means that different types of Gemini surfactants may one day be developed to replace monomeric surfactants so that much less total material is required for the process to form micelles.

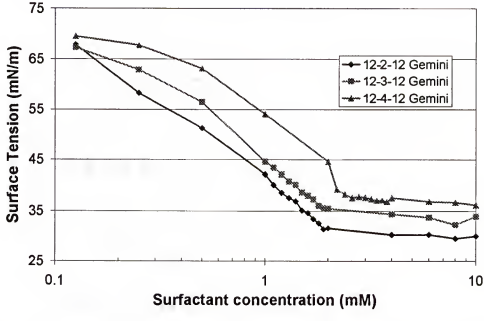

Figure 5-15. Surface tension vs. surfactant concentration for 12-2-12, 12-3-12, and 12-4-12 quaternary ammonium bromide Gemini surfactants.

5.6.2 Gemini Micelle Stability

A recent publication by Ulbricht and Zana (2001) has shown that Gemini surfactants with short spacer groups do in fact show typical micelle formation and breakup kinetics. Using the pressure-jump technique with conductivity detection, they found that the same quaternary ammonium bromide-based Gemini surfactants used in this study display fast (τ_1) and slow (τ_2) relaxation time constants. Interestingly, they

found that the fast relaxation time constant, τ_1, is about 10^3 times larger than for similar conventional surfactants. This surprising observation implies that the residence time of a single Gemini surfactant molecule within the micelle is very large. A possible explanation for this is that surfactant dimers with a short spacer group experience increased energy due to steric hindrance between the two adjacent chains. This steric hindrance may force the dimer molecule to adopt a conformation where the two alkyl chains are in a *trans* position with respect to one another (Ulbricht and Zana, 2001), causing the molecule to enter and exit the micelle in a step-wise process involving first one alkyl chain, then the other--a much slower process than that by a conventional monomeric surfactant molecule. By this line of reasoning, as the spacer group increases in length, the steric hindrance would decrease, allowing the Gemini to enter and exit the micelle much quicker.

Table 5-1. Comparison of experimental and literature values of 12-2-12 12-3-12, and 12-4-12 Gemini surfactant cmc.

Surfactant	cmc (mM) Literature values*	cmc (mM) Experimental values (from this study)
12-2-12	0.940 – 0.960	1.41
12-3-12	0.918 – 1.02	1.33
12-4-12	0.931 – 1.40	1.66

* Ref: Menger et al., 2000.

Figure 5-16 shows micelle stability (τ_2) of 12-2-12, 12-3-12, and 12-4-12 Gemini surfactants using the stopped-flow method with Merocyanine 540 dye. This figure clearly shows that micelle stability for these Gemini's is quite long--on the order of tens

of seconds. The figure also shows that micelle stability decreases with increasing spacer chain length, which seems to follow the above argument regarding steric hindrance of individual chains in the molecule. Another possible reason for a decrease in micelle stability with spacer chain length is the effect of molecular packing within the micelle. As Figure 5-17 demonstrates, Gemini surfactants with shorter spacer groups (e.g., 12-2-12 Gemini) are able to pack more closely in the micelle than those with longer groups (e.g., 12-4-12 Gemini). Closer packing would increase the tail-tail hydrophobic interactions and increase the stability of the monomers within the micelle.

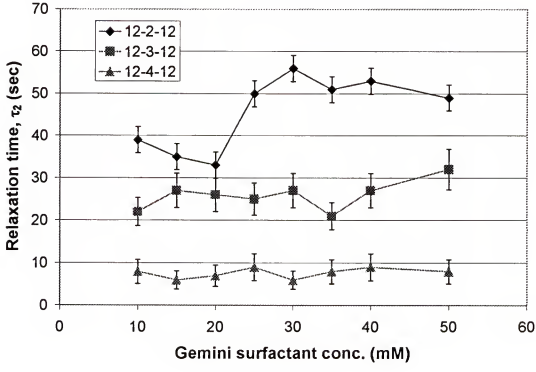

Figure 5-16. Micelle stability of 12-2-12, 12-3-12, and 12-4-12 quaternary ammonium bromide Gemini surfactants at 25 °C using stopped-flow method.

Furthermore, while the 12-3-12 and 12-4-12 Gemini show a relatively flat τ_2 profile, the data suggest that some type of transition is encountered for 12-2-12 in the 20-25 mM concentration range. As previously mentioned, Zana and Talmon (1993) have

shown the 12-2-12 Gemini to form long wormlike micelles at approximately 25 mM. It is possible that this transition is seen here. Unfortunately, the stopped-flow instrument used was unable to determine the micelle stability of these surfactants above approximately 50 mM. It was also unable to detect a noticeable transition range from spherical to cylindrical micelles for 12-3-12 and 12-4-12 Gemini surfactants.

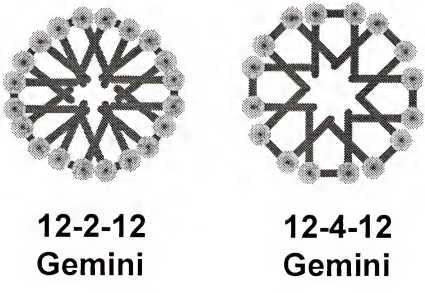

Figure 5-17. Schematic illustration of effect of Gemini spacer group on molecular packing within a micelle. 12-2-12 Gemini surfactants are able to pack closer than 12-4-12 Gemini surfactants.

5.6.3 Gemini Desorption at the Air-Water Interface

The aspect of Gemini surfactant micelles that allows them to have such high stability compared to conventional surfactants appears to be the surfactant monomer's rate constant of exit from the micelle. Similarly, the desorption rate constant of this surfactant from an interface is probably quite small (i.e., the molecule tends to remain adsorbed much longer to the interface). In order to study the desorption rate of Gemini surfactants from interfaces, a simple experiment was devised whereby small amounts of

surfactant were spread onto a clean air/water interface, and the surface tension was monitored over time (Figure 5-18).

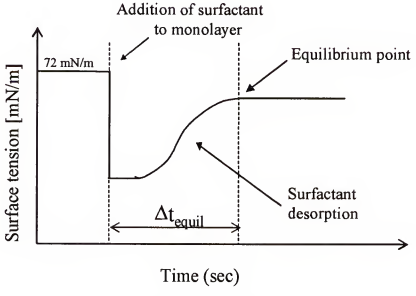

Figure 5-18. Sample surface tension vs. time curve for surfactant desorption measurements.

These curves were used to plot the surface tension (mN/m) versus time. Also obtained from these desorption data were the times required for each surfactant system to reach a new equilibrium surface tension. This time was labeled t_e (equilibration time).

Figure 5-19 is a graph of average values of surface tension vs. time for each Gemini surfactant as well as C_{12}TAB. As can be seen from this figure and from Table 5-2, all three Gemini surfactants have similar desorption characteristics and similar equilibration times. Also, these equilibration times are much longer than that of C_{12}TAB. The 12-4-12 Gemini equilibration time is shorter than the equilibration times of the other two Gemini surfactants. These results are in agreement with Ulbricht's and Zana's (2001) statement that Gemini surfactants with longer spacer groups should desorb more quickly than those with shorter spacer groups. The results are also in agreement with the

surfactant micelle kinetics data (Figure 5-16) showing the breakup time of 12-4-12 Gemini micelles to be the shortest of the three Gemini surfactants studied.

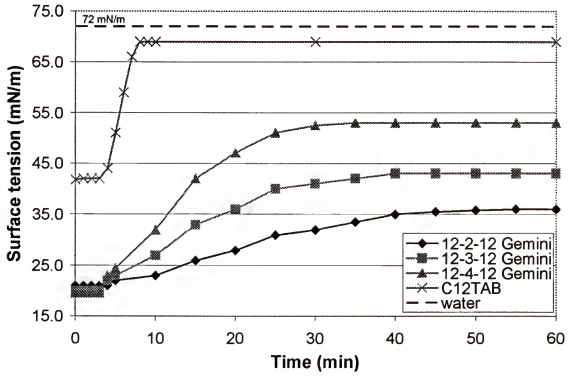

Figure 5-19. Surface tension vs. time and equilibration times (t_e) of $C_{12}TAB$ and various Gemini surfactants after spreading 100 μL of 1:1:3 methanol:chloroform:n-hexane + surfactant (1 mg/ml ratio) solution on a clean surface of 0.05 M NaCl.

Table 5-2. Equilibrium surface tension, initial desorption rate, and equilibration time of $C_{12}TAB$ and various Gemini surfactants.

Surfactant	ST_{eq} (mN/m)	$(\Delta ST/\Delta t)_o$ (mN m^{-1} min^{-1})	Equil. time (t_e) (min)
$C_{12}TAB$	69	7.4	7.2
12-2-12	36	0.43	34.3
12-3-12	43	0.86	27.7
12-4-12	53	1.75	22

The results shown in Figure 5-19 and Table 5-2 also make sense when one considers the probably molecular packing of the Gemini surfactants at the air/water interface. As Figure 5-20 suggests, 12-2-12 Gemini surfactants most likely are able to pack much closer than 12-3-12 and 12-4-12 Gemini surfactants. The increased chain-chian interactions slow the desorption of molecules from the surface to the bulk solution. Also, because surface tension is ultimately a measurement of the crowding of molecules at the interface, it is not surprising that the 12-2-12 Gemini surfactant solution yields the lowest equilibrium surface tension while 12-4-12 yields the highest surface tension of the three Gemini surfactants studied.

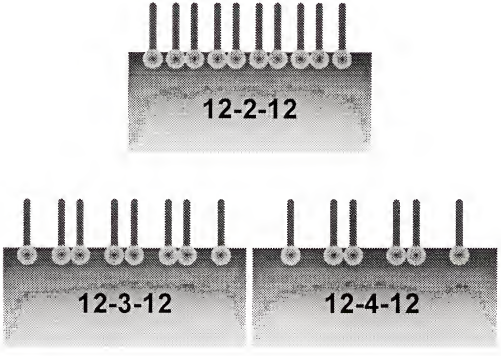

Figure 5-20. Schematic illustration of effect of Gemini spacer group on molecular packing within a monolayer. 12-2-12 Gemini surfactants are able to pack closer than 12-4-12 Gemini surfactants.

5.7 Conclusions

It has been shown that the addition of small amounts of fatty acid to a micellar solution of SDS stabilizes the micelle at low pH ($pH < pK_a$) due to a charge-shielding phenomenon similar to that encountered in the stabilization of SDS micelles using long-chain alcohol. At higher pH ($pH > pK_a$), however, the majority of fatty acid molecules have a negative charge and do not effectively reduce the repulsive force encountered by the molecules in the micelle or ionized fatty acid does not partition in the micelles. As a result, the micelle stability remains similar to values found for pure SDS. Addition of small amounts of fatty acid to a micellar solution of C_{12}TAB also stabilizes the micelle at low pH ($pH < pK_a$) due to a charge shielding effect. At higher pH ($pH > pK_a$), the micelle stability increases significantly due to the charge neutralization effect encountered between cationic C_{12}TAB molecules and anionic fatty acid molecules. Furthermore, addition of approximately 10% Triton X-100 to the SDS system increased the micelle stability four-fold.

The micelle stability of 12-2-12, 12-3-12, and 12-4-12 quaternary ammonium bromide Gemini (or dimeric) surfactants have been shown to be much higher than the stability of micelles of their monomeric equivalent surfactants (i.e., C_{12}TAB). Gemini micelle stability has been shown to be of the order of tens of seconds. The Gemini surfactants studied also have cmc values of approximately 1 mM, which is an order of magnitude lower than the cmc of C_{12}TAB (16 mM). Finally, the Gemini surfactants studied have been shown to have very slow desorption times. The desorption rate order is 12-4-12 > 12-3-12 > 12-2-12.

CHAPTER 6
CORRELATION OF PARTICULATE DISPERSION STABILITY WITH THE STRENGTH OF SELF-ASSEMBLED GEMINI SURFACTANT FILMS

6.1 Introduction

Surfactant adsorption onto solid surfaces is a phenomenon of vital importance to various industrial processes ranging from ore flotation, lubrication, and paint technology to enhanced oil recovery (Rosen, 1989). At interfaces, the self-assembly process is influenced by surfactant-surfactant, surfactant-surface, surfactant-solvent, and solvent-surface interactions. These include the free energy of adsorption, roughness, surface heterogeneities, charge, and crystallinity (Rosen, 1989).

Atomic force microscopy (AFM) has been used in the past to directly image and measure forces felt by surfactant adsorbed at the solid/liquid interface (Adler et al., 2000; Manne et al., 1994; Manne and Gaub, 1995). The main assumption is that the micellar structures, as revealed by AFM on flat pieces of mica or silica, are also present on spherical particles. Different adsorption structures are possible as depicted in Figure 6-1. Surfactant molecules can form bilayers, semi-cylinders, full cylinders, semi-spheres and full spheres adsorbed onto the surface, and it has been found that the surface has an important influence in controlling aggregate structure (Adler et al., 2000, Manne et al., 1994; Manne and Gaub, 1995). For example, in quaternary ammonium surfactant systems, mica tends to form full cylindrical micelles while amorphous silica forms full spheres (Manne et al., 1994; Ducker and Wanless, 1999). Figure 6-2 (Patist, 1999)

shows AFM images of mica immersed in water (Fig 6-2A) and in $C_{14}TAB$ cationic surfactant (Fig. 6-2B).

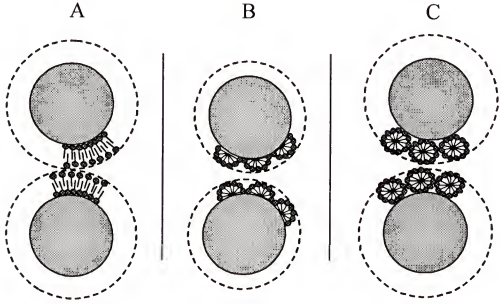

Figure 6-1 Schematic diagram showing the possible structures of surfactants adsorbed at the solid/liquid interface. A) bilayer formation; B) semi-cylindrical micelles or semi-spheres; C) full cylinders or spheres.

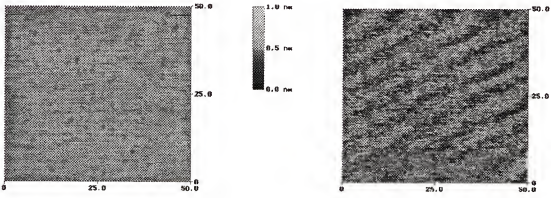

Figure 6-2. Top view AFM image of mica immersed in (A) water (pH 6), and (B) 2 cmc $C_{14}TAB$ solution (pH 6). Size: 50 by 50 nm. The diagonal stripes in (b) represent full cylindrical micelles, with an intermicellar distance of 5.2 nm.

Force-distance curves of C_nTAB samples were measured in a fluid cell using AFM contact mode. An example of a typical force-distance curve is given in Figure 6-3 (Patist, 1999).

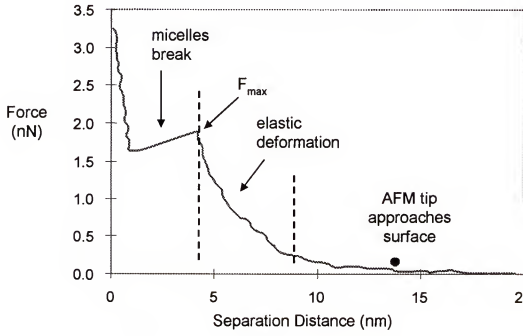

Figure 6-3. Force-distance curve for a 2 cmc $C_{12}TAB$ solution showing the different stages as the tip approaches the mica surface.

It was proposed by Patist (1999) and Adler et al. (2000) that the maximum compressive force of the adsorbed surfactant aggregates, F_{max}, is directly related to the stability of solid/liquid dispersions. This can be seen in Figure 6-4, which very clearly shows that as the $C_{12}TAB$ surfactant concentration increases from 8 to 10 mM, the interaction forces between the AFM tip and the silica substrate increase significantly and concurrently with the onset of suspension stability.

Furthermore, it was found that the chain length of the adsorbed surfactant plays an important role in the maximum repulsive force, F_{max}. As Figure 6-5 shows, F_{max} was found to increase with surfactant alkyl chain length.

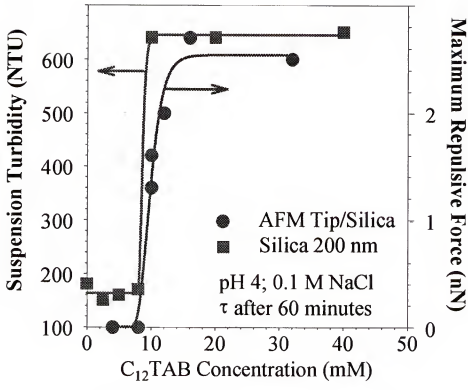

Figure 6-4. Measured interaction forces between an AFM tip and a silica substrate as well as turbidity in NTU (nephelometric turbidity units) of silica particles after 60 min in a solution of 0.4 M NaCl at pH 4 as a function of $C_{12}TAB$ concentration.

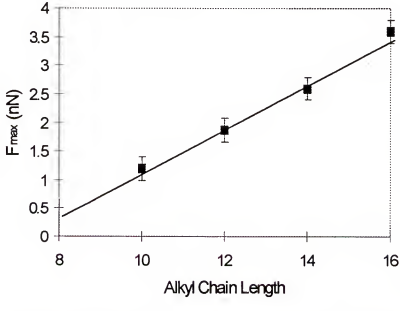

Figure 6-5. Maximum compressive force as function of alkyl chain length for 2 cmc solutions of C_nTAB (for n = 10, 12, 14 and 16) on mica.

Patist (1999) and Adler et al. (2000) found other factors influencing the magnitude of the maximum repulsive force, F_{max}. Among these are the type of substrate used as well as the presence of added co-surfactant. For example, the repulsive forces are significantly higher and first observed at lower concentrations for mica than for silica. This is possibly due to the different atomic structures of the substrates (Adler et al., 2000).

Also, addition of small amounts of SDS to a C_{12}TAB solution increases the maximum repulsive force significantly (Patist, 1999). Similarly to the increased stabilization of bulk micelles caused by charge repulsion, the addition of SDS to a C_{12}TAB solution can greatly enhanced stability at the solid/liquid interface due to the introduction of ion-ion or ion-dipole interactions. In order to show this concept a small amount of SDS was added to a C_{12}TAB solution. Figure 6-6 shows the maximum repulsive force, F_{max}, for C_{12}TAB cylindrical micelles with increasing SDS concentration. The C_{12}TAB concentration was kept constant at twice the cmc. The maximum compressive force increases linearly with SDS concentration and levels off beyond approximately 20 mol% of SDS.

Each of the above methods used to increase the maximum repulsive force, F_{max}, between the AFM tip and the solid substrate deals with the surfactant-surfactant, surfactant-surface, surfactant-solvent, and solvent-surface interactions mentioned previously. Yet another way to increase the maximum repulsive force between particles in a dispersion with adsorbed surfactants is by changing the nature of the surfactant itself. Research reported in the previous chapter on Gemini surfactant systems have shown that Gemini surfactants tend to adsorb more strongly to an interface than their monomeric

counterparts. They also form micelles at lower concentrations and have very slow micelle formation/disintegration kinetics. For this reason, it was decided to continue the study of surfactant adsorption to solids by investigating the performance of selected quaternary ammonium Gemini surfactants and comparing them to their single-chained counterparts. Specifically, the adsorption behavior of Gemini quaternary ammonium bromide surfactants onto a mica surface were investigated as a function of alkyl spacer group length using AFM. Values of F_{max} were obtained for these surfactant systems and they were compared to dispersion turbidity results to attempt to correlate the maximum repulsive force to dispersion stability.

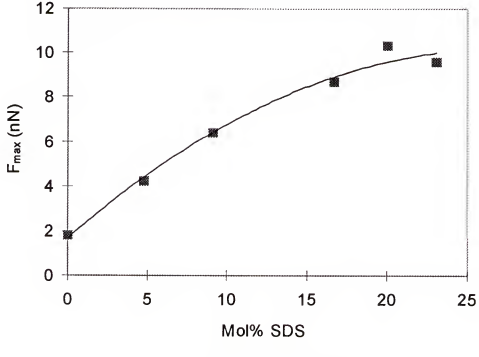

Figure 6-6. Maximum repulsive force as function of SDS concentration for a 2 cmc C_{12}TAB solution on mica.

6.2 Materials and Methods

6.2.1 Materials

Dodecyltrimethylammonium bromide (C_{12}TAB) (99%) was supplied by Acros Organics (Fair Lawn, NJ). Bis(dodecyldimethylammonium bromide) (i.e., 12-n-12) Gemini cationic surfactants with ethylene (12-2-12), propylene (12-3-12), and butylene (12-4-12) spacer groups were generously supplied by Prof. Krister Holmberg of Chalmers University in Göteborg, Sweden. Silica particles (200 nm) were obtained from Geltech Corporation (Orlando, FL). Deionized water was passed through a Milli-Q water purification system before use. All experiments were performed at 23 ± 1 °C.

6.2.2 AFM Microscopy

Force-distance curves were obtained using a Nanoscope III AFM (Digital Intruments, Santa Barbara, CA) using silicon nitride cantilevers with a spring constant of 0.12 N/m in contact mode. A freshly cleaved mica surface was placed in the cell and allowed to equilibrate with the surfactant solution for ten minutes. Manne et al. [1995] found that mica immersed for several days showed no difference in the aggregate structure, indicating that the adsorbate reaches equilibrium configuration in a few minutes. Experiments were performed with at least three freshly prepared samples on different days (Figure 6-7).

6.2.3 Turbidity/Dispersion Stability Measurements

The turbidity of dispersions of 200 nm silica particles (0.05 wt% solids at pH 4) was measured by a Hach turbidimeter, model 2100A (Hach Chemical Corporation). The intensity of scattered light at 90° was recorded versus time in NTU units (nephelometric turbidity units).

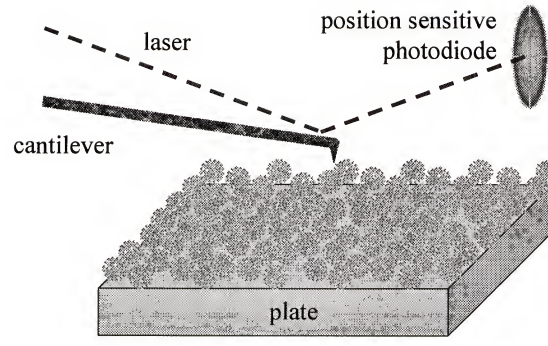

Figure 6-7. Schematic diagram of an AFM instrument.

6.2.4 Surfactant Orientation Measurements using FT-IR/ATR

FT-IR/ATR experiments were conducted on silicon single-crystal parallelepiped internal reflection elements (IRE) (55 mm x 5 mm x 2 mm, 45° incedent angle) obtained from Spectra-Tech Inc. using a nitrogen-purged Nicolet Magna 760 spectrometer equipped with a DTGS (deuterated triglycine sulfate) detector. The procedure followed is similar to that outlined by Singh et al. (2001). All the spectra were the results of 512 co-added scans at a resolution of 4 cm^{-1}. The background spectrum was measured with 0° and 90° plane-polarized light, obtained using a wire grid polarizer, to calculate the dichroic ratio (dichroism). All the spectra were obtained five times, and the result presented is the average for the measurements.

The spectra of 12-2-12 and 12-4-12 Gemini surfactants were measured at various surfactant concentrations to investigate the average orientation of hydrocarbon chains in

the surfactant films adsorbed on the crystal. Asymmetrical CH_2 stretching mode peaks (near 2920 cm^{-2}) were used for the calculation of dichroism. The order parameter (S) was calculated from the dichroism using a model developed by Rabinovich et al. (1993). An order parameter of -0.5 indicates parallel orientation of surfactant adsorbed at the surface; a value of 1.0 indicates surfactant orientation normal (perpendicular) to the surface; a value of 0 indicates a "random" orientation (Figure 6-8) (Stein, 1958; 1961).

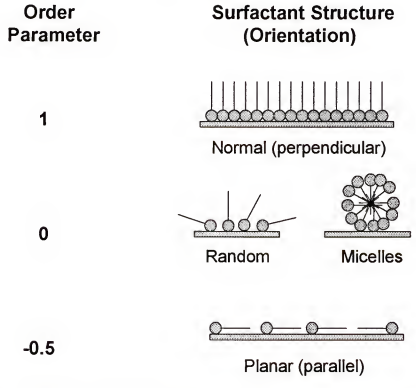

Figure 6-8. Schematic representation of the order parameter associated with adsorbed surfactant structures and orientation.

6.3 Structures of Gemini Surfactant Micelles Adsorbed at a Solid/Liquid Interface

Figure 6-9 shows AFM images of 12-2-12 and 12-4-12 Gemini surfactant adsorbed onto a mica substrate (Manne et al., 1997). As the figure shows, surface structures formed by these surfactants were found to vary with surfactant geometry. The

images indicate that 12-2-12 gave rise to featureless images indicative of a planar aggregate, while 12-4-12 forms parallel rows of cylindrical micelles or stripes similar to those of conventional CTAB surfactants (Manne et al., 1997). The measured stripe spacing (4.3 ± 0.4 nm) was a little over twice the length of a dodecane tail group, and cylinders of 12-4-12 were on average oriented parallel to the mica symmetry axes.

The images shown in Figure 6-9 obtained by Manne et al. (1997) indicate that alkyltrimethylammonium bromide Gemini surfactants with ethylene spacer groups (12-2-12) form bilayers while those with *n*-butylene spacer groups (12-4-12) form parallel rows of cylindridal micelles. This conclusion is supported by surfactant orientation measurements using FT-IR/ATR.

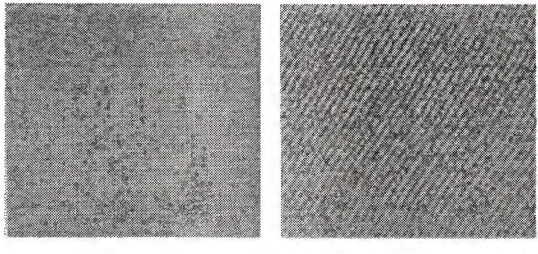

Figure 6-9. AFM images of 12-2-12 and 12-4-12 alkyltrimethylammonium Gemini surfactants on the cleavage plane of mica. 12-2-12 Gemini surfactants form a bilayer while 12-4-12 Gemini surfactants form parallel cylindrical micelles.

While a systematic study of Gemini surfactant orientation at the solid/liquid interface was not performed, preliminary experiments have shown that 12-2-12 Gemini

surfactants do indeed show a much higher order parameter when adsorbed to the silicon crystal surface than do 12-4-12 Gemini surfactants. 12-2-12 Gemini surfactants at 1.0 mM with 0.1 M NaCl added demonstrated an average orientation number of 0.388 while 12-4-12 Gemini surfactants at the same surfactant and salt concentration had an average orientation number of 0.068. The error for these experiments was ± 0.1. As Figure 6-8 shows, an orientation number greater than zero indicates adsorption normal to the surface (e.g. monolayer or bilayer), while an orientation number close to zero indicates either random orientation or spherical or cylindrical packing.

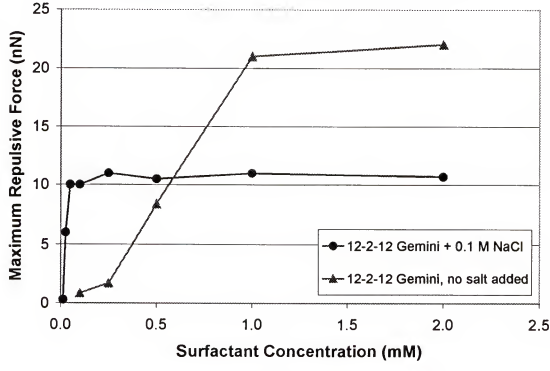

Figure 6-10. Maximum repulsive force between an AFM tip and a mica substrate in 12-2-12 alkyltrimethylammonium Gemini surfactant solution.

Figures 6-10 and 6-11 show the maximum repulsive force (F_{max}) versus surfactant concentration from force-distance experiments of 12-2-12 and 12-4-12 Gemini

surfactants, respectively, using AFM microscopy. As can be seen from these figures, the maximum repulsive force for 12-2-12 Gemini is twice that of 12-4-12 Gemini, both with and without added salt. It seems that the self-assembled bilayer formed by 12-2-12 Gemini is much more effective in repelling the AFM tip from the surface than the self-assembled cylindrical micelles formed by 12-4-12 Gemini.

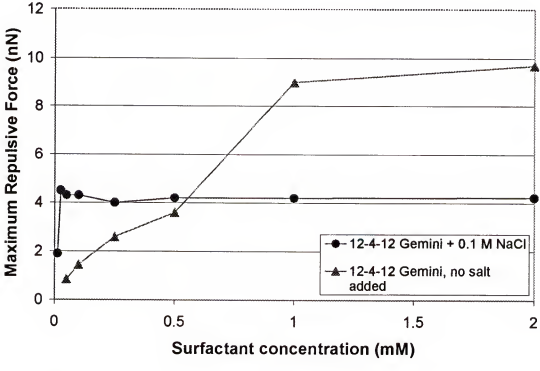

Figure 6-11. Maximum repulsive force between an AFM tip and a mica substrate in 12-4-12 alkyltrimethylammonium Gemini surfactant solution.

Interestingly, the maximum repulsive force of 12-4-12 Gemini is approximately equal to that of $C_{12}TAB$ (Figure 6-12). This makes sense since both 12-4-12 and $C_{12}TAB$ form parallel cylindrical micelles on the silica and mica surface. However, one must note the difference in concentration at onset of the repulsive barrier for 12-4-12 and $C_{12}TAB$ surfactants. $C_{12}TAB$ shows a barrier onset at 6 mM, while 12-4-12 (as well as 12-2-12) shows barrier onset at approximately 0.025 mM.

Figure 6-12 also highlights the great difference in maximum repulsive force between the bilayer structure formed by 12-2-12 Gemini and the cylindrical micelle structure formed by 12-4-12 Gemini and $C_{12}TAB$.

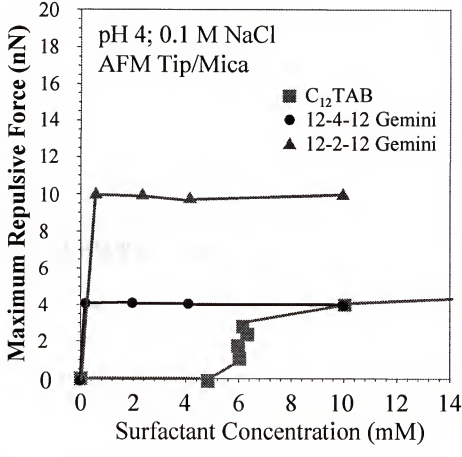

Figure 6-12. Comparison of maximum repulsive force of $C_{12}TAB$ with those of 12-2-12, and 12-4-12 Gemini surfactants.

Because Gemini surfactants demonstrate a barrier onset at concentrations well below the $C_{12}TAB$ barrier onset concentration, it makes sense that dispersion stability experiments using Gemini surfactants should show stable dispersions corresponding to these very low surfactant concentrations. Adler et al. (2000) reported the formation of a stable silica suspension in the 8-10 mM $C_{12}TAB$ concentration range. As Figure 6-13 shows, Gemini surfactants can be used to form a stable suspension at a concentration well

below 10 mM. 12-2-12 forms a stable suspension at 0.5 mM while 12-4-12 Gemini stabilizes the suspension at 1.0 mM. The difference in performance in this area between 12-2-12 and 12-4-12 Gemini is most likely attributed to the difference in maximum barrier force (Figure 6-12).

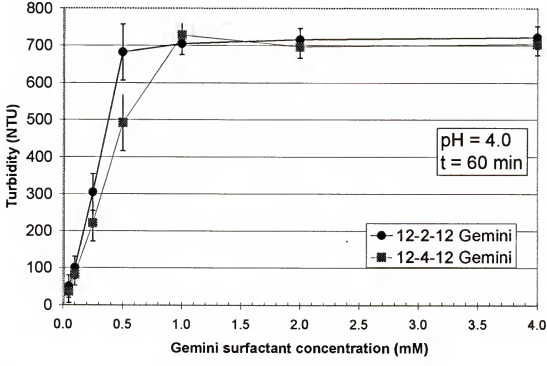

Figure 6-13. Turbidity of silica dispersions vs. concentration of 12-2-12 and 12-4-12 alkyltrimethylammonium bromide Gemini surfactants at pH 4.0 after 60 min.

6.4 Conclusions

The force-distance curves of 12-2-12 and 12-4-12 Gemini surfactants were correlated with AFM images in order to elucidate the mechanism by which these surfactants adsorb to the surface and the aggregation structures they form. Also, as mentioned earlier, the strength of the adsorbed surfactant film on particles (i.e., the stability of the adsorbed micellar layer) is an important parameter in the stability of

dispersions. The AFM force-distance results obtained for the Gemini surfactants were used along with turbidity measurements to determine how adsorption of Gemini surfactants affects dispersion stability.

CHAPTER 7
SUMMARY AND RECOMMENDATIONS FOR FUTURE WORK

7.1 Effect of pH on Molecular Interactions of Long-Chain Fatty Acids

It has been shown that soap exhibits optimum properties at a pH near its pKa in various technological processes. Specifically, foam height, foam stability and bubble lifetime show maximum values, and contact angle on PMMA and water evaporation rate show minimum values at the bulk pKa of sodium laurate. Further studies indicate that an increase in the chain length of the soap molecule results in a shift in pKa towards a greater value due to molecular cooperativity induced by van der Waals interactions between hydrophobic chains and greater interactions among polar groups.

7.2 Effect of Chain Length Compatibility and Degree of Unsaturation on Fatty Acid pKa

The results presented in this work show that the degree of unsaturation of long-chain fatty acids affects the pKa of the fatty acid. Specifically, the pKa decreases from stearic to oleic, linoleic, and linolenic acids as the degree of unsaturation increases. Results further correlate the pKa value of a long-chain fatty acid with the intermolecular distance between the fatty acid molecules as measured from monolayer experiments. The greater the intermolecular distance, the lower is the pKa value of the acid.

Furthermore, upon mixing long-chain fatty acids of unequal chain lengths, pKa value decreases as compared with those of pure acids. This decrease is due to increased area per molecule caused by thermal motion of the mismatched chains. Retardation of

water evaporation from the films of pure vs. mixed fatty acids were carried out to show that the greater evaporation occurs in mixed films, indicating poorer molecular packing and hence increased intermolecular distance, and greater rate of evaporation.

7.3 Effect of Premicellar Aggregation on Fatty Acid pKa

It has been shown that an increase in the chain length of a fatty acid from C_8 to C_{18} increases the apparent pKa of the solution. However, fatty acids of chain length C_6 and below have a constant pKa of about 4.8. pKa values are found to decrease upon dilution of C_8-C_{12} fatty acid solutions below cmc. However, they have to be reduced from 10^{-6} to 10^{-11} M to reach the pKa of short chain fatty acids, by extrapolation. These results indicate that even in nanomolar solutions of fatty acids of C_8-C_{12}, substantial molecular association exists in *premicellar aggregates* and in an *adsorbed film*. The association between the ionized and unionized polar groups in such premicellar aggregates will shift the measured pKa to a higher value than 4.8 for true monomers, depending upon its intermolecular distance.

7.4 Kinetics of Mixed and Gemini Micelles

It has been shown that the addition of small amounts of fatty acid to a micellar solution of SDS stabilizes the micelle at low pH ($pH < pK_a$) due to a charge-shielding phenomenon similar to that encountered in the stabilization of SDS micelles using long-chain alcohol. At higher pH ($pH > pK_a$), however, the majority of fatty acid molecules have a negative charge and do not effectively reduce the repulsive force encountered by the molecules in the micelle or ionized fatty acid does not partition in the micelles. As a result, the micelle stability remains similar to values found for pure SDS. Addition of small amounts of fatty acid to a micellar solution of C_{12}TAB also stabilizes the micelle at

low pH ($pH < pK_a$) due to a charge shielding effect. At higher pH ($pH > pK_a$), the micelle stability increases significantly due to the charge neutralization effect encountered between cationic $C_{12}TAB$ molecules and anionic fatty acid molecules. Furthermore, addition of approximately 10% Triton X-100 to the SDS system increased the micelle stability four-fold.

The micelle stability of 12-2-12, 12-3-12, and 12-4-12 quaternary ammonium bromide Gemini (or dimeric) surfactants have been shown to be much higher than the stability of micelles of their monomeric equivalent surfactants (i.e., $C_{12}TAB$) (see Figure 5-16). Gemini micelle stability has been shown to be of the order of tens of seconds. The Gemini's studied also have cmc values of approximately 1 mM, which is an order of magnitude lower than the cmc of $C_{12}TAB$ (16 mM). Finally, the Gemini surfactants studied have been shown to have very slow desorption rates as compared to $C_{12}TAB$. The desorption rate order is 12-4-12 > 12-3-12 > 12-2-12.

7.5 Dispersion of Particles Using Gemini Surfactants

The force-distance curves of 12-2-12 and 12-4-12 Gemini surfactants were correlated with AFM images in order to elucidate the mechanism by which these surfactants adsorb to the surface and the aggregation structures they form. Also, the strength of the adsorbed surfactant film on particles (i.e., the stability of the adsorbed layer) was correlated to the stability of dispersions. The AFM force-distance results obtained for the Gemini surfactants were used along with turbidity measurements to determine how adsorption of Gemini surfactants affects dispersion stability.

7.6 Recommendations for Future Work

7.6.1 Fatty Acids

The understanding of the effect of fatty acid chain length and structure on molecular interactions in fatty acid soap solutions is not yet complete. Recommendations for further research and development are given below:

1) Pressure-jump and stopped-flow experiments could be designed to explore the formation and breakup kinetics of fatty acid soap micelles in the spherical and cylindrical micelle concentration range as a function of pH.

2) Adsorption/desorption experiments at the air/water and oil/water interfaces could be conducted as a function of solution pH using the Wilhelmy plate surface tension method. These experiments would provide further insight as to the molecular interactions of fatty acid soaps in a monolayer.

3) Items (1) and (2) above could be repeated with different and mixed fatty acid chain lengths, or with addition of cationic surfactant (e.g. 1%, 5%, 10%, 25% dodecylamine added to lauric acid solution).

5) A thorough investigation of dynamic surface tension, equilibrium interfacial tension, and micelle stability could be performed for the C_{12} soap+oil+water or C_{12} soap+water+air systems.

6) Infrared spectroscopy (IR or FT-IR) studies to quantitatively determine the ratio of R-COOH to $R\text{-}COO^-$ and acid-soap complex present in solution at a given pH could be performed to further study the molecular interactions in bulk solution or at an interface.

7.6.2 Gemini Surfactant Micelle Kinetics

Research on the new types of surfactants called Gemini surfactants is still in its infancy. Particularly the effect that these surfactants have on micelle stability in pure and mixed solutions has yet to be thoroughly explored. Recommendations for further research on the kinetics of Gemini and mixed micelles are given below:

1) Once the pressure-jump apparatus is again operational, pressure-jump studies of 12-s-12 Gemini surfactants should be conducted immediately to verify results obtained by stopped-flow.

2) Pressure-jump and stopped-flow studies of mixed systems containing Gemini, SDS, and/or nonionic surfactants should be performed to determine the change in micelle kinetics caused by mixing Gemini's with other surfactants.

3) Pressure-jump studies of Gemini surfactants with different chains and spacers (e.g., unsaturated or branched chains) should be performed to determine how Gemini structure affects kinetics of micelle formation and disintegration.

7.6.3 Dispersion Stability Using Surfactants

The ability to use the mechanical strength of surfactant aggregates adsorbed at the solid/liquid interface to stabilize a particulate dispersion is a novel and promising line of research. Below are several recommendations for further research on dispersion stability using surfactants:

1) Add SDS to Gemini surfactant solution to see how much it increases the maximum repulsive force, F_{max}, by AFM force-distance plot.

2) Maximize barrier strength (F_{max}) by adding oppositely charged surfactants, cosurfactants, salts, or polymers to the Gemini system, and correlate with the dispersion stability or shelf-life of the dispersion.

3) Conduct a systematic study of Gemini surfactant orientation using FT-IR/ATR method.

4) Study kinetics of adsorption and desorption of surfactants at the solid/liquid, air/water, and oil/water interfaces, and correlate to dispersion stability and shelf life of product.

7.7 Publications

1. **Kanicky, J. R.** and Shah, D. O., Effect of Premicellar Aggregation on the pKa of Fatty Acid Soap Solutions, *Langmuir* (in press).

2. **Kanicky, J. R.** and Shah, D. O., Effect of Degree, Type and Position of Unsaturation on the pKa of Long-Chain Fatty Acids, *J. Colloid Interface Sci.* 256 (1), 1, 2002 (in press).

3. Patist, A., **Kanicky, J. R.**, Shukla, P. K., and Shah, D. O., Importance of Micellar Kinetics in Relation to Technological Processes, *J. Colloid Interface Sci.* 245 (1), 1, 2002 **(feature article)**.

4. **Kanicky, J. R.**, Lopez-Montilla, J. C., Pandey, S., and Shah, D. O., Surface Science in the Petroleum Industry, in K. Holmberg (Ed.), Handbook of Applied Colloid and Surface Chemistry, Wiley, 2001.

5. Bagwe, R.P., **Kanicky, J. R.**, Palla, B.J., Patanjali, P.K. and Shah, D.O., Improved Drug Delivery Using Microemulsions: Rationale, Recent Progress and New Horizons, *Critical Reviews™ in Therapeutic Drug Carrier Systems* **18** (1), 77-140, 2001.

6. **Kanicky, J. R.**, Poniatowski, A. F., Mehta, N. R., and Shah, D. O., Cooperativity Among Molecules at Interfaces in Relation to Various Technological Processes: Effect of Chain Length on the pKa of Fatty Acid Salt Solutions, *Langmuir* **16**, 172-177, 2000.

7. **Kanicky, J. R.**, Patist, A., Oh, S. G., and Shah, D.O., Performance Characteristics and Design Strategies for the 21st Century Laundry Detergent, Proceedings of the 39th International Detergency Conference, Luxembourg, Sept. 6-8, 1999.

8. Pillai, V., **Kanicky, J. R.**, and Shah, D. O., Applications of Microemulsions in Enhanced Oil Recovery, in P. Kumar and K. L. Mittal (Eds.), Handbook of Microemulsion Science and Technology, New York: Marcel Dekker, Inc., 1999.

9. Jha, B. K., **Kanicky, J. R.**, Patist, A., Subramani, S., Patel, H. and Shah, D.O., Performance Characteristics and Design Strategies for the 21st Century Laundry Detergent, Proceedings of the New Horizons Conference sponsored by AOCS & CMS, Williamsburg, VA, Sept. 16-18, 1998.

APPENDIX A
DETERMINATION OF AREA/MOLECULE OF AN ADSORBED SURFACTANT MONOLAYER USING THE GIBBS ADSORPTION ISOTHERM

This appendix will discuss the thermodynamic treatment of the variation of surface tension with concentration, and show how the Gibbs Equation can be used to calculate area per molecule and intermolecular distance of an adsorbed monomolecular film. The treatment is due to Gibbs (1931) but has been amplified in a more convenient readable way by Guggenheim and Adam (1933). We now proceed to the derivation of the 3rd fundamental equation of surface chemistry (the Laplace and Kelvin equations are the other two), known as the *Gibbs Equation.*

For a small, reversible change dE in the energy of a system, one has (Adamson and Gast, 1997)

$$dE = dE^{\alpha} + dE^{\beta} + dE^{\sigma} \tag{A.1}$$

where

$$dE^{\alpha} = T\,dS^{\alpha} + \sum(\mu_i\,dn_i^{\alpha}) - P^{\alpha}\,dV^{\alpha} \tag{A.2}$$

$$dE^{\beta} = T\,dS^{\beta} + \sum(\mu_i\,dn_i^{\beta}) - P^{\beta}\,dV^{\beta} \tag{A.3}$$

$$dE^{\sigma} = T\,dS^{\sigma} + \sum(\mu_i\,dn_i^{\sigma}) + \gamma\,dA \tag{A.4}$$

α and β are two separate phases, σ represents the surface or interface, S is entropy, T is temperature, μ_i is the chemical potential of species i, n_i is the number of moles of i, P is pressure, V is volume, A is area, and γ is the surface or interfacial tension.

If one allows the energy, entropy, and amounts (n_i) to increase from zero to some finite value, keeping T, A, and n_i^σ constant, Equation A.4 becomes

$$E^\sigma = T S^\sigma + \Sigma(\mu_i \, dn_i^\sigma) + \gamma A \tag{A.5}$$

Equation A.5 is generally valid and may now be differentiated in the usual manner to give

$$dE^\sigma = T \, dS^\sigma + S^\sigma dT + \Sigma(\mu_i \, dn_i^\sigma) + \Sigma(n_i^\sigma d\mu_i) + \gamma dA + A \, d\gamma \tag{A.6}$$

If Equation A.6 is set equal to Equation A.4, one gets

$$0 = S^\sigma dT + \Sigma(n_i^\sigma d\mu_i) + A \, d\gamma \tag{A.7}$$

or, per unit area:

$$d\gamma = -S^\sigma dT - \Sigma(\Gamma_i^\sigma d\mu_i) \tag{A.8}$$

where Γ_i^σ denotes the surface excess per unit area.

For solutions consisting of the solvent and only one solute (i.e., for a two-component system) at constant temperature, Equation A.8 reduces to

$$d\gamma = -\Gamma_1^\sigma d\mu_1 - \Gamma_2^\sigma d\mu_2 \tag{A.9}$$

But (Atkins, 1990)

$$\mu_i = \mu_i^* + RT \ln a_i \tag{A.10}$$

where μ_i^* is the chemical potential of pure i, and a_i ($= x_i f_i$) is the activity, x_i is mole fraction, and f_i is activity coefficient of i. So Equation A.10 becomes

$$d\gamma = -RT(\Gamma_1^\sigma d \ln a_1 - \Gamma_2^\sigma d \ln a_2) \tag{A.11}$$

For dilute solutions (10^{-2} M or less) (Rosen, 1989) containing only one nondissociating surface-active solute, the activity of the solvent and the activity

coefficient of the solute can both be considered to be constant and the mole fraction of the solute x_2 may be replaced by its molar concentration C_2. Thus

$$d\gamma = -RT\,\Gamma_2^{\sigma}\,d\ln C_2 \qquad \text{(A.12)}$$

However, calculations are easier to perform with the log_{10} of concentration rather than log_e (i.e., *ln*). *Ln* is 2.303 times as large as log_{10}. Therefore, we can use log_{10} in Equation A.12 as long as we multiply by 2.303. What results is the form of the *Gibbs Equation* used for calculation of area/molecule of ***nonionic surfactants*** containing no other materials:

$$d\gamma = -2.303\,RT\,\Gamma\,d\log C \qquad \text{(A.13)}$$

or

$$\boxed{\Gamma = -\frac{1}{2.303\,RT}\frac{d\gamma}{d\log C}} \qquad \text{(A.14)}$$

For solutions of a completely dissociated surfactant of the 1:1 electrolyte type, A^+B^-, as the only solute,

$$d\gamma = -RT\,(\Gamma_A^+\,d\ln a_A^+ - \Gamma_B^-\,d\ln a_B^-) \qquad \text{(A.15)}$$

Since $\Gamma_A^+ = \Gamma_B^- = \Gamma$ to maintain electroneutrality and $a_A^+ = a_B^- = C \times f_{\pm}$ without significant error, then

$$d\gamma = -2RT\,\Gamma d\,(\ln C + \ln f_{\pm}) \qquad \text{(A.16)}$$

where $f_{\pm}$ is the mean activity coefficient of the surfactant. For dilute solutions (10^{-2} M or less),

$$d\gamma = -2RT\,\Gamma d\ln C \qquad \text{(A.17)}$$

or written in log_{10} form:

$$d\gamma = -4.606\,RT\,\Gamma\,d\log C \qquad \text{(A.18)}$$

or

$$\boxed{\Gamma = -\frac{1}{4.606\,RT}\frac{d\gamma}{d\log C}} \qquad (A.19)$$

(for ***ionic surfactants***) without significant error.

For mixtures of ionic and nonionic surfactants in aqueous solution in the absence of added electrolyte, the coefficient decreases from 4.606 to 2.303 with a decrease in the concentration of the ionic surfactant at the interface.

The Gibbs Equation can also be written in the form:

$$\boxed{\Gamma = -\frac{1}{2.303\,nRT}\frac{d\gamma}{d\log C}} \qquad (A.20)$$

where n takes the value 2 for an ionic surfactant where the surfactant ion and counterion are univalent, and 3 for a dimeric (i.e., Gemini) surfactant made up of a divalent surfactant ion and two univalent counterions, in the absence of a swamping electrolyte.

For dilute solutions of a completely dissociated surface-active 1:1 electrolyte in the presence of a swamping, constant amount of electrolyte containing a common non-surfactant counterion, one can use $n = 1$ since under these conditions the change in activity of the non-surfactant common ion with adsorption is zero.

Γ is the surface excess per unit area of surfactant measured, and has units of [moles/area].

Given a series of surface tension (γ) versus concentration data, one simply needs to select the portion of their data to include in the calculation, and plot it on a γ vs. logC graph. The slope of the resulting line is equal to the ($d\gamma$/dlogC) term in Equations A.14 and A.19.

Care must be taken when choosing units of surface tension (i.e., mN/m vs. dynes/cm), because these units must match with those in the gas constant, R. In order to calculate area/molecule, one may simply multiply Γ by Avogadro's number, N_{Av}, and take the inverse of the product:

$$\text{Area per molecule} = (N_{Av}\,\Gamma)^{-1} \quad \text{with units of [area/molecule]} \tag{A.21}$$

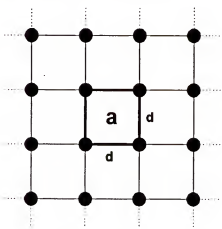

Figure A-1. Area per molecule of an adsorbed monolayer.

If we assume that the molecules are arranged in a square grid-like pattern (see Figure A-1), the area per molecule can be thought of as one square in this grid, and therefore the intermolecular distance is equal to a side of the square, and can be calculated by taking the square root of area/molecule.

Sample Calculations

Given the following data (nonionic species):

C (mM)	γ (mN/m)
4.50	28.8
2.25	30.4
1.12	31.8
0.56	40.2
0.28	52.7
0.14	62.7
0.07	69.3
0.04	71.9
0.02	71.9

Plot data on a γ vs. logC graph, draw line through linear portion, and set the slope of this line equal to (dγ/dlogC). The units for slope in this particular example are [dynes/cm] (logC has no units). For this example, the slope is -14.07 dynes/cm.

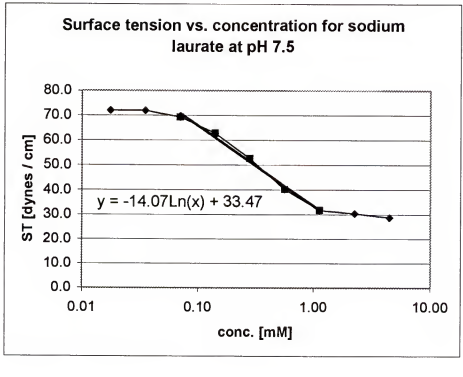

Choose a value for temperature, T, in Kelvin temperature units. For this example, T = 298 K. Choose a value for R, the gas constant, and convert to proper units

e.g., R = 0.08206 *l atm mol*$^{-1}$ *K*$^{-1}$

After unit conversion: R = 8.3147 x 10^{7} *dynes cm mol*$^{-1}$ *K*$^{-1}$

Plug all these values into Equation A.14:

$$\Gamma = -\frac{1}{2.303RT}\frac{d\gamma}{d\log C}$$

Γ = -(1 / 4.606 / 8.3147 x 10^{7} [dynes cm mol^{-1} K^{-1}/ 298 [K]) * (-14.07 [dynes/cm])

Γ = 2.466 x 10^{-10} mol cm^{-2}

Convert area to Å^{2}:

Γ = 2.466 x 10^{-26} mol Å^{-2}

Area per molecule = $(N_{Av}\,\Gamma)^{-1}$

Area per molecule = [(6.023 x 10^{23} [molecules mol^{-1}]) * (2.466 x 10^{-26} [mol Å^{-2}])]$^{-1}$

Area per molecule = 67.3 ≈ **<u>67 Å^{2} / molecule</u>**

Intermolecular distance = (area per molecule)$^{1/2}$

Intermolecular distance = (67.3 [Å^{2} / molecule])$^{1/2}$

Intermolecular distance = 8.2 ≈ **<u>8 Å</u>**

APPENDIX B
AREA/MOLECULE CALCULATIONS OF VARIOUS GEMINI SURFACTANTS

In this appendix, the thermodynamic concepts presented in Appendix A are used to calculate the area per molecule and intermolecular distance of bis(dodecyldimethylammonium bromide) (i.e., 12-n-12) Gemini cationic surfactants with ethylene (12-2-12), propylene (12-3-12), and butylene (12-4-12) spacer groups using surface tension versus concentration data for each of these surfactants. The surface tension versus concentration plots of each of these surfactants was presented in Figure 5-15, and is recreated in Figure B-1 for convenience.

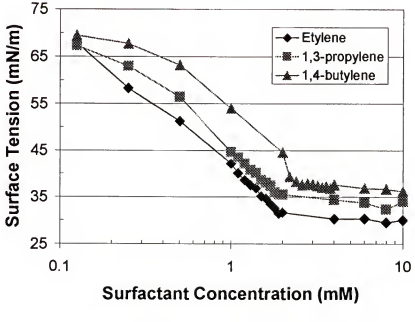

Figure B-1. Surface tension vs. surfactant concentration for 12-2-12, 12-3-12, and 12-4-12 quaternary ammonium bromide Gemini surfactants.

In order to calculate area per molecule, one must first determine the concentration at which this value will be calculated. As can be seen in Figure B-1, when concentration is graphed on a log plot, there exist two unique parts to the resulting curve: a linear dependence of surface tension on concentration below cmc, and another linear dependence above cmc. Because we are interested in the area per molecule prior to cmc, that is where the line fit will be made. The resulting line fit for each surfactant, along with the equations for each line, are shown in Figure B-2.

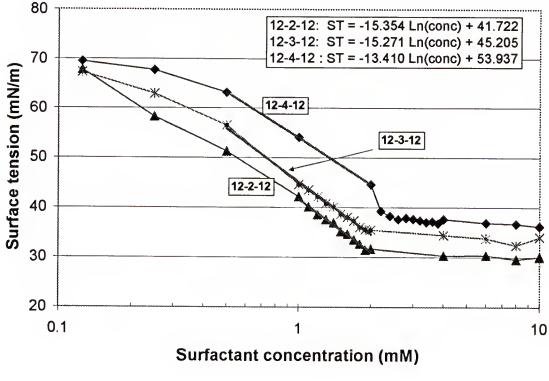

Figure B-2. Line fit of surface tension vs. concentration curves of 12-2-12, 12-3-12, and 12-4-12 quaternary ammonium bromide Gemini surfactants.

The slope of each line is obtained from the equations in Figure B-2. The area per molecule can then be calculated from the equation:

$$\Gamma = -\frac{1}{2.303\, nRT}\frac{d\gamma}{d\log C} \qquad \text{(A.20)}$$

where $n = 2$ for ionic Gemini surfactants on the assumption that one of the two charged groups is neutralized by a bound counterion, or $n = 3$ if it assumed that the Gemini surfactant is completely dissociated from its counterions (Zana, 2002). Li et al. (1999) found using neutron reflectivity that most Gemini surfactants in the 12-s-12 series tend to fit in the $n = 2$ category. Therefore, $n = 2$ was used for the calculations below.

For the 12-2-12 Gemini surfactant:

$n = 2$

R = 8.3147×10^7 *dynes cm* mol^{-1} K^{-1}

$\Gamma = -(1 / 4.606 / 8.3147 \times 10^7$ [dynes cm mol^{-1} K^{-1}/ 298 [K]) * (-15.35 [dynes/cm])

$\Gamma = 1.345 \times 10^{-10}$ mol cm^{-2}

Convert area to $Å^2$:

$\Gamma = 1.345 \times 10^{-26}$ mol $Å^{-2}$

Area per molecule = $(N_{Av}\,\Gamma)^{-1}$

Area per molecule = $[(6.023 \times 10^{23}$ [molecules mol^{-1}]) * $(1.345 \times 10^{-26}$ [mol $Å^{-2}$])$]^{-1}$

Area per molecule = 123.4 ≈ **<u>123 $Å^2$ / molecule</u>**

Intermolecular distance = (area per molecule)$^{1/2}$

Intermolecular distance = (123.4 [$Å^2$ / molecule])$^{1/2}$

Intermolecular distance = 11.11 ≈ **11 Å**

Similar calculations for the 12-3-12 and 12-4-12 Gemini surfactants yield the results in Table B-1.

Table B-1. Tabulated values of area per molecule and intermolecular distance of 12-2-12, 12-3-12, and 12-4-12 quaternary ammonium bromide Gemini surfactants adsorbed at the air/water interface at concentrations below cmc (C ~ 1mM).

Gemini Surfactant	Slope (mN/m)	Γ (mol/cm^2)	Γ (mol/Å^2)	Area per molecule (Å^2/molecule)	Intermolecular Distance (Å)
12-2-12	15.35	1.34E-10	1.34E-26	123.4	11.11
12-3-12	15.27	1.34E-10	1.34E-26	124.1	11.14
12-4-12	13.41	1.18E-10	1.18E-26	141.3	11.89

APPENDIX C
CALCULATION OF GEMINI SURFACTANT MONOLAYER DESORPTION RATES

This appendix describes the calculations performed to obtain the initial rates of desorption and times required to reach equilibrium surface tension for $C_{12}TAB$ and various Gemini surfactants spread onto a clean surface of 0.05 M NaCl. Calculations are based on results shown in Figure 5-19, which has been reproduced below and labeled Figure C-1.

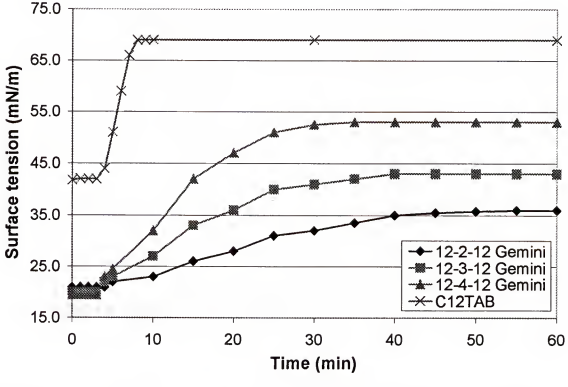

Figure C-1. Surface tension (mN/m) vs. time and equilibration times (t_e) of $C_{12}TAB$ and various Gemini surfactants after spreading 100 μL of 1:1:3 methanol:chloroform:n-hexane + surfactant (1 mg/ml ratio) solution on a clean surface.

When comparing the rates of desorption of the different surfactants, of particular interest are the initial desorption rates. Figure C-1 shows an initial constant surface tension that is a result of depositing an excess amount of surfactant at the surface. As the surfactant desorbs from the air/water interface and enters the bulk solution, the surface tension begins to increase at a constant rate, resulting in a linear portion of the surface tension vs. time graph. Figure C-2 shows curve fits of the initial change in surface tension with time of each surfactant, which can be directly correlated to the desorption rate of the surfactant. The relative initial rates of desorption can be determined from the slope of each line (see equations in Figure C-2).

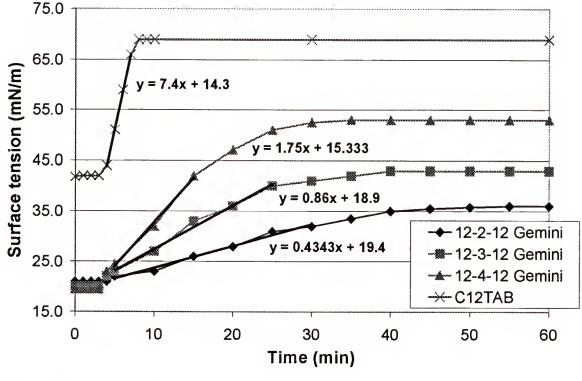

Figure C-2. Line fit of initial surface tension vs. time curves of C_{12}TAB as well as 12-2-12, 12-3-12, and 12-4-12 quaternary ammonium bromide Gemini surfactants.

The initial rate of change in surface tension of $C_{12}TAB$ is 7.4 mN m^{-1} min^{-1}. The initial "desorption" rates of 12-2-12, 12-3-12, and 12-4-12 Gemini surfactants are much lower: 0.43, 0.86, and 1.75 mN m^{-1} min^{-1}, respectively.

Equilibration time (t_e) was determined by drawing tangent lines at the initial linear surface tension vs. time plot and at the final equilibrium values of each surfactant (Figure C-3). The equilibration time was taken as the time corresponding to the intersection of these two lines. As Figure C-3 shows, the equilibration times for $C_{12}TAB$, 12-2-12 Gemini, 12-3-12 Gemini, and 12-4-12 Gemini are approximately 7.2, 34.3, 27.7, and 22 minutes, respectively.

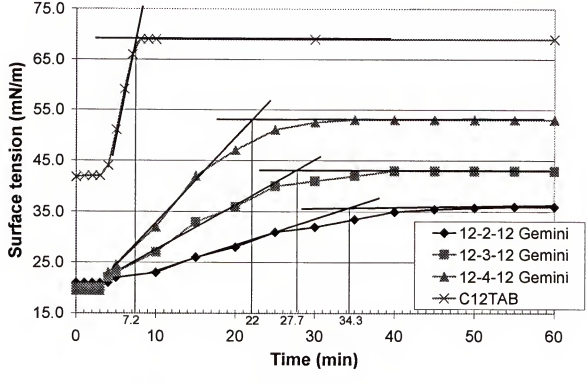

Figure C-3. Determination of equilibration time (t_e) by construction of intersecting lines.

LIST OF REFERENCES

Acosta-Rivera, S. L., *Factors Influencing Foaming Ability and Foam Stability*, Master's Thesis, University of Florida, 1994.

Adam, N. K., *Proc. Roy. Soc. (London)* **A99**, 336 (1921).

Adam, N. K., and Miller, J. G. F., *Proc. Roy. Soc. (London)* **A142**, 401 (1933).

Adamson, A. W., and Gast, A. P., *Physical Chemistry of Surfaces*, John Wiley & Sons (6th ed.), New York, 1997.

Adler, J. J., Singh, P. K., Patist, A., Rabinovich, Y. I., Shah, D. O., and Moudgil, B. M., *Langmuir* **16**, 7255 (2000).

Ahn, D. J., and Franses, E. I., *J. Chem Phys.* **95**, 8486 (1991).

Allen, M. P., and Tildesley, D. J., *Computer Simulation of Liquids*, Oxford University Press, New York, 1987.

Ananthapadmanabhan, K. P., *Associative Interactions in Surfactant Solutions and Their Role in Floatation*, Ph.D. Dissertation, Columbia University, 1980.

Aniansson, E. A. G., *Progr. Coll. Polym. Sci.* **70**, 2 (1985).

Aniansson, E. A. G., and Wall, S. N., *J. Phys. Chem.* **78**, 1024 (1974).

Aniansson, E. A. G., and Wall, S. N., *J. Phys. Chem.* **79**, 857 (1975).

Aniansson, E. A. G., Wall, S. N., Almgren, M., Hoffmann, H., Kielmann, I., Ulbricht, W. J., Zana, R., Lang, J. and Tondre, C., *J. Phys. Chem.* **80**, 905 (1976).

Atkins, P. W., *Physical Chemistry*, W. H. Freeman & Co. (4th ed.), New York, 1990.

Attwood, D., and Florence, A. T., *Surfactant Systems*, Chapman and Hall, New York, 1983.

Bangs, L. B., *Surfactant Dimers and Their Adsorption*, Ph.D. Dissertation, Massachusetts Institute of Technlogy, 1964.

Bennion, B. C., and Eyring, E. M., *J. Colloid Interface Sci.* **32**, 286 (1970).

Bennion, B. C., Tong, L. K. J., Holmes, L. P., and Eyring, E. M., *J. Phys. Chem.* **73**, 3288 (1969).

Bergethon, P. R., and Simons, E. R., *Biophysical Chemistry: Molecules to Membranes*, Springer-Verlag, New York, 1990.

Bernheim-Groswasser, A., Zana, R., and Talmon, Y., *J. Phys. Chem. B* **104**, 4005 (2000).

Budavari, S. (Ed.), *Merck Index*, Merck Research Labs (12th ed.), Whitehouse Station, NJ, 1996.

Care, C. M., *J. Phys. C: Solid State Phys.* **20**, 689 (1987).

Chandler, D., *Introduction to Modern Statistical Mechanics*, Oxford University Press, New York, 1987.

Chattopadhyay, A. K., Ghaicha, L., Oh, S. G., and Shah, D. O., *J. Phys. Chem.* **96**, 6509 (1992).

Christodoulou, A. P., and Rosano, H. L., *Adv. Chem. Ser.* **84**, 210 (1968).

Cook, M. A., *J. Phys. Colloid Chem.* **55**, 383 (1951).

Cooke, S. R. B., Iwasaki, I., and Choi, H. S., *Trans. AIME* **217**, 76 (1960).

Davies, J. T. and Rideal, E. K., *Interfacial Phenomena*, Academic Press, New York, 1961.

Davies, J. T., and Rideal, E. K., *Interfacial Phenomena*, Academic Press (2nd ed.), New York, 1963.

Dawson, R. M. C. (Ed.), *Data for Biochemical Research*, Clarendon Press, Oxford, 1959.

De Castro, F. H. B., and Borrego, A. G., *J. Colloid Interface Sci.* **173**, 8 (1995).

DeBolt, S. E., and Kollman, P. A., *J. Am. Chem. Soc.* **117**, 5316 (1995).

Devinsky, F., Lacko, I., Bittererova, F., and Tomeckova, L., *J. Colloid Interface Sci.* **114**, 314 (1986).

Devinsky, F., Lacko, I., Mlynarcik, D., Racansky, V., and Krasnec, L., *Tensides Detergents* **22**, 1 (1985).

Ducker, W. A., and Wanless, E. J., *Langmuir* **15**, 160 (1999).

Dutta, P., *Colloids Surfaces A* **171**, 59 (2000).

Eagland, D. and Franks, F., *Trans. Far. Soc.* **61**, 2468 (1965).

Ekwall, P., *Kolloid Z.* **92**, 141 (1940).

Ekwall, P., in *Chemistry, Physics and Applications of Surface Active Sustances* (p. 98), J. Th. G. Overbeek (Ed.), Gordon and Breach Science Publisher, New York, 1967.

Ekwall, P., and Lindblad, L. G., *Kolloid Z.* **94**, 42 (1941).

Esselink, K., Hilbers, P., van Os, N., Smit, B., and Karaborni, S., *Colloid Surf.* **91**, 155 (1994).

Fainerman, V. B., Miller, R., and Joos, P., *Colloid Polym. Sci.* **272**, 731 (1994).

Fainerman, V. B., Vollhardt, D., and Johann, R., *Langmuir* **16**, 7731 (2000).

Fang, H., and Shah, D. O., *J. Colloid Interface Sci.* **205**, 531 (1998).

Fendler, J., *Catalysis in Micellar and Macromolecular Systems*, Academic Press, New York, 1975.

Fox, M. A., and Whitesell, J. K., *Organic Chemistry*, Jones and Barlett, Boston, 1994.

Franks, F., Quickender, M. J., Ravenhill, J. R. and Smith, H. T., *J. Phys. Chem.* **72**, 2668 (1968).

Frenkel, D., and Smit, B., *Understanding Molecular Simulation. From Algorithms to Applications*, Academic Press, London, 1996.

Frindi, M., Michels, B., and Zana, R., *J. Phys. Chem.* **98**, 6607 (1994).

Garrett, P. R., and Ward, D. R., *J. Colloid Interface Sci.* **132**, 475 (1989).

Gibbs, J. W., *The Collected Works of J. W. Gibbs* (Vol. I), Longmans & Green, New York, 1931, p. 219.

Gloxhuber, C., and Kunstler, K., *Anionic Surfactants: Biochemistry, Toxicology, Dermatology*, Marcel Dekker (2nd ed.), New York, 1992.

Goddard, E. D., and Ackilli, J. A., *J. Colloid Sci.* **18**, 585 (1963).

Goddard, E. D., Goldwasser, S., Goliken, G., and Kung, H. C., *Advan. Chem. Ser.* **84**, 67 (1968).

Gormally, J., Gettings, W. J., and Wyn-Jones, E., in *Molecular Interactions* (Vol. 2, p. 143), H. Ratajczak and W. J. Orville-Thomas (Eds.), Wiley, New York, 1980.

Graber, E., and Zana, R., *Kolloid-Z. Z. Polym.* **238**, 479 (1970).

Gratzel, M., and Kalyanasundaram, K., *Kinetics and Catalysis in Microheterogeneous Systems*, Marcel Dekker, New York, 1991.

Guggenheim, E. A., and Adam, N. K., *Proc. Roy. Soc. (London)* **A139**, 218 (1933).

Haliloglu, T., and Mattice, W. L., *Chem. Eng. Sci.* **49**, 2851 (1994).

Hall, D. G., *J. Chem. Soc. Faraday Trans. I* 77, 1973 (1981).

Halliday, D., Resnick, R., and Walker, J., *Fundamentals of Physics*, John Wiley & Sons (4th ed.), New York, 1993.

Hartley, G. S., *Aqueous Solutions of Paraffin-Chain Salts*, Hermann, Paris, 1936.

Hartley, G. S., Collie, B., and Samis, C. S., *Trans. Faraday Soc.* **32**, 795 (1936).

Heikkila, R. E., Deamer, D. W., and Cornwell, D. G., *J. Lipid Res.* **11**, 195 (1970).

Heikkila, R. E., Kwong, C. N., and Cornell, D. G., *J. Lipid Res.* **11**, 190 (1970).

Herrmann, C.-U., and Kahlweit, M., *J. Phys. Chem.* **84**, 1536 (1980).

Hiemenz, P. C., and Rajagopalan, R., *Principles of Colloid and Surface Chemistry*, Marcel Dekker (3rd ed.), New York, 1997.

Hifeda, Y. M., and Rayfield, G. W., *J. Colloid Interface Sci.* **104**, 209 (1985).

Higashiyama, T. and Takenaka, T. *J. Phys. Chem.* **78**, 941 (1974).

Hoffmann, H., Nagel, R., Platz, G., and Ulbricht, W. J., *Colloid Polym. Sci.* **254**, 812 (1976).

Holmberg, K., *Novel Surfactants: Preparation, Applications, and Biodegradability*, Marcel Dekker, New York, 1998.

Horozov, T. S., Kralchevsky, P. A., Danov, K. D., and Ivanov, I. B., *J. Disp. Sci. Technol.* **18**, 593 (1997).

Hughes, A. H. and Rideal E. K., *Proc. Roy. Soc. (London)* **A140**, 253 (1933).

Huibers, P. D. T., Oh, S. G., and Shah, D. O., in *Surfactants in Solution* (p. 146), A. K. Chattopadhyay and K. L. Mittal (Eds.), Marcel Dekker, Inc., New York, 1996.

Hunter, R. J., *Foundations of Colloid Science*, Oxford University Press, New York, 1987.

Iliev, Tz. H., and Dushkin, C. D., *Colloid Polym. Sci.* **270**, 370 (1992).

Imam, T., Devinsky, F., Lacko, I., Mlynarcik, D., Krasnec, L., *Pharmazie H.5* **38**, 308 (1983).

In, M., Bec, V., Aguerre-Chariol, O., and Zana, R., *Langmuir* **16**, 141 (2000).

Innoue, T., Tashiro, R., Shibuya, Y., and Shimozawa, R., *J. Colloid Interface Sci.* **73**, 105 (1980).

Israelachvili, J. N., *Intermolecular and Surface Forces*, Academic Press (2nd ed.), London, 1991.

Israelachvili, J. N., Mitchell, D. J., and Ninham, B. W., *J. Chem. Soc. Faraday Trans. 1* **72**, 1525 (1976).

Israelachvili, J. N., and Pashley, R. M., *Nature* **300**, 341 (1982).

Iwahashi, M., Yamaguchi, Y., Kato, T., Horiuchi, T., Sakurai, I., and Suzuki, M., *J. Phys. Chem.* **95**, 445 (1991).

James, A. D., Robinson, B. H., and White, N. C., *J. Colloid Interface Sci.* **59**, 328 (1977).

Johann, R., and Vollhardt, D., *Mat. Sci. Eng. C* **8-9**, 35 (1999).

Johann, R., Vollhardt, D., and Möhwald, H., *Langmuir* **17**, 4569 (2001).

Jung, R. F., *Oleic Acid Adsorption at the Goethite Water Interface*, Master's Thesis, University of Melbourne, 1976.

Kahlweit, M., *J. Colloid Interface Sci.* **90**, 92 (1982).

Kahlweit, M., and Teubner, M., *Adv. Colloid Interface Sci.* **13**, 1 (1980).

Kanicky, J. R., Poniatowski, A. F., Mehta, N. R., and Shah, D. O., *Langmuir* **16**, 172 (2000).

Kanicky, J. R., and Shah, D. O., *J. Colloid Interface Sci* (2002), in press, doi: 10.1006/jcis.2001.8009.

Kato, S., Harada, S., and Sahara, H., *J. Phys. Chem.* **99**, 12570 (1995).

Knoche, W., and Wiese, G., *Rev. Sci. Intrum.* **47**, 220 (1976).

Kralova, K., Sersen, F., *Tenside Surf. Det.* **31**, 192 (1994).

Kresheck, G. C., Hamori, E., Davenport, G., and Scheraga, H.A., *J. Amer. Chem. Soc.* **88**, 246 (1966).

Kulkarni R. D., and Somasundaran, P., *Trans. AIME* **120**, 262 (1977).

Kulkarni, R. D., and Somasundaran, P., *Colloids Surf.* **1**, 387 (1980).

Kunjappu, J. T., and Somasundaran, P., *Langmuir* **11**, 428 (1995).

Lang, J., Auborn, J. J., and Eyring, E. M., *J. Colloid Interface Sci.* **41**, 484 (1972).

Lang, J., and Eyring, E. M., *J. Polym. Sci. A-2* **10**, 89 (1972).

Lang, J., Tondre, C., Zana, R., Bauer, R., Hoffmann, H., and Ulbricht, W. J., *J. Phys. Chem.* **79**, 276 (1975).

Lang, J., and Zana, R., *J. Phys. Chem.* **90**, 5258 (1986).

Lang, J., and Zana, R. in *Chemical Relaxation Methods in Surfactants in Solution –New Methods of Investigation* (p. 14), R. Zana (Ed.), Marcel Dekker, New York, 1987.

Langmuir, I., *J. Amer. Chem. Soc.* **39**, 1848 (1917).

Larson, R. G., Scriven, L. E., and Davis, H. T., *J. Chem. Phys.* **83**, 2411 (1985).

Lasic, D., *Liposomes: From Physics to Applications*, Elsevier Scientific, Amsterdam, 1993.

Laughlin, R. G., *The Aqueous Phase Behavior of Surfactants*, Academic Press, New York, 1994.

Lessner, E., Teubner, M., and Kahlweit, M., *J. Phys. Chem.* **85**, 1529 (1981a).

Lessner, E., Teubner, M., and Kahlweit, M., *J. Phys. Chem.* **85**, 3167 (1981b).

Leung, R., and Shah, D. O., *J. Colloid Interface Sci.* **113**, 484 (1986).

Levy, J., in *Fatty Acids and Their Industrial Applications* (p. 209), E. S. Pattison (Ed.), Marcel Dekker, New York, 1968.

Li, Z. X., Dong, C. C., Thomas, R. K., *Langmuir* **15**, 4392 (1999).

Lide, D. R., and Milne, G. W. A., *Handbook of Data on Common Organic Compounds* (Vol I), CRC Press, Boca Raton, 1995.

Lucassen, J., *J. Phys. Chem.* **70**, 1824 (1966).

Mackie, A. D., Onur, K., and Panagiotopoulos, A. Z., *J. Chem. Phys.* **104**, 3718 (1996).

Maillet, J., Lachet, V., and Coveney, V., *Phys. Chem. Chem. Phys.* **1**, 5277 (1999).

Manne, S., Cleveland, J. P., Gaub, H. E., Stucky, G. D., Hansma, P. K., *Langmuir* **10**, 4409 (1994).

Manne, S. and Gaub, H. E., *Science* **270**, 1480 (1995).

Manne, S., Shäffer, T. E., Huo, Q., Hansma, P. K., Morse, D. E., Stucky, G. D., and Aksay, I. A., *Langmuir* **13**, 6382 (1997).

Marrink, S. J., Tieleman, D. P., and Mark, A. E., *J. Phys. Chem B* **104**, 12165 (2000).

Mavelli, F., and Maestro, M., *J. Chem. Phys.* **111**, 4320 (1999).

Mayer, B., and Rasmussen, S., *Int. J. Mod. Phys. C* **11**, 809 (2000).

McBain, J. W., *Trans. Faraday Soc.* **9**, 99 (1913a).

McBain, J. W., *Kolloid Z.* **12**, 256 (1913b).

McBain, J. W., and McHan, H., *J. Am. Chem. Soc.* **70**, 38 (1948).

McBain, J. W. and Salmon, C. S., *J. Amer. Chem. Soc.* **42**, 426 (1920).

McBain, J. W. and Stewart, A., *J. Chem. Soc.* **13**, 1392 (1927).

Menger, F. M., Keiper, J. S., Mbadugha, B. N. A., Caran, K. L., and Romsted, L. S., *Langmuir* **16**, 9095 (2000).

Michels, B., and Waton, G., *J. Phys. Chem. B* **104**, 228 (2000).

Mijnlieff, P. F., and Ditmarsch, R., *Nature* **208**, 889 (1965).

Miller, C. A., and Neogi, P., *Interfacial Phenomena, Equilibrium and Dynamic Effects*, Surfactant Science Series, Vol. 17, Marcel Dekker, New York, 1985.

Mitchell, D. J., and Ninham, B. W., *J. Chem. Soc. Faraday Trans. 2* 77, 601 (1981).

Mlynarcik, D., Lacko, I., Devinsky, F., Krasnec, L., *Pharmazie* **31**, 407 (1976).

Mukerjee, P., *J. Phys. Chem.* **62**, 1397 (1958a).

Mukerjee, P., *J. Phys. Chem.* **62**, 1404 (1958b).

Mukerjee, P. and Mysels, K. J., *J. Phys. Chem.* **62**, 1390 (1958).

Mukerjee, P., *J. Phys. Chem.* **69**, 2821 (1965).

Mukerjee, P. and Mysels, K. J. *Critical Micelle Concentrations of Aqueous Surfactant. Systems*, GPO, Washington, D. C., 1971.

Muller, N., *J. Phys. Chem.* **76**, 3017 (1972).

Muller, N., in *Solution Chemistry of Surfactants* (Vol. 1, p. 167), K. L. Mittal (Ed.), Plenum Press, New York, 1979.

Myers, D., *Surfaces, Interfaces and Colloids: Principles and Applications*, VCH Publishers, New York, 1991.

Mysels, K. J., *Introduction to Colloid Chemistry*, Interscience Publishers: New York, 1959, p 79.

Nelson, P. H., Rutledge, G. C., and Hatton, T. A., *J. Chem. Phys.* **107**, 10777 (1997).

Nikolov, A. D., Kralchevsky, P. A., Ivanov, I. B., and Wasan, D. T., *J. Colloid Interface Sci.* **133**, 1 (1989).

Nikolov, A. D., and Wasan, D. T., *J. Colloid Interface Sci.* **133**, 13 (1989).

Oh, S. G., Jobalia, M., and Shah, D. O., *J. Colloid Interface Sci.* **155**, 511 (1993).

Oh, S. G., Klein, S. P., and Shah, D. O., *AIChE Journal* **38**, 149 (1992).

Oh, S. G., and Shah, D. O., *Langmuir* **7**, 1316 (1991).

Oh, S. G., and Shah, D. O., *Langmuir* **8**, 1232 (1992).

Oh, S. G., and Shah, D. O., *J. Am. Oil Chem. Soc.*, **70**, 673 (1993a).

Oh, S. G., and Shah, D. O., *J. Phys. Chem.* **97**, 284 (1993b).

Patel, S. S., Kumar, K., Shah, D. O., and Delfino, J. J., *J. Colloid Interface Sci.* **183**, 603 (1996).

Patil, G. S., Matthews, R. H., and Cornwell, D. G., *J. Lipid Res* **13**, 574 (1972).

Patist, A., *Tailoring Micellar Stability to Control Interfacial Properties and Behavior of Dispersed Systems*, Ph.D. Dissertation, University of Florida, 1999.

Patist, A., Axelberd, T., and Shah, D. O., *J. Colloid Interface Sci.* **208**, 259 (1998).

Patist, A., Chhabra, V., Pagidipati, R., and Shah, D. O., *Langmuir* **13**, 432 (1997).

Patist, A., Devi, S., Shah, D. O., *Langmuir* **15**, 7403 (1999).

Patist, A., Kanicky, J. R., Shukla, P. K., and Shah, D. O., *J. Colloid Interface Sci.* **245**, 1 (2002).

Patist, A., Oh, S. G., Leung, R., and Shah, D. O., *Colloid Surf. A* **176**, 3 (2000).

Patist, A., Oh, S. G., Shiao, S. Y., Ling, T. F., Lee, H. K., Sharma, M. K., Devi, S., and Shah, D. O., in *Emulsions, Foams, and Thin Films* (p. 31), K. L. Mittal and P. Kumar (Eds.), Dekker, New York, 2000.

Peltonen, J. P. K., and Rosenholm, J. B., *Thin Solid Films* **179**, 543 (1989).

Peng, J. B., Barnes, G. T., and Gentle, I. R., *Adv. Colloid Interface Sci.* **91**, 163 (2001).

Peng, J. B., Barnes, G. T., Gentle, I. R., and Foran, G. J., *J. Phys. Chem. B* **104**, 5553 (2000).

Peng, J. B., Foran, G. J., Barnes, G. T., and Gentle, I. R., *Langmuir* **13**, 1602 (1997).

Peters, R. A., *Proc. Roy. Soc. (London)* **A133**, 140 (1931).

Pryde, E. H. (Ed.), *Fatty Acids*, AOCS, Champaign, 1979.

Pugh, R. J., *Colloids Surf.* **18**, 19, 1986.

Rabinovich,Y. I., Guzonas, D. A., Yoon, R. H., *J. Colloid Interface Sci.* **155**, 221 (1993).

Rao, Y. K., and Shah, D. O., *J. Colloid Interface Sci.* **137**, 25 (1990).

Rassing, J., Sams, P., and Wyn-Jones, E., *J. Chem. Soc., Faraday Trans. 2* **70**, 1247 (1974).

Reiss-Husson, F., and Luzzati, V., *J. Phys. Chem.* **68**, 3504 (1964).

Rosano, H. L., Breindel, K, Schulman, J. H., and Eydt, A. J., *J. Colloid Interface Sci.* **22**, 58 (1966).

Rosen, M. J., *Surfactants and Interfacial Phenomena*, John Wiley & Sons (2nd ed.), New York, 1989.

Rosen, M. J., *Chemtech* **23**, 30 (1993).

Sams, P. J., Wyn-Jones, E., and Rassing, J., *Chem. Phys. Lett.* **13**, 233 (1972).

Schmitt, V., Schosseler, F., Lequeux, F., *Europhys. Lett.* **30**, 31 (1995).

Schneider, V. L., Holman, R. T., and Burr, G. O., *J. Phys. Colloid Chem.* **53**, 1016 (1949).

Schulman, J. H., and Hughes, A. H., *Proc. Roy. Soc. (London)* **A138**, 430 (1932).

Seelig, A., and Seelig, J., *Biochemistry* **16**, 45 (1977).

Seidell, A. *Solubilities of Organic Compounds* (Vol 2), D. van Nostrand Co. (3rd ed.), New York, 1941.

Shah, D. O. (Ed.), *Macro- and Microemulsions: Theory and Applications*, ACS Symposium Series 272, American Chemical Society, Washington, D.C., 1985.

Shah, D. O., in *Micelles, Microemulsions and Monolayers* (p. 1), D. O. Shah (Ed.), New York, Marcel Dekker, 1998.

Shah, D. O., and Schulman, J. H., *J. Lipid Res.* **6**, 341 (1965).

Shah, D. O., and Schulman, J. H., *J. Lipid Res.* **8**, 215 (1967a).

Shah, D. O., and Schulman, J. H., *J. Colloid Interface Sci.* **25**, 107 (1967b).

Sharma, M. K., Shah, D. O., and Brigham, W. E., *SPE Reservoir Engineering*, 253, May 1986.

Sharma, M. K., and Shah, D. O., *Ind. Eng. Chem. Fundam.* **23**, 213 (1984).

Shiao, S. Y., Chhabra, V., Patist, A., Free, M. L., Huibers, P. D. T., Gregory, A., Patel, S., and Shah, D. O., *Adv. Colloid Interface Sci.* **74**, 1 (1998).

Shiao, S. Y., Patist, A., Free, M. L., Chhabra, V., Huibers, P. D. T., Gregory, A., Patel, S., and Shah, D. O., *Colloids Surfaces A* **128**, 197 (1997).

Shinoda, K., and Nakagawa, T., *Colloidal Surfactants: Some Physicochemical Properties*, Academic Press, New York, 1963.

Singh, C. P., and Shah, D. O. , *Colloids Surfaces A* 77, 219 (1993).

Singh, P. K., Adler, J. J., Rabinovich, Y. I., and Moudgil, B. M., *Langmuir* **17**, 468 (2001).

Small, D. M., *The Physical Chemistry of Lipids, Handbook of Lipid Research* (Vol. 4), Plenum Press, New York, 1986.

Smit, B., Hilbers, P., Esselink, K., Rupert, L., van Os, N., and Schlijper, A., *J. Phys. Chem.* **95**, 6361 (1991).

Somasundaran, P., Ananthapadmanabhan, K. P., and Ivanov, I. B., *J. Colloid Interface Sci.* **99**, 128 (1984).

Somasundaran, P. and Moudgil, B. M. (Eds.) *Reagents in Mineral Technology*, New York, Marcel Dekker, 1988.

Stein, R. S., *J. Polym. Sci.* **31**, 327 (1958).

Stein, R. S., *J. Polym. Sci.* **50**, 339 (1961).

Sutherland, I. O., *Comprehensive Organic Chemistry: The Synthesis and Reactions of Organic Compounds* (Vol 2); Pergamon Press, New York, 1979.

Takeda, K., Tatsumo, T. N., and Yasunaga, T., *J. Colloid Interface Sci.* **47**, 128 (1974).

Talsania, S. K., Wang, Y., Rajagopalan, R., and Mohanty, K. K., *J. Colloid Interface Sci.* **190**, 92 (1997).

Tandon, P., Forster, G., Neubert, R., and Wartewig, S., *J. Mol. Struct.* **524**, 201 (2000).

Tanford, C., *The Hydrophobic Effect. Formation of Micelles and Biological Membranes*, Wiley (2nd ed.), New York, 1980.

Tarek, M., Bandyopadhyay, S., and Klein, M. L., *J. Mol. Liq.* **78**, 1 (1998).

Teubner, M., Diekmann, S., and Kahlweit, M., *Ber. Bunsenges. Phys. Chem.* **82**, 1278 (1978).

Tieleman, D. P., van der Spoel, D., and Berendsen, H. J. C., *J. Phys. Chem. B* **104**, 6380 (2000).

Tomoaia-Cotisel, M., Zsako, J., Mocanu, A., Lupea, M., and Chifu, E., *J. Colloid Interface Sci.* **117**, 464 (1987).

Tondre, C., Lang, J., and Zana, R., *J. Colloid Interface Sci.* **52**, 372 (1975).

Turner, M. S., and Cates, M. E., *J. Phys. France* **51**, 307 (1990).

Ueno, S., Miyazaki, A., Yano, J., Furukawa, Y., Suzuki, M., and Sato, K., *Chem. Phys. Lipids* **107**, 169 (2000).

Ulbricht, W., and Zana, R., *Colloid Surf A* **183-185**, 487 (2001).

van Deenen, L., L., M., Houtsmuller, U., M., T., de Haas, G., H., and Mulder, E., *J. Pharm. Pharmacol.* **14**, 429 (1962).

van Ee, J. H., Misset, O., and Baas, E. J., *Enzymes in Detergency*, Marcel Dekker, New York, 1997.

von Gottberg, F.K., Smith, K.A., and Hatton, T.A., *J. Chem. Phys.* **108**, 2232 (1998).

Walstra, P., in *Encyclopedia of Emulsion Technology* (Vol. 1, p. 235), P. Becher (Ed.), Dekker, New York, 1983.

Wang, Y., Diermeier, R. G., and Rajagopalan, R., *Langmuir* **13**, 2348 (1997).

Wangnerud, P., Jonsson, B., *Langmuir* **10**, 3542 (1994).

Wasan, D. T., Gupta, L., and Vora, M. K., *AIChE J.* **17**, 1287 (1971).

Waton, G., *J. Phys. Chem. B* **101**, 9727 (1997).

Wymore, T., Gao, X. F., and Wong, T. C., *J. Mol. Struct.* **485-486**, 195 (1999).

Wyn-Jones, E., *Chemical and Biological Aspects of Relaxation Spectroscopy*, D. Reidel, Boston, 1975.

Yasunaga, T., Fujii, S., and Miura, M., *J. Colloid Interface Sci.* **30**, 399 (1969).

Yasunaga, T., Oguri, H., and Miura, M., *J. Colloid Interface Sci.* **23**, 352 (1967).

Yasunaga, T., Takeda, and K., Harada, S., *J. Colloid Interface Sci.* **42**, 457 (1973).

Zana, R., in *Structure-Performance Relationships in Surfactants* (p. 255), Esumi, K. and Ueno, M. (Eds.), Marcel Dekker, New York, 1997.

Zana, R., *Adv. Colloid Interface Sci.* **97**, 205 (2002).

Zana, R., and Lang, J., C. R. *Acad. Sci., Ser. C* **266**, 893 (1968a).

Zana, R., and Lang, J., C. R. *Acad. Sci., Ser. C* **266**, 1347 (1968b).

Zana, R., and Talmon, Y. *Nature* **362**, 228 (1993).

Zhu, Y. P., Masuyama, A., Kobata, Y., Nakatsuji, Y., Okahara, M., and Rosen, M. J., *J. Colloid Interface Sci.* **158**, 40 (1993).

BIOGRAPHICAL SKETCH

James Rene Kanicky was born to James F. and Anne-Marie D. Kanicky on December 6, 1975, at the U.S. Naval Station in Rota, Spain. He spent most of his childhood in Chipiona, Spain, and completed high school at David Glasgow Farragut (DGF) High School (Class of 1993). He went on to study at Rose-Hulman Institute of Technology (Terre Haute, IN), where he completed his bachelor's degree in chemical engineering in 1997. He then joined the chemical engineering department at the University of Florida in August 1997 and began work in Professor Dinesh O. Shah's research group in 1998. He completed his Ph.D. degree under the supervision of Dr. Shah in 2002 and began work with DuPont in January of 2003.

I certify that I have read this study and that in my opinion it conforms to acceptable standards of scholarly presentation and is fully adequate, in scope and quality, as a dissertation for the degree of Doctor of Philosophy.

D. O. Shah

Dinesh O. Shah, Chairman
Professor of Chemical Engineering

I certify that I have read this study and that in my opinion it conforms to acceptable standards of scholarly presentation and is fully adequate, in scope and quality, as a dissertation for the degree of Doctor of Philosophy.

B. M. Moudgil

Brij M. Moudgil
Professor of Materials Science and Engineering

I certify that I have read this study and that in my opinion it conforms to acceptable standards of scholarly presentation and is fully adequate, in scope and quality, as a dissertation for the degree of Doctor of Philosophy.

Gar B. Hoflund

Gar Hoflund
Professor of Chemical Engineering

I certify that I have read this study and that in my opinion it conforms to acceptable standards of scholarly presentation and is fully adequate, in scope and quality, as a dissertation for the degree of Doctor of Philosophy.

A Chauhan

Anuj Chauhan
Assistant Professor of Chemical Engineering

This dissertation was submitted to the Graduate Faculty of the College of Engineering and to the Graduate School and was accepted as partial fulfillment of the requirements for the degree of Doctor of Philosophy.

December, 2002

Pramod Khargonekar
Dean, College of Engineering

Winfred M. Phillips
Dean, Graduate School